Solubility and Leaching of Radionuclides in Site Decommissioning Management Plan (SDMP) Slags
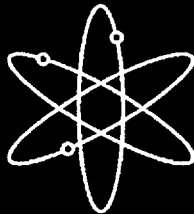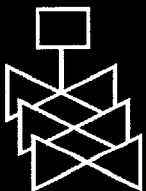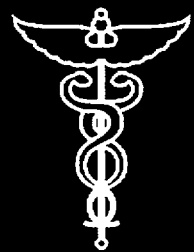
Pacific Northwest National Laboratory

U.S. Nuclear Regulatory Commission
Office of Nuclear Regulatory Research
Washington, DC 20555-0001

AVAILABILITY OF REFERENCE MATERIALS
IN NRC PUBLICATIONS

NRC Reference Material

As of November 1999, you may electronically access NUREG-series publications and other NRC records at NRC's Public Electronic Reading Room at www.nrc.gov/NRC/ADAMS/index.html.
Publicly released records include, to name a few, NUREG-series publications; *Federal Register* notices; applicant, licensee, and vendor documents and correspondence; NRC correspondence and internal memoranda; bulletins and information notices; inspection and investigative reports; licensee event reports; and Commission papers and their attachments.

NRC publications in the NUREG series, NRC regulations, and *Title 10, Energy*, in the Code of *Federal Regulations* may also be purchased from one of these two sources.
1. The Superintendent of Documents
   U.S. Government Printing Office
   Mail Stop SSOP
   Washington, DC 20402–0001
   Internet: bookstore.gpo.gov
   Telephone: 202-512-1800
   Fax: 202-512-2250
2. The National Technical Information Service
   Springfield, VA 22161–0002
   www.ntis.gov
   1–800–553–6847 or, locally, 703–605–6000

A single copy of each NRC draft report for comment is available free, to the extent of supply, upon written request as follows:
Address: Office of the Chief Information Officer,
          Reproduction and Distribution
            Services Section
          U.S. Nuclear Regulatory Commission
          Washington, DC 20555-0001
E-mail: DISTRIBUTION@nrc.gov
Facsimile: 301–415–2289

Some publications in the NUREG series that are posted at NRC's Web site address www.nrc.gov/NRC/NUREGS/indexnum.html are updated periodically and may differ from the last printed version. Although references to material found on a Web site bear the date the material was accessed, the material available on the date cited may subsequently be removed from the site.

Non-NRC Reference Material

Documents available from public and special technical libraries include all open literature items, such as books, journal articles, and transactions, *Federal Register* notices, Federal and State legislation, and congressional reports. Such documents as theses, dissertations, foreign reports and translations, and non-NRC conference proceedings may be purchased from their sponsoring organization.

Copies of industry codes and standards used in a substantive manner in the NRC regulatory process are maintained at—
          The NRC Technical Library
          Two White Flint North
          11545 Rockville Pike
          Rockville, MD 20852–2738

These standards are available in the library for reference use by the public. Codes and standards are usually copyrighted and may be purchased from the originating organization or, if they are American National Standards, from—
          American National Standards Institute
          11 West 42nd Street
          New York, NY 10036–8002
          www.ansi.org
          212–642–4900

Legally binding regulatory requirements are stated only in laws; NRC regulations; licenses, including technical specifications; or orders, not in NUREG-series publications. The views expressed in contractor-prepared publications in this series are not necessarily those of the NRC.

The NUREG series comprises (1) technical and administrative reports and books prepared by the staff (NUREG–XXXX) or agency contractors (NUREG/CR–XXXX), (2) proceedings of conferences (NUREG/CP–XXXX), (3) reports resulting from international agreements (NUREG/IA–XXXX), (4) brochures (NUREG/BR–XXXX), and (5) compilations of legal decisions and orders of the Commission and Atomic and Safety Licensing Boards and of Directors' decisions under Section 2.206 of NRC's regulations (NUREG–0750).

Solubility and Leaching of Radionuclides in Site Decommissioning Management Plan (SDMP) Slags

Prepared by
A. R. Felmy, D. Rai, S. A. Hartley,
V. L. LeGore

Pacific Northwest National Laboratory
Richland, WA 99352

P. Reed, NRC Project Manager

ABSTRACT

Samples of disposed wastes at three U.S. Nuclear Regulatory Commission (NRC) Site Decommissioning Management Plan (SDMP) sites were studied to determine 1) the key radionuclides and their concentrations present in the waste, 2) the solubility limits and solubility limiting phases for these radionuclides, 3) the rate of attainment of solubility equilibrium, 4) the observed leaching rate for radionuclides which may or may not be solubility controlled, and 5) the potential for radiocolloid formation. In order to achieve these goals batch studies of ground or fractured samples were conducted over ranges of solution pH values (2 - 12), solid to solution ratio, and particle size. In addition, flow-through column studies were conducted of selected samples to help verify the mechanisms and predictive relations identified in the batch experiments. Three slag containing sites were selected for study. The results for slags at all three sites show that the major radionuclides present in the wastes were Th and U with their associated daughter products. Th daughters were in secular equilibrium with the parent Th-232 in all samples. U-238 daughters were in secular equilibrium in certain highly solidified non-porous samples but escape of Rn-222 had occurred from more porous samples perturbing the U-238 secular equilibrium. Analysis of solution phase concentrations and solid phase composition indicated that aqueous Th concentrations are solubility controlled, most likely by thoranite, $ThO_2(c)$, which sets an upper limit on the dissolved Th concentrations. Uranium also appears to be solubility controlled in certain waste samples (thoriated slags) high in pH and alkaline earth cations (Ca, Sr, Ba), upper limits on the observed solubilities apparently being set by the secondary formation of alkaline earth uranates. Comparisons of filtered and unfiltered analyses of samples from flow-through columns did not show any evidence for the presence of radiocolloids. Maximum dissolved concentrations (solubility limits) and radionuclide leaching rates have been calculated for three sites for use in performance assessment calculations. Observed Th and U solubilities were quite low (maximum Th solubilities of 3.2×10^{-8} M, 4×10^{-8} M, and 3.2×10^{-9}; maximum U solubilities were 2.5×10^{-8} M, 6.3×10^{-8} M, and 8.9×10^{-9}M all for sites A, B, and C respectively). Observed leaching rates for the three sites were 100, 1 and 0.2 pCi/yr for Th and 260, 8 and 2 pCi/yr for U again for sites A, B, and C respectively. Chemical modeling of well water compositions at site C indicates that the low concentrations of soluble uranium are primarily present as anionic uranium carbonate complexes. Statistical analysis of the batch, column, and solubility data showed that the uncertainties in the dissolved Th and U concentrations can be described using a lognormal distribution with a meanlog of −17.7 and a sdlog of 0.57 for U and a meanlog of −19.5 and an sdlog of 1.7 for Th. These parameters are valid for all three sites.

CONTENTS

FIGURES

TABLES

EXECUTIVE SUMMARY

Each year the NRC receives requests to discontinue licensed operations that involve the use of radioactive materials (NRC 1993). However, the termination of some licenses and the possible release of the site for unrestricted or other uses are sometimes non-routine owing to the level, volume, or complex nature of the radiological contamination. In such cases a more clear scientific understanding of the nature, both physical and chemical, of the radiological contamination is required to make informed judgments as to the level of site remediation that may be required. As part of such an overall effort this report summarizes the findings from solubility, batch, and soil/waste column studies conducted on wastes from three NRC Site Decommissioning Management Plan (SDMP) sites. These studies were designed to determine 1) the key radionuclides and their concentrations present in the waste, 2) the solubility limits and solubility limiting phases for these radionuclides, 3) the rate of attainment of solubility equilibrium, 4) the observed leaching rate for radionuclides which may or may not be solubility controlled, and 5) identify, if possible, the potential for radiocolloid formation. Three sites were selected for study, labeled Sites A, B, and C, which provided a range of materials for analysis that covered different processing conditions and represented differences in chemical and physical properties of the slags. The results for all three sites showed that the major radionuclides present in the wastes were Th and U with their associated daughter products. Analysis of solution phase concentrations and solid phase composition indicated that aqueous Th concentrations are solubility controlled, most likely by thoranite, $ThO_2(c)$, which sets an upper limit
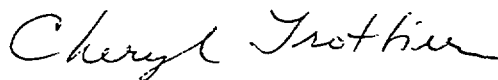
on the dissolved Th concentrations. U also appears to be solubility controlled in certain waste samples (thoriated slags). Comparisons of filtered and unfiltered analyses of samples from flow-through columns did not show any evidence for the presence of radiocolloids. Maximum dissolved concentrations (solubility limits) and radionuclide leaching rates have been calculated for use in performance assessment calculations. Observed Th and U solubilities were quite low (maximum Th solubilities of 3.2×10^{-8} M, 4×10^{-8} M, and 3.2×10^{-9} M ; maximum U solubilities were 2.5×10^{-8} M, 6.3×10^{-8} M, and 8.9×10^{-9} M all for sites A, B, and C respectively). Observed leaching rates for the three sites were 100, 1 and 0.2 pCi/yr for Th and 260, 8 and 2 pCi/yr for U again for sites A, B, and C respectively. Chemical modeling of well water compositions at site C indicates that the low concentrations of soluble uranium are primarily present as anionic uranium carbonate complexes. Statistical analysis of the batch, column, and solubility data showed that the uncertainties in the dissolved Th and U concentrations can be described using a lognormal distribution with a meanlog of -17.7 and a sdlog of 0.57 for U and a meanlog of -19.5 and an sdlog of 1.7 for Th. These parameters are valid for all three sites. These results thus provide experimental evidence of the nature of the contamination present at these sites and the range of conditions under which the radionuclides are likely to be either soluble and mobile in the groundwater or insoluble and immobile. It is anticipated that such results will assist in the evaluation of effective remediation strategies for these sites.

FOREWORD

This contractor technical report, NUREG/CR-6632, was prepared by Pacific Northwest National Laboratory[1] under their DOE Interagency Work Order (JCN W6409) with the Radiation Protection, Environmental Risk and Waste Management Branch, Division of Systems Analysis and Regulatory Effectiveness, Office of Nuclear Regulatory Research, U.S. Nuclear Regulatory Commission. This report is the first in a series of three contractor reports documenting PNNL's research results on slag and soil samples collected at Site Decommission Management Plan (SDMP) sites.

The PNNL research study was undertaken to support licensing needs for reviewing radiological and chemical data and information for estimating site-specific dose assessment modeling as outlined in the NMSS Decommissioning Standard Review Plan, NUREG-1727. This PNNL report provides information on uranium and thorium solubilities, release rates, and colloidal data and information from three SDMP slag sites. Uranium and thorium solubilities are presented in both deterministic and probabilistic distribution functions for use in commonly-used dose assessment codes (i.e., RESRAD). The report also includes site radiological data for uranium and thorium isotopes in slags, chemical data for slags and ground water samples, and information on secular equilibrium behavior of uranium and thorium parent and daughter isotopes at the three slag sites.

NUREG/CR-6632 is not a substitute for NRC regulations, and compliance is not required. The approaches and/or methods described in this NUREG/CR report are provided for information only. Publication of this report does not necessarily constitute NRC approval or agreement with the information contained herein. Use of product or trade names is for identification purposes only and does not constitute endorsement by the NRC or Pacific Northwest National Laboratory.

Cheryl A. Trottier, Chief
Radiation Protection, Environmental Risk
 and Waste Management Branch
Division of Systems Analysis and Regulatory Effectiveness
Office of Nuclear Regulatory Research.

---

[1]Pacific Northwest National Laboratory is operated for the U.S. Department of Energy by Battelle Memorial Institute under contract DE-AC06-76RLO 1830.

LIST OF ABBREVIATIONS

Ac	Actinium
(am)	amorphous
Al	Aluminum
BET	Brunauer-Emmett-Teller
Bi	Bismuth
(c)	crystalline
Ca	Calcium
Ci/ml	Curies per milliliter
DU	Depleted Uranium
EDXRF	Energy dispersive x-ray fluorescence
Fe	Iron
g	gram
(gl)	glass
GM	Gieger-Müller
IC	Ion Chromatograph
ICP	Inductively coupled plasma spectroscopy
ICP-MS	Inductively coupled plasma mass spectrometry
kev	one thousand electron volts
kgs	kilograms
m	meter
mg/l	milligrams per liter
ml	milliliter
mm	millimeter
M	molarity (moles/l)
Mo	Molybdenum
Nb	Niobium
NRC	United States Nuclear Regulatory Commission
ORISE	Oak Ridge Institute for Science and Education
Pb	Lead
PCi/g	picocuries per gram
PCi/yr	picocuries per year
pH	Negative log of the activity of H^+
PNNL	Pacific Northwest National Laboratory
ppm	parts per million
Ra	Radium
Rn	Radon
SDMP	Site Decommissioning Management Plan
Si	Silicon
Ta	Tantalum
Th	Thorium
U	Uranium
XRF	X-ray fluorescence

1 INTRODUCTION

The U.S. Nuclear Regulatory Commission (NRC) has identified 51 sites around the U.S. that have radionuclide contamination that exceeds NRC criteria for unrestricted use (NRC 1995). All of these sites require some degree of remediation before sites can be released for unrestricted use. One of the principal types of contaminants present at these sites is thoriated slags produced as byproducts from processing ferrocolumbium alloys or tin slag. The thoriated slags were then mixed with site material (i.e. soils, building rubble, or other wastes) and disposed either in unlined slag piles, over embankments, or by other means (NRC 1995). As a result, the NRC is currently in the process of conducting performance assessments of these sites to better ascertain the potential for radionuclides solubilization, leaching or migrate off site. As part of this overall effort, the Pacific Northwest National Laboratory (PNNL) was contracted to obtain selected samples from different SDMP sites and conduct batch and flow-through column leaching studies of these wastes to determine the radionuclides present in the waste, the maximum leachable concentrations (solubility limits) for important radionuclides, the time required for radionuclides to reach solubility equilibrium, the overall radionuclide leaching rates, and, if possible, identify the potential impact of colloids in transporting radionuclides.

This report presents detailed results of PNNL studies on three selected SDMP sites, which represent a range of slag compositions and disposal practices. Disposal practices ranged from gathering the waste materials and placing into barrels or a slag pile (site A) to direct disposal over embankments (site B) or a combination of such practices (site C). The radionuclide containing wastes at these sites are principally thoriated slags produced from processing tin slag or ferrocolumbium alloys. The following sections of this report describe site sampling and sample selection, chemical analysis, radiological analysis, solubility and leaching studies, and investigations of radiocolloids.

1

2 SITE SAMPLING AND SAMPLE SELECTION

Samples from Site A were sent to PNNL following a visit to the site. Four samples of the disposed slags with the highest radionuclide content (>1000pCi/g) in the slag pile were obtained. All of the samples were large pieces (~1-1.5kgs)of grayish slag with a rust and white coating. The samples from Site B were obtained by both PNNL and NRC staff from diggings near the edge of the embankment. A total of 21 samples from Site B were obtained and shipped to PNNL. Preliminary gamma scans were performed on all samples and three of the samples with the highest radioactivity were selected for detailed study. These samples were 1) 2 kgs of slag pieces mixed with some soil (sample C-9), 2) a relatively small (280g) grayish green sample of slag/ore (sample C-19), and 3) 1 kg of sandy soil mixed with pieces of slag (sample C-20).

PNNL received two sets of samples from Site C. The first set was collected by staff at the Center for Nuclear Waste Regulatory Analyses (CNWRA), San Antonio TX and sent to PNNL for analysis. Only a limited amount of radiological and chemical analyses were performed on these samples owing to the small size of the samples. Many of these samples were non-radioactive. Appendix A presents a complete description of these samples and the analyses conducted by PNNL. A second set of samples was then collected by NRC, Commonwealth of Pennsylvania, and SCIENTECH, Inc. staff at site C in 2001 and shipped to PNNL for more detailed analysis. These samples consisted of six well water or river water samples and two samples of slag. All of the well water samples contained suspended or particulate material of a brownish to rust color upon arrival. As a result the samples were filtered to remove solids and determine dissolved concentrations. Both the unfiltered and filtered samples were analyzed.

3 METHODS AND MATERIALS

The presence of a solubility controlling solid phase in a soil or slag sample means that the radionuclide concentration in equilibrium with this phase will vary only with the chemistry of the water in contact with the soil or sediment and will be independent of time, particle size, and solid to solution ratio. Therefore, all of these factors must be varied in the experimental design in order to establish that a solubility controlling phase is present. The experimental design outlined here attempts to accomplish these goals by 1) conducting studies as a function of water chemistry (pH, CO_2 content), 2) conducting long term studies with both coarse and fine material to test the independence of particle size, and 3) conducting studies at different solid to solution ratios. In the latter case we chose to conduct studies at high solid to solution ratio and these studies were most easily done by using flow through columns. The column studies also allow insight to be gained into the rate of the reactions. It is often difficult to vary the chemistry (particularly the pH) of the samples at high solid to solution ratio since large concentrations of acid or base must be added. Therefore the pH varying studies (labeled "solubility" henceforth) were conducted at low solid to solution ratios and using fine material to enhance the reaction rate. The other studies that were conducted were done at low solid to solution ratio without the addition of acid or base. These studies were done wherever possible using both fine and coarse material to evaluate the possible influence of the particle size effect. These latter studies are labeled as "batch" studies

The selected samples from the different sites were treated in the following manner (see Figure 3-1).

First, for the samples that contained large pieces of slag it was necessary to fracture the material into smaller pieces in order to conduct column or batch studies. This fractured material is subsequently referred to as "coarse" (2mm < particle size < 7mm) material. In addition, samples of the fractured material were ground to a very fine size (< 2mm) for chemical analysis, radiological analysis, and for use in the solubility studies. The use of fine material in the solubility studies was necessary to speed the reaction rate and achieve, if possible, equilibrium between solid phase components of the samples and the solutions. Surface area analysis was conducted on both the coarse and fine material using a Micrometrics Model 2010 BET analyzer.

Following sample fracturization the materials were used in the following general manner. Samples of fine material were sent for chemical, radiological, particle size (selected samples only) analysis and were used in all solubility studies. In addition, selected fine material was used in "fine" batch studies to contrast the leaching characteristics of the fine and coarse material. Coarse material was used only in the batch and column studies. The following discussion provides more details on the analysis procedures and sample preparation for the solubility, batch, and column studies.
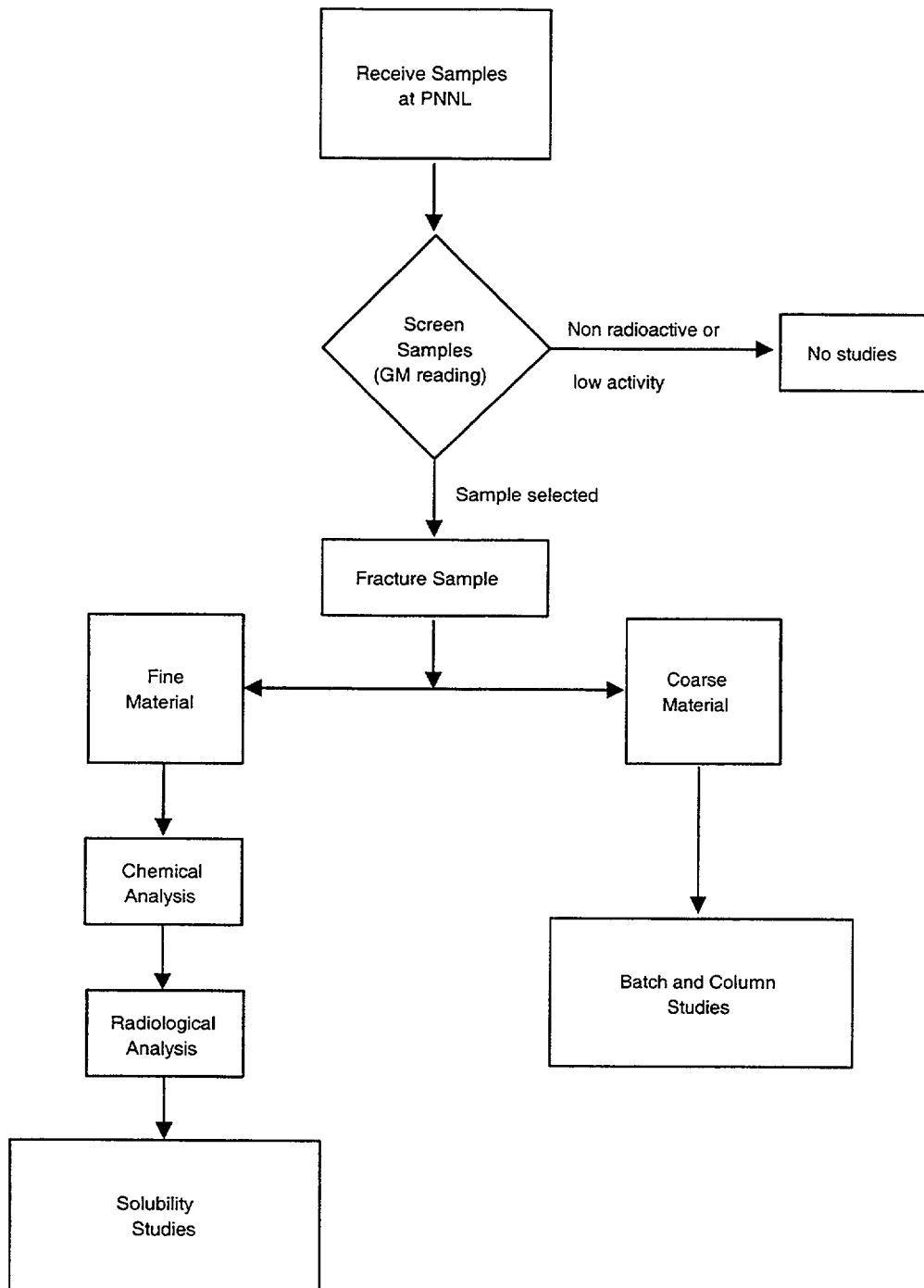
Figure 3-1. Schematic outline of sample treatment and analysis.

3.1 Chemical Analysis Procedures

Total chemical analysis of solid materials was performed by energy dispersive x-ray fluorescence (EDXRF) with low (ppm) detection limits for most elements from Al to Ce.

Chemical analysis of solutions was performed by inductively coupled plasma spectroscopy (ICP) analysis, except for samples with low concentrations of Th, U, or Nb, which were determined by inductively coupled plasma mass spectrometry (ICP-MS). Selected samples for anion analysis were also conducted using a model 4000i Dionex ion chromatograph. All analyses were performed under guidelines provided in PNNL QA good laboratory practice procedures: ICPMS (PNNL-AGG-415); ICP (PNNL – AGG-ICP-AES); IC (EPA method 300, "The determination of inorganic anions in water by ion chromatography); and XRF (use of NBS standard reference materials).

3.2 Radiological Analysis

Radiological analysis of solid and solution samples were conducted using a high-efficiency intrinsic Germanium detector calibrated over the energy range 60 to 2000 kev. The following energy peaks was used to determine the radionuclide concentrations: Ac-228, 911 kev; Bi-212, 727 kev; Pb-212, 239 kev; Ra-226, 186 kev; Bi-214, 609 kev; Pb-214, 352 kev; Th-234, 62.3 kev; Tl-208 583 kev. All analyses were performed on duplicate or triplicate samples. The Ra-226 values were corrected by a factor of 0.57 to account for the coincident natural U-235 peak. Selected solid samples were also dissolved with $KOH-KNO_3$ fusion and chemically separated the U and Th. Uranium was then measured by kinetic phosphorescence and Th isotopes by alpha spectroscopy.

3.3 Solubility and Batch Studies

Solubility studies were conducted in a controlled atmosphere chamber under an atmosphere of ultrapure argon. Solubility studies were conducted in initially de-ionized water which had been pH adjusted using HCL to cover a broad range of pH values extending from approximately 1 to 12 depending upon the specific samples examined. Batch studies were conducted both in an atmospheric chamber in the absence of CO_2 and on the bench top where CO_2 was allowed into the samples. De-ionized water was used in all batch studies. The bench top studies were conducted as both "long term" and "short term" experiments. In the "long term" studies the samples were kept lightly capped but there was no forced equilibration with atmospheric CO_2. ($pCO_2 \sim 10^{-3.5}$ atm). In the "short term" studies the samples were vigorously bubbled with air over a three-day period to insure the equilibration with atmospheric CO_2. The introduction of CO_2 is potentially important owing to the possible formation of either Th(IV) carbonate complexes (Felmy et al. 1997) or U carbonate complexes (Grenthe et al. 1992). All of the batch studies were conducted at the "natural" pH of the sample, which varied with reaction time, and conditions, as the samples dissolved. No pH adjustments were made by adding acid or base. Both fine and coarse material was used in the batch experiments. All of the fine batch and solubility suspensions were prepared in the following manner. For each site sample a solid/solution suspension was

7

prepared by placing approximately one gram of fine material in 30ml of deionized water in each 50ml centrifuge tube. Approximately 24 such suspensions were prepared for each sample in the solubility studies. Each sample was independently adjusted to a different pH value within the prescribed range using reagent grade HCl or NaOH. The batch samples were prepared in the same manner but only two suspensions (duplicates) were prepared for each site sample. All suspensions were then placed on an orbital shaker and shaken until sampling. Sampling of the solubility and batch suspensions consisted of pH measurements followed by centrifugation at 2000 x g for 7 to 10 min. A sample of the supernatant was then filtered through Amicon type F-25 Centriflo membrane cones with effective 2500-molecular-weight cutoffs and approximately 0.0018-μm pore sizes. The membrane were pretreated by washing with pH adjusted deionized water (to the approximate pH of the sample) followed by filtration of a 0.5 ml to 1.0 ml aliquot of sample to saturate any adsorption sites. The aliquot of the sample was then discarded. This pretreatment process was then followed by filtration of approximately 5ml of sample. Approximately 1ml of this sample was then withdrawn and acidified for ICP or ICP-MS and radiological analysis. The remaining unacidified sample was retained for anion analysis by IC.

The coarse batch studies were conducted in the identical manner to the fine batch studies except that approximately 6g of sample were added to 180ml of deionized water in 500ml polypropylene bottles. This procedure maintained the same solid/solution ratio as in the fine batch but allowed more particles of the larger material to be included in each sample.

3.4 Column Studies

Flow through column experiments were conducted using 32ml Savelex® teflon columns, Figure 3-2, connected to 3M modular infusion pumps operating at a flow rate of 0.1 ml/hr. Each 32ml column was then packed with 30 to 40g of slag material depending upon the exact particle size. The final solution volume in each column (pore volume) was then approximately 16 to 17mls. Porous frits were placed at the top and bottom of each column to prevent any fine suspended material from passing through the column. The solutions entered the columns through the bottom and passed out the top into a sealed collection bottle. Samples from the collection bottle were taken, pH measurements made, and filtered as described for solubility and batch studies. Filtrates were split into acidified and unacidified aliquots for analysis by ICP or ICP-MS and IC. Radiological analysis was also performed on acidified sample.

To Sample Collection

Flow Direction

Teflon Screen

Soil

pH port

Frit

SP98030148.1
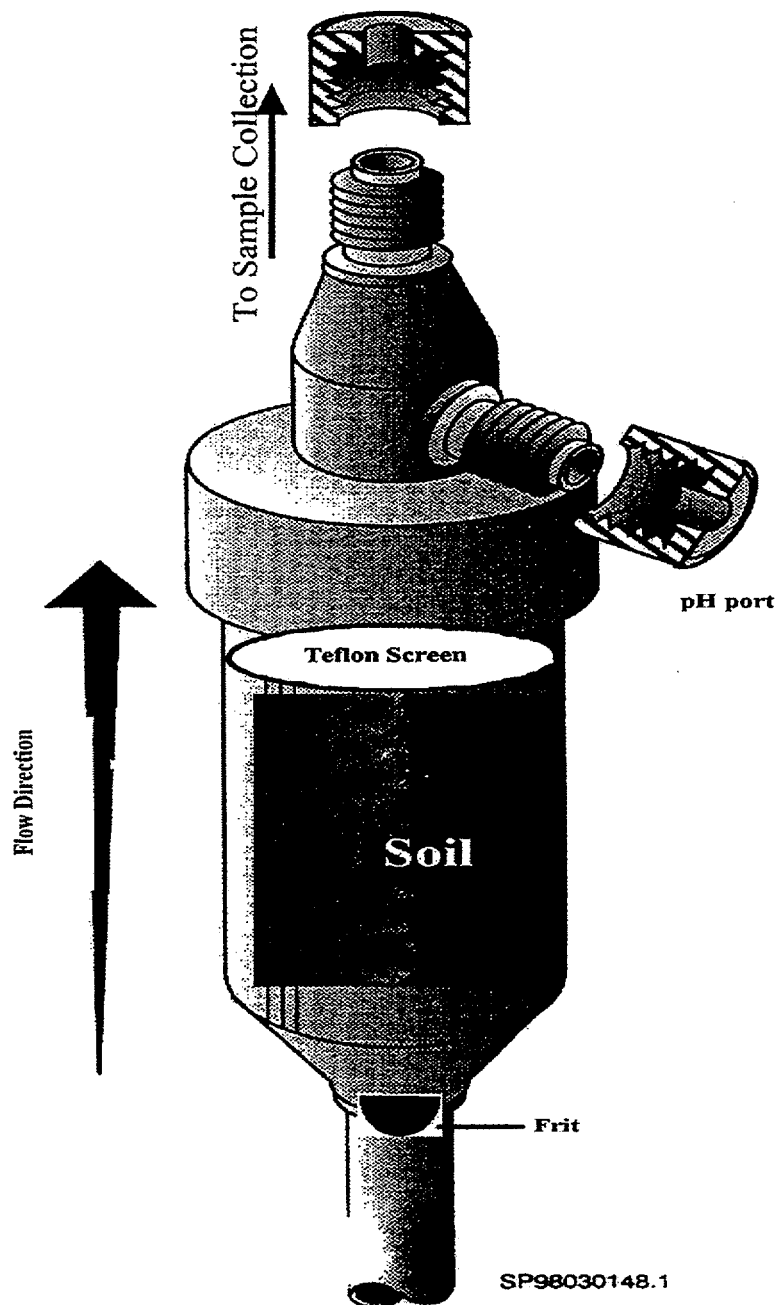
Figure 3-2. Schematic of Column Apparatus. The designation "soil" represents soil or slag depending upon the specific sample. The pH port, which was present on only a few columns, was not used. All pH measurements were made in the sample collecting vessel.

4 RESULTS AND DISCUSSION

4.1 Chemical Analysis

The total chemical analysis of the soil and slag samples at all three sites, Tables 4-(1-3), show a bulk composition dominated by Al, Si, and Ca characteristic of alumino-silicate minerals or calcium alumino-silicate minerals with significant amounts of Fe and significant amounts of Nb. These same general chemical characteristics, with somewhat lower Fe content, have been reported elsewhere (Pickett et al. 1998) and have been correlated with the presence of several alumino-silicate minerals including gehlenite, wollastonite, and pervoskite (Table 4-4). The presence of high concentrations of Nb, and to a lesser extent Ta, at least Site C, being a clear indication of materials originating from the ferro-columbium smelting process. Also, of interest is the presence of significant amounts of Zr which is correlated with the presence of zirconate minerals (calzirtite and zirconolite; Table 4-4) and a relatively high Mo content in slags from Site A.

The element in highest concentration with radioactive isotopes is Th. Th occurs in significant concentration in all samples, as high as 1.4% in Site A samples. The concentration of U is fairly uniform in all samples averaging approximately 200ppm. The mineral phases in which these radionuclides are incorporated in does vary somewhat between the sites. The major Th bearing phase is perovskite at sites A and C (Veblen et al. 2000). However, significant amounts of thorianite (ThO_2) also present at site A (Table 4-4). At site B the Th and U are primarily contained in perovskite, calzirtite, and pyrochlore.

Chemical analysis of well and surface waters were also conducted at Site C. The analyses are reported for filtered samples in Table 4-5 and unfiltered samples in Table 4-6. Filtration was necessary since the samples as received at PNNL contained brownish to rust colored solids. The well waters are all predominately Na, Ca, Mg, SO_4, HCO_3 solutions at near neutral pH values. Well #8 contains the highest concentrations of these components and hence has the highest ionic strength. Dissolved Th and U concentrations were quite low in all samples with Th concentrations at or below the analytical detection limit. Dissolved U concentrations were detectable but quite low (~ 1ug/l). No other radionuclides were present at concentrations >1pCi/l in any water sample taken at the site.

The analyses of the unfiltered samples showed the same trends as the filtered samples with the exception of significant concentrations of Fe, Si, and sometimes Al in the analyses. These components are indicative of the inclusion of solids in the analyses. The particulate material associate with well #10 is clearly aluminosilicate dominated from the high fractions of Al and Si as well as the enriched K concentration. The other samples are somewhat more difficult to distinguish owing to the relatively high detection limits for Al and Si. However, there does appear to be some enrichment in Fe, most likely as the result of precipitation of iron oxide/hydroxides in the sample upon exposure to air. Such a conclusion is partially supported by the on-site dissolved oxygen (DO) readings (Table 4-5), which show depressed values especially for well sample #9. Eh measurements of these samples taken at

11

PNNL all showed relatively high and oxidizing readings (~500mv vs SHE), indicating that the samples were initially oxidized or became oxidized during shipping and storage.

The well water analyses shown in Table 4-5 for Site C were also used as input for geochemical modeling calculations using the MINTEQA2 equilibrium model (Allison et al. 1991). These results showed that the soluble chemical species for U were dominated by aqueous carbonate complexes, principally by the dicarbonate species $UO_2(CO_3)_2^{2-}$ at the pH of the samples (6-7), Figure 4-1 Such anionic species can be highly mobile in groundwater systems, although the total species concentration was quite low as the data in Table 4-5 indicate. The chemical modeling calculations also indicated that the well waters are near saturation with the mineral calcite ($CaCO_3$). If the laboratory pH values are used in these calculations calcite appears to be slightly supersaturated. However, if the lower field pH values are used in the calculations calcite appears to be in equilibrium or slightly undersaturated. No other mineral equilibrium was indicated in the modeling calculations.

Table 4-1. Chemical composition of slags at Site A.

Element (ppm)	Site A Slag 1	Site A Slag 2	Site A Slag 3	Site A Slag 4
Al	200000±17000	192000±17000	234000±19000	229000±1800
Si	88800±7400	928000±7900	86100±7500	90400±7600
K	1110±160	1450±180	1050±170	1130±160
Ca	75700±5300	85100±6000	85100±6000	82200±5800
Mn	840±160	950±180	690±170	660±160
Fe	27300±1900	31200±2200	26000±1900	26700±1900
Ni	<57±57	<64±64	<64±64	<57±57
Cu	218±34	250±39	223±36	436±47
Zn	66±20	84±23	<38±38	103±20
Ga	<32±32	<34±34	<35±35	<32±32
Hg	<23±23	<24±24	<21±21	<22±22
Se	<35±35	<33±33	<35±35	<332±33
Br	<18±18	<17±17	<17±17	<17±17
Rb	<19±19	<18±18	<18±18	<18±18
U	248±22	218±20	230±21	262±23
Sr	169±28	330±25	382±28	372±28
Y	68±11	67.3±10	64±10	76±11
Nb	27500±1900	23600±1700	26900±1900	26800±1900
Mo	2980±210	3530±250	2260±160	2460±170
Th	13290±940	12060±850	14190±1000	13760±970

Table 4-2. Chemical composition of samples collected at Site B.

Element (ppm)	Slag A (96T-C-9)	Ore (96T-C-19)	Soil B5 (96T-C-20)	Ore (96-T-C-21)
Al	45000±3900	315000±23000	543000±5000	95200±7400
Si	337000±24000	119400±8700	281000±20000	164000±1200
P	<1500±1500	<2900±2900	<2600±2600	
Cl	<110±110	<250±250	<190±190	<260±260
K	6500±460	3640±270	6200±450	1510±140
Ca	26500±1900	137500±9600	98900±6900	217000±15000
Ti	8270±580	19800±1400	25700±1800	66000±4600
Mn	2420±180	2270±190	5600±410	5070±380
Fe	59400±4200	26500±1900	91700±6400	13730±970
Ni	71±15	82±24	77±32	<53±53
Ta	1230±100	5070±360	7750±560	12130±860
Pb	461±34	28100±2000	1600±110	<28±28
As	280±22	1062±92	616±48	
U	75.8±6	243±18	213±16	371±27
Th	364±27	2240±160	1108±79	2380±170
Sr	125±9	144±11	165±12	162±12
Y	274±19	1312±92	849±60	2460±190
Zr	4070±290	15600±1100	11740±820	23600±1600
Nb	3860±270	7120±500	13290±930	8320±580
Mo	<7.0±7	<16±16	<28.7±7.3	<18±18
W	803±67	191±63	2330±190	1970±150
S	1290±200	2060±610	1110±33	
Cd	26±10	66.9±9	<17±8.2	<8.7±8.7
Sn	1059±76	1490±110	1970±140	205±12
Sb	<23±23	931±66	183±16	<11±11
Ba	402±41	197±28	243±31	<48±48
La	598±61	2690±200	1600±120	3220±170
Ce	1540±130	6340±450	3970±290	7370±380

Table 4-3. Chemical composition of slag samples 1 and 2 at Site C.

Element (ppm)	Site C Slag 1	Site C Slag 2
Al	376000±27000	420000±30000
Si	102600±8300	34700±4400
K	4700±340	5110±370
Ca	59200±4200	41700±2900
Mn	5110±420	420±130
Fe	23600±1700	17300±1200
Ni	11320±800	230±30
As	250±20	1130±80
U	260±20	280±20
Sr	1000±70	1550±110
Y	660±50	450±30
Nb	42900±3000	63400±4400
Mo	160±10	260±20
Zr	3490±240	3940±280
Th	2130±150	10170±710

Table 4-4. Minerals present at sites A, B, and C (Veblen et al. 2000).

Phase	Ideal formula	Site where present
Calzirtite*	$(Ca,U,Th)ZrTi_2O_7$	all
Zirconolite*	$(Ca,Th,Ce)Zr(Ti,Nb)_2O_7$	all
Perovskite*	$CaTiO_3$	all
Perovskite (Loparite)	$(Ca,Ce,Th)(Ti,Nb)O_3$	Site A and B
Zirconolite	$(Ca_{2.45}Th_{0.03}REE_{0.04})Zr_{0.34}Al_{0.30}Ti_{1.24}Nb_{0.15}Ta_{0.12}O_7$	Site B
Zirconolite	$(Ca_{1.18}Ce_{0.61}Th_{0.11}REE_{0.26})Zr_{0.02}Al_{1.17}Ti_{1.14}Nb_{0.08}O_7$	Site B
Pyrochlore (Betafite)	$(Ca,U,Ce)_2(Nb,Ti)_2O_6$	Site A and B
Pyrochlore	$(Ca,Th,Ce)_2(Nb,Ti)_2O_6$	all
Glass	Si,Al,Ca,Ti,U,Th	all
Hibonite	$(Ca,Ce)_9(Ti,Al)_{12}O_{19}$	Sites A and C
Barium Aluminate*	$Ba,Ce(Ti,Al)_{12}O_{19}$	Site A and Site B
Spinel*	AB_2O_4 A = Co, Fe, Mg, Mn, Ni B = Al, Cr, Fe, Mg, Mn, V	all
Periclase	MgO	Site B
Wustite	FeO	Site B
Monticellite	$CaMgSiO_4$	Site B
Gehlenite	$Ca_2Al(AlSi)O_7$	all
Melilite	$(Ca,Na)_2(Mg,Fe,Al,Si)_3O_7$	Site C
Clinopyroxene	$Ca(Zr,Ti,Al)(Al,Si,Ti)_2O_6$	Site C
Feldspar	$CaAl_2Si_2O_8$	all
Wollastonite	$CaSiO_3$	Site C
Ce-Silicate	Ce,Si	Site C
Ce-Aluminosilicate	Ce,Si,Al	Site C
Barium Aluminosilicate	$BaAl_2Si_2O_8$	Site A
Gypsum	$Ca(SO)_4$	Site A
Tridymite	SiO_2	all
Groundmass	Ca,Ba,Al; Ca,Ba,S,Cl,Al	Site A
* indicates SYNROC phases		

16

Table 4-5. Chemical analysis of filtered water and well samples at Site C. Field data supplied by SCIENTECH Inc. DO represents dissolved oxygen. Concentrations in mg/l, pH in units. Inorganic carbon (IC) in mg/l as C. Alkalinity is reported as mg/l as $CaCO_3$ with the value in parentheses converted to mg/l as C for comparison with the IC analysis.

	MW #1	MW #5	MW #6	MW #8	MW #9	MW #10	River
pH (lab)	7.48	7.52	7.52	7.55	7.86	7.48	7.32
pH (field)	-	-	-	6.38	6.97	6.80	-
DO (field)	-	-	-	4.2	0.60	6.8	-
Na	16	45	32	101	34	45	10
K	2.0	11	5.6	27	2.1	8	2.0
Ca	135	48	99	293	201	120	24
Mg	23	22	22	49	49	60	5
Cl	18	14	20	24	80	25	18
F	0.2	1.2	0.9	0.7	0.1	0.6	0.1
IC*	75	30	57	66	65	59	16
Alkalinity	205 (49)	132 (32)	248 (59)	240 (58)	-	182 (44)	65 (16)
SO_4	131	156	120	815	400	287	0.2
Th (ug/l)	< 0.25	<0.25	< 0.25	< 0.25	< 0.25	< 0.25	<0.25
U (ug/l)	1.0	0.35	1.6	0.63	0.76	1.2	<0.25

17

Table 4-6. Chemical analysis of unfiltered water and well samples at Site C. Concentrations in mg/l, pH in units. Values in parentheses are the corresponding values for filtered samples to assist in distinguishing the chemical composition of the solids in the samples.

	MW #1	MW #5	MW #6	MW #8	MW #9	MW #10
pH	7.42 (7.48)	7.50 (7.52)	7.49 (7.52)	7.55 (7.55)	- (7.86)	7.46 (7.48)
Al	<135	<126	<165	<147	<132	221
K	2.6 (2.0)	12 (11)	16 (5.6)	25 (27)	5.0 (2.1)	47 (8)
Ca	94 (135)	40 (48)	89 (99)	208 (293)	157 (201)	107 (120)
Mn	3.4	<0.048	0.9	0.28	0.38	2.1
Cl	24 (18)	19 (14)	27 (20)	36 (24)	87 (80)	30 (25)
Si	<49	<49	188	<59	<53	860
Fe	16.6	1.9	34	1.5	2.2	102
SO_4	134 (131)	156 (156)	127 (120)	657 (815)	344 (400)	268 (287)
Th (ug/l)	< 0.1	< 0.09	< 0.1	< 0.1	< 0.08	< 0.1
U (ug/l)	< 0.1	< 0.08	< 0.1	< 0.1	< 0.07	< 0.1
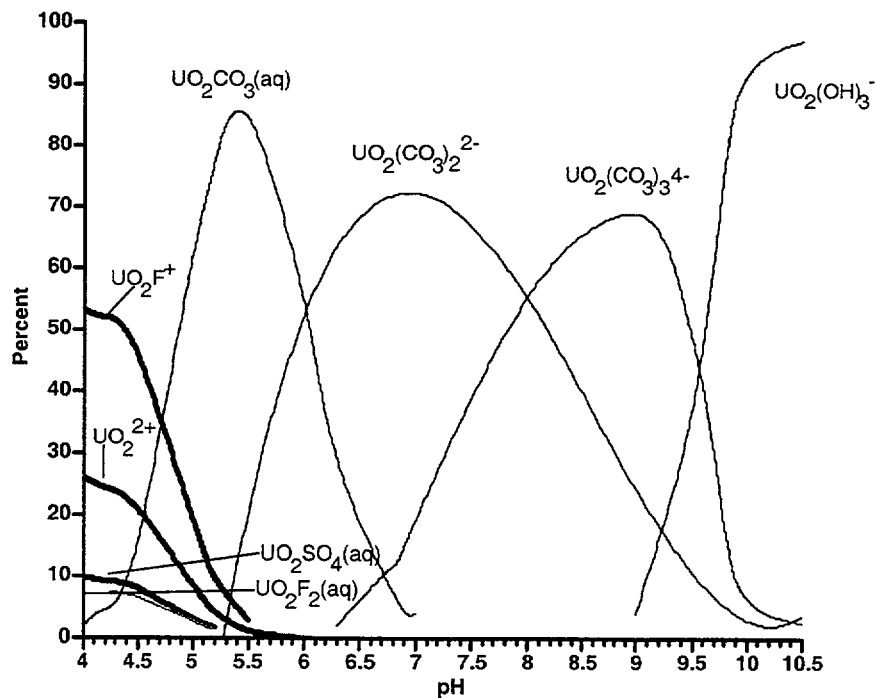
Figure 4-1. Calculated uranium species distribution for well #10 as a function of pH at site C. Anionic uranium complexes are the dominant species at the pH of the well sample, 6.8.

18

4.2 Radiological Analysis

Radiological analyses of site materials yields the isotopic composition of the radioactive elements. Such analyses are important not only for more detailed analyses of possible health effects but also the relative ratios of the various isotopes yields important information on isotopic separation processes that may have occurred at the site. This information is key to understanding the site history and waste disposal practices at the site.

The ferrocolumbian slag at Site A contains about 1.3% Th-232 (Table 4-1 and 4-7) and is in secular equilibrium with all of its daughter products (see Table 4-7). The U-238 appears to be in secular equilibrium with Ra-226 but not with the Ra-226 daughters, presumably as a result of the continuous escape of Rn-222 gas since disposal. These facts indicate the slags have a certain porous structure that allows escape of the Rn-222. This fact contrasts sharply with the results for Site B slags, described below, which do not show such a porous structure.

In the case of Site B samples (Table 4-8), all four samples have Th-232 and U-238 in secular equilibrium with all their daughter products. Apparently the processing conditions at Site B did not result in the separation of the U-238 daughters. In addition, unlike at Site A, the Ra-226 daughters are in secular equilibrium,

indicating only negligible escape of Rn-222 has occurred since disposal. This is apparently related to the refractory nature and low permeability of Site B slag samples.

In the case of Site C samples (Table 4-9) both samples show the slag samples to be in secular equilibrium with the U-238 daughters. It is likely that Th-232 is also in secular equilibrium with its daughters, although this is clearly apparent only for slag 2. The radiological analysis of slag 1 shows only about 65% of the Th-232 can be seen in the daughters. This is most likely a slight subsampling error since the same effect is seen in subsample 1 of slag 2 but not subsample 2 of slag 2.

The U and Th isotopic analyses (Table 4-10) support the above results based upon gamma spectroscopy. Th-232 and daughters are in secular equilibrium. In the case of U-238, the Th-230 daughter appears to be somewhat lower in activity than the parent U-238 but this lower activity is in proportion to the lower activities observed for the other Th isotopes, Th-232 and Th-228, relative to the gamma spectroscopy analyses. Apparently not all of the Th was dissolved in the KOH-KNO_3 fusion process before alpha spectroscopy and the presence of undissolved solids was noted for these samples. The undissolved solids apparently contained small quantities of insoluble Th. Examples of alpha spectroscopy analysis for sites A and B are shown in Figures 4-2 and 4-3, respectively.

Table 4-7. Radiological analysis of slags at Site A. All analyses represent the average of three subsamples of each slag. Values in pCi/g.

Nuclide	Site A Slag 1	Site A Slag 2	Site A Slag 3	Site A Slag 4
Th Series				
Th-232	(1460)	(1330)	(1560)	(1510)
Ac-228	1,270	1,100	1,360	1,250
Th-228	1,190	980	1,200	1,200
Ra-224	1,440	1,300	1,500	1,390
Pb-212	1,390	1,200	1,490	1,370
Bi-212	1,530	1,310	1,610	1,510
U-238 Series				
U-238	(80)	(70)	(75)	(85)
Ra-226	90	75	90	80
Pb-214	45	45	40	45
Bi-214	40	45	35	40
U-235 Series	**			

** Uranium values are close to detection limit and because of interferences are hard to quantify with the counting system. Values in parenthesis are calculated from the XRF data for thorium and uranium assuming all of the Th is Th-232 $(1.1 \times 10^{-7} Ci/g)$ and all of the U is U-238 $(3.3 \times 10^{-7} Ci/g)$.

Table 4-8. Radiological analysis of Site B samples. Slag A(96T-C-9),Grayish Green Ore(96T-C-19), Soil Site B5(96T-C-20), and Ore (96T-C-21). Results in pCi/g.

Nuclide	Site B Slag A	Site B Ore	Site B Soil B5	Site B 96T-C-21 Ore
Th Series				
Th-232	(40)	(246)	(120)	(262)
Ac-228	43	176	97	246
Pb-212	42	160	100	238
Bi-212	49	197	112	266
U-238 Series				
U-238	(25)	(80)	(70)	(123)
Th-234				140
Ra-226	33	121	78	180
Pb-214	29	111	70	210
Bi-214	27	101	63	192
U-235 Series	**			

** Uranium values are close to detection limit and because of interferences are hard to quantify with the counting system. Values in parenthesis are calculated from the XRF data for thorium and uranium assuming all of the Th is Th-232 (1.1×10^{-7}Ci/g) and all of the U is U-238 (3.3×10^{-7}Ci/g).

Table 4-9. Radiological analysis of Site C samples. Results in pCi/g.

Nuclide	Site C Slag 1	Site C Slag 2
Th Series		
Th-232	(230)	(1120)
Th-228	159	941
Ac-228	136	921
Pb-212	151	944
Bi-212	161	1060
Tl-208	142	951
U-238 Series		
U-238	84	142
Pb-214	75	105
Bi-214	74	112
U-235 Series		
U-235	5	6

Values in parenthesis are calculated from the XRF data for thorium assuming all of the Th is Th-232 $(1.1 \times 10^{-7} \text{Ci/g})$.

Table 4-10. Uranium and thorium isotopic analyses of selected samples. Results in pCi/g.

Nuclide	Site A Slag 1	Site B Sample C-19
Th Series		
Th-232	946	64
Th-228	955	63
U-238 Series		
U-238	81	72
U-234	81	72
Th-230	59	38
U-235	3.8	3.4
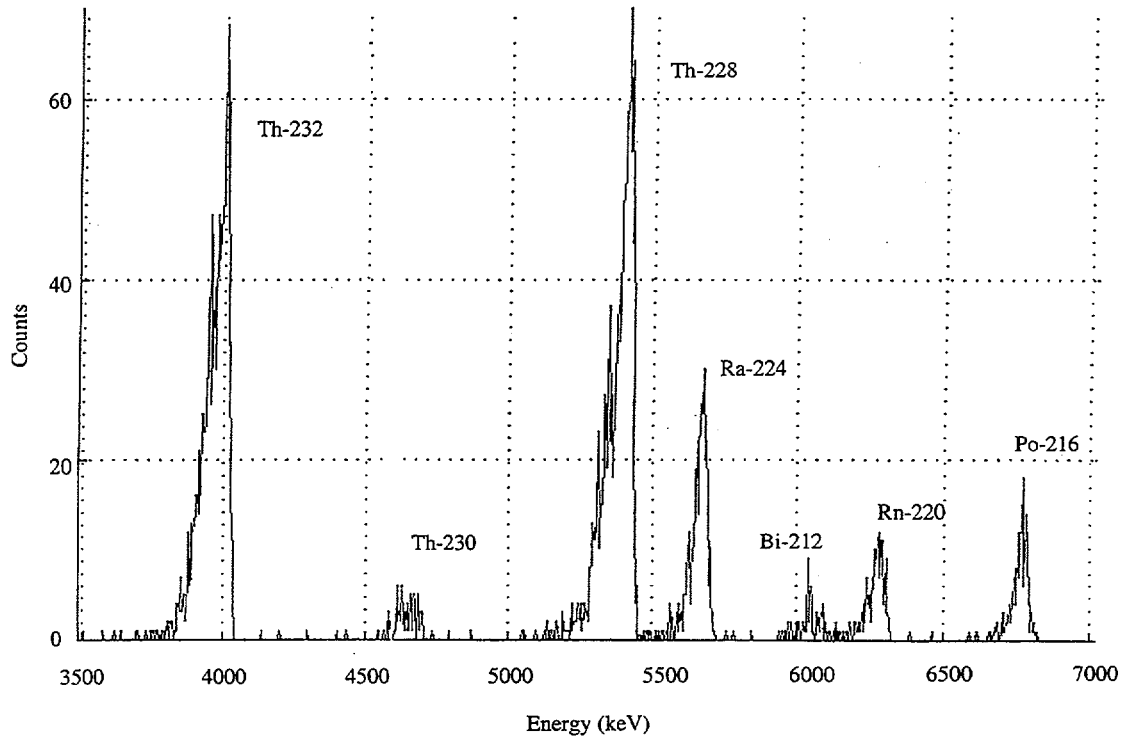
Figure 4-2. Example Alpha Spectra of Site A samples.
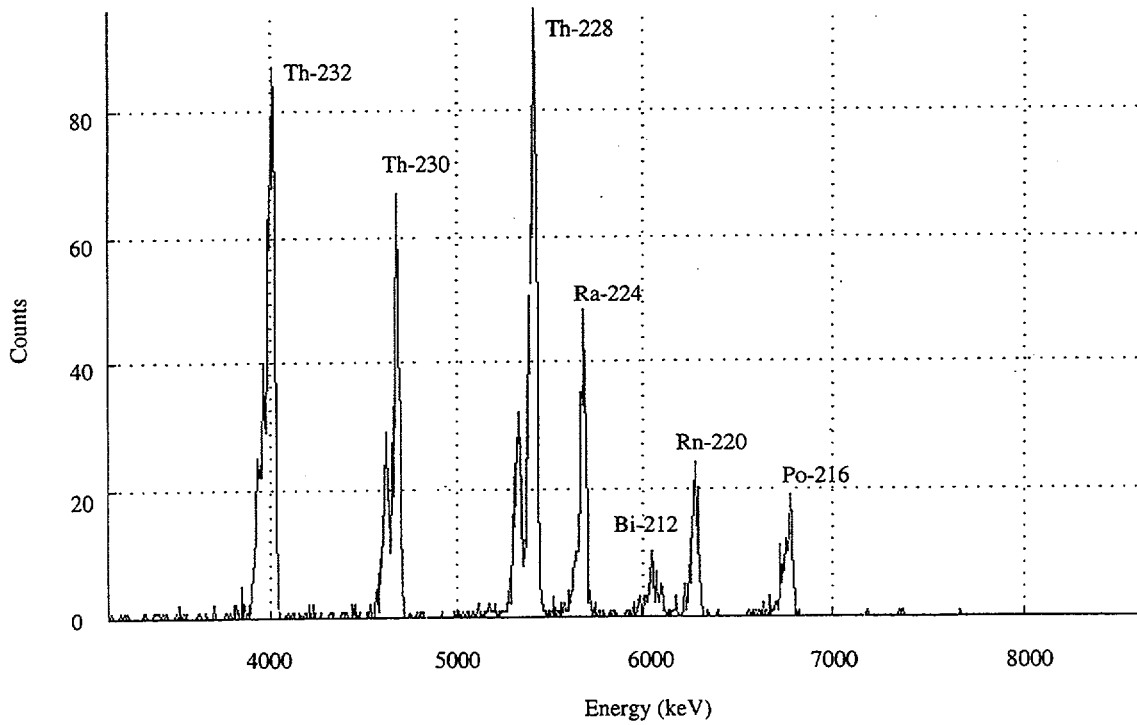
Figure 4-3. Example Alpha Spectra of Site B samples.

23

4.3 Solubility and Leaching Studies

4.3.1 Site A

4.3.1.1 THORIUM

The solubility data for Th at Site A show very low solubilities except at low pH values (<5) where the solubilities increase rapidly (Figure 4-4). A comparison of these solubility data with the calculated solubilities for possible Th solid phases, solid and dashed lines in Figure 4-4, show that the aqueous Th concentrations are most likely controlled by thorianite ($ThO_2(c)$) or possibly, at very low pH a Th-silicate (i.e.$ThSiO_4(gl)$). Mineralogical analysis of these samples (Table 4-5), show the presence of some thorianite. The presence of this phase leads credence to the possibility that this phase is the primary solubility control. If a $ThSiO_4(gl)$ phase does form it is most likely a secondary phase precipitated as a result of the dissolution of large concentrations (> 200mg/l) of Si at low pH. The difference in observed solubility between the thorianite solubility at the somewhat higher observed solubilities between pH 4 and 5 also indicates the presence of a small amount of amorphous $ThO_2(am)$. In any event, the Th concentrations in Site A samples appear to be solubility limited, either by $ThSiO_4(gl)$ at very low pH, $ThO_2(c)$, or by trace amounts of $ThO_2(am)$, and show very low solubilities over a broad range of pH values.

The batch leaching data for Site A samples show that the slag materials tend to buffer the solution pH values in the alkaline region (> 10, see Table 4-11). Although we cannot be sure, these high pH values are most likely related to the dissolution of alkaline earth compounds containing either Ca or Ba that are present in these samples. As seen from the solubility data, these high pH values are expected to maintain the dissolved Th concentrations at very low levels. The observed Th concentrations in the batch leaching studies, Figure 4-5, follow this expected trend. Th concentrations are uniformly low in both the coarse and fine material with maximum concentrations about $10^{-7.5}$M (3.2×10^{-8}M). As expected, if a solubility controlling solid was present, there should be no clear differences between coarse and fine material (i.e. no surface area or particle size effect). The pH values for the "long term" samples exposed to CO_2, Table 4-12, show very similar values to those in the absence of CO_2 indicating that the light capping of these samples prevented influx of sufficient CO_2 to equilibrate the solutions, with the possible exception of the longest term (45 day) samples. However, the "short term" studies with vigorous bubbling show much lower pH values more typical of equilibration with atmospheric CO_2. However, even with this introduced CO_2 the dissolved Th concentrations remained at or near the detection limit of $10^{-8.5}$M. This fact appears to result from the relatively low final inorganic carbon content (<0.002M) which was constrained either by the dilute nature of the solutions or the apparent precipitation of carbonate minerals owing to the high concentrations of alkaline earth cations in some samples.

The pH values in the column experiments, Table 4-13, show a trend of much lower values than in the batch experiments. This results from the leakage of small amounts of atmospheric CO_2 into the sampling bottle during the duration of the column study. However these pH values also fall in the low solubility region, see Figure 4-4. The observed Th concentrations in the column

24

experiments, Figure 4-6, follow this expected trend with all of the Th concentrations all at or below the analytical detection limit of approximately $10^{-8.5}$M.
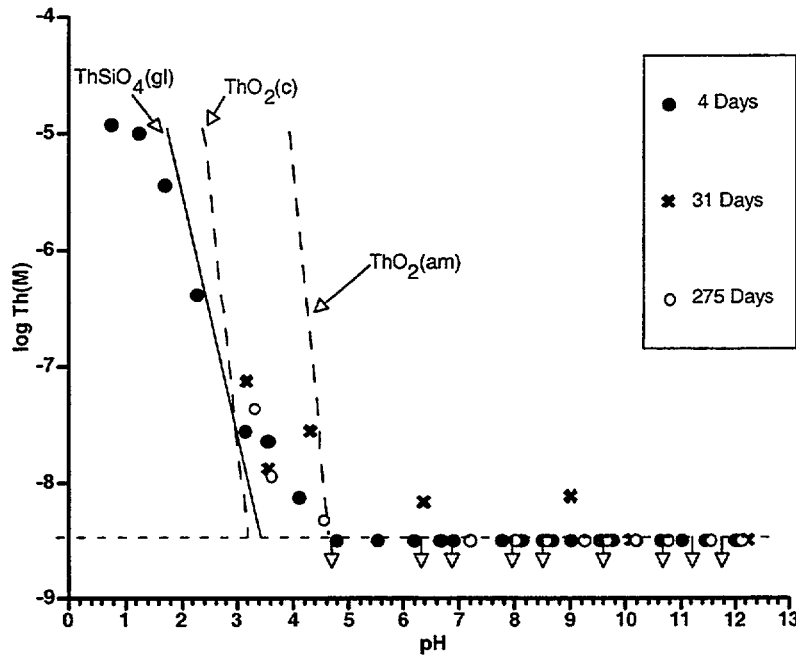
Figure 4-4. Th concentrations in Site A Solubility Studies.
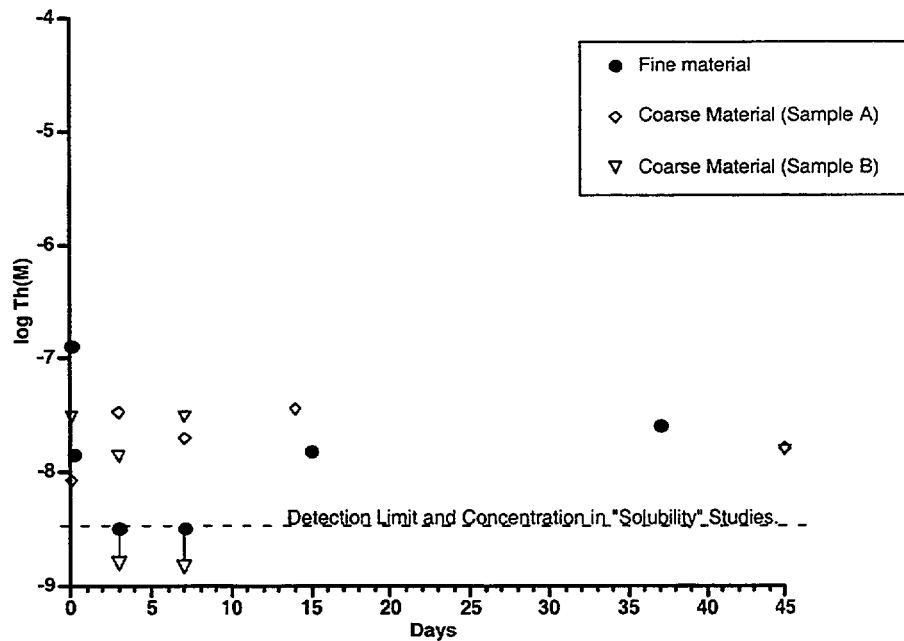
Figure 4-5. Th concentrations in Site A Batch Leaching Studies.
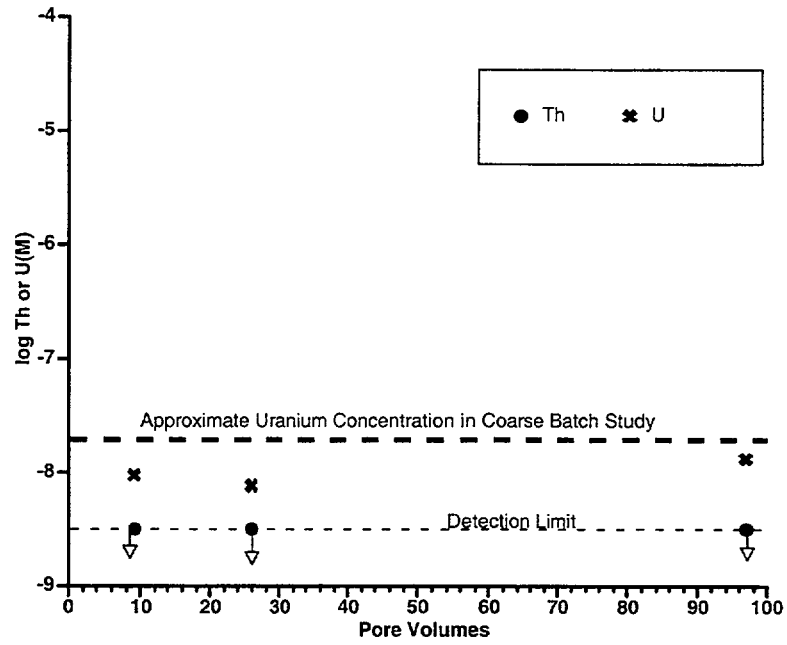
Figure 4-6. Th and U concentrations in Site A Column Studies.

Table 4-11. Measured pH values in batch leaching studies as a function of time.

Leaching Time	Site A Fine Material	Site A Coarse Material
2 hrs.	9.39	7.62
6 hrs. CO_2	9.75	
3 days	10.15	10.33
7 days	10.45	10.33
15 days	10.31	9.84
37 days	10.23	
45 days		10.66

26

Table 4-12. pH values measured in batch studies exposed to atmospheric CO_2.

		"Long Term"				"Short Term"	
	2 hrs.	3 days	7 days	14 days	45 days	0.75 days	3 days
Site A	9.29	10.26	10.4	10.37	10.55	8.07	7.97
Site B(C-9)	8.41	9.44	9.48	9.38	9.34	7.76	8.03
Site B(C-19)	7.62	8.71	8.84	8.61	9.25	7.73	7.89
Site B(C-20)	7.39	8.56	8.36	8.10	7.74	7.73	7.83

Table 4-13. Measured pH values in column studies as a function of time.

Leaching Time	Site A	Site B
4 days	7.96	
5 days		8.23
8 days		8.21
11 days	7.64	
30 days	8.22	8.43
72 days	8.38	
78 days		8.29

In summary, the aqueous Th concentrations in Site A samples are solubility controlled, either by $ThO_2(c)$, $ThO_2(am)$, or at very low pH, $ThSiO_4$. The presence of a solubility limiting phase results in the leachable Th concentrations being independent of total sample particle size or surface area. The apparent rapid dissolution of the solubility limiting phase(s) results in consistent results between the solubility, batch, and column studies. The solubility controlling solid phases for Th are all very insoluble at pH values > 5.

4.3.1.2   URANIUM

Uranium, even if present as insoluble U(IV) solid phases, is easily oxidized in solution to U(VI). The majority of U(VI) containing solid phases (Krupka and Serne 1998) are highly soluble (>10^{-4}M). One of the major exceptions to this rule of insoluble U(VI) phases is in solutions of high pH, low carbonate, and high concentrations of alkaline earth cations. These solutions result in the precipitation of insoluble alkaline earth uranates {i.e. strontium uranate ($SrUO_4(c)$), or becquerelite ($CaU_6O_{19} \cdot 11H_2O$)}. These are precisely the conditions found for Site A samples, Table 4-11 and Figure 4-7. As a result, such phases, particularly the calcium uranates could limit U (VI) solubilities at Site A. Unfortunately, experimental data on the solubility of these phases is very limited. As a result, in another task of this project, the solubility of becquerelite was measured over a broad range of pH values and dissolved Ca

27

concentrations (see Appendix C). A summary of the results is presented in Figure 4-8. Interestingly, these data show that solid phases such as bequerelite can maintain quite low (10^{-7}M) dissolved U (VI) concentrations at the high pH and dissolved Ca concentrations that could occur at Site A. The actual solubility data for U in samples from Site A, Figure 4-9, show quite low solubilities across the entire pH range. Although these concentrations are obviously not limited by becquerelite at low pH values, the solubilities at higher pH (>8) could be limited by the solubility of such phases.

The batch leaching data for U in the absence of CO_2 also show low dissolved concentrations (Figure 4-10) with some difference between fine and coarse material. The "solubility" data at the same pH appearing to be intermediate between the fine and coarse batch results. The differences do not appear to be due to differences in Ca concentrations, which are

very consistent between the coarse batch, fine batch, and solubility studies (i.e. 100 - 120mg/l as Ca). The results for the batch studies in the presence of CO_2 all show U concentrations at or near the detection limit (~$10^{-8.5}$ M), indicating no significant solubilization effect on U of introduced CO_2. The results for the column studies, Figure 4-6, also show quite low solubilities and are in excellent agreement with the coarse batch studies.

In summary, although the solubility controlling mechanism for U in Site A samples is not precisely known, the fact that the U concentrations are relatively low is not entirely unexpected for these high pH, low carbonate, high alkaline earth solutions. The solubilities can be limited by becquerelite at high pH values. The dissolved concentrations of U are consistent between the coarse batch and the column studies, which allows useful calculations to be made on solubility and leaching rates (see below).
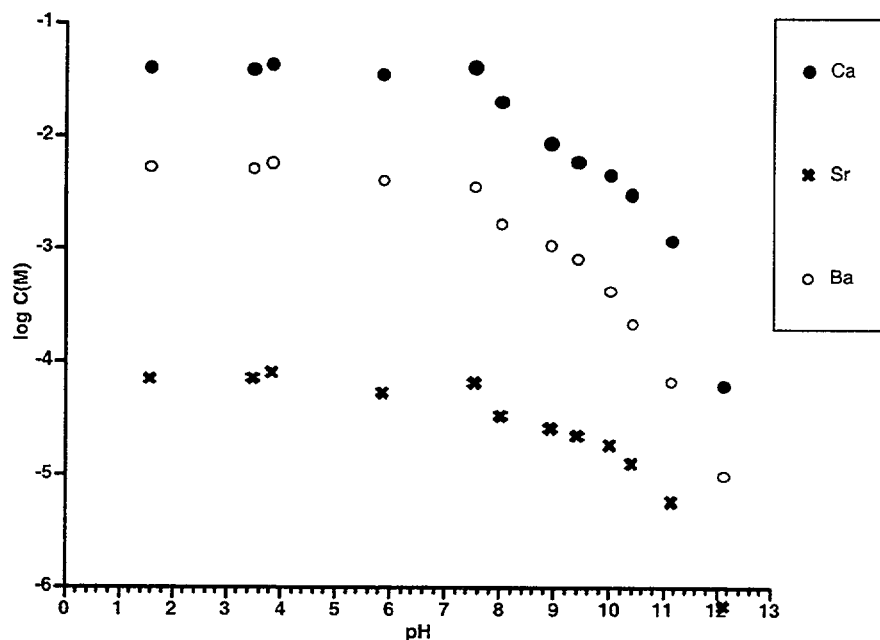
Figure 4-7. Alkaline Earth Cation Solubilities in Site A Samples.
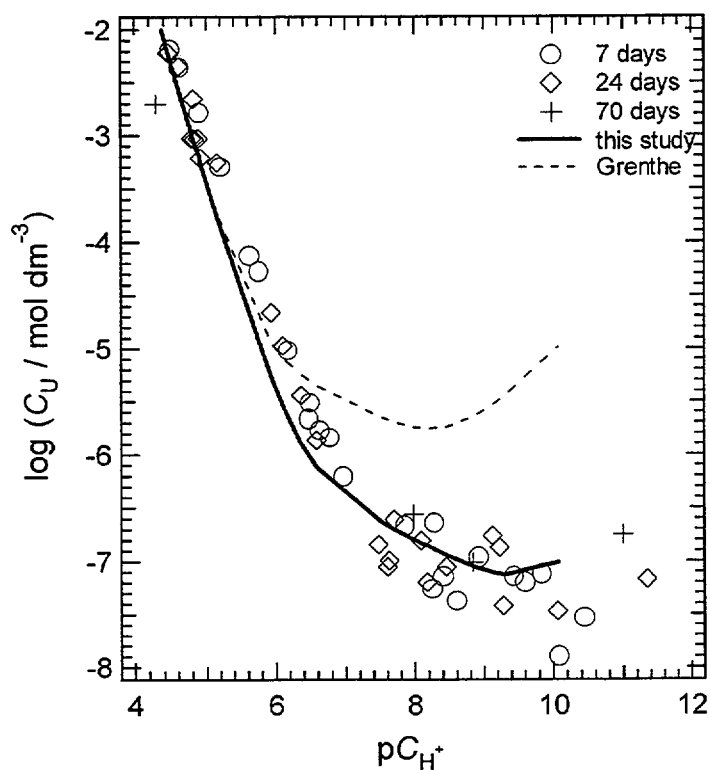
Figure 4-8. Aqueous uranium concentrations contacting becquerelite suspensions in 0.1M $CaCl_2$ and over a range of hydrogen ion concentrations (pC_{H+} values). The designation (mol/dm^{-3}) is equivalent to moles/l. See Appendix C for a detailed explanation.
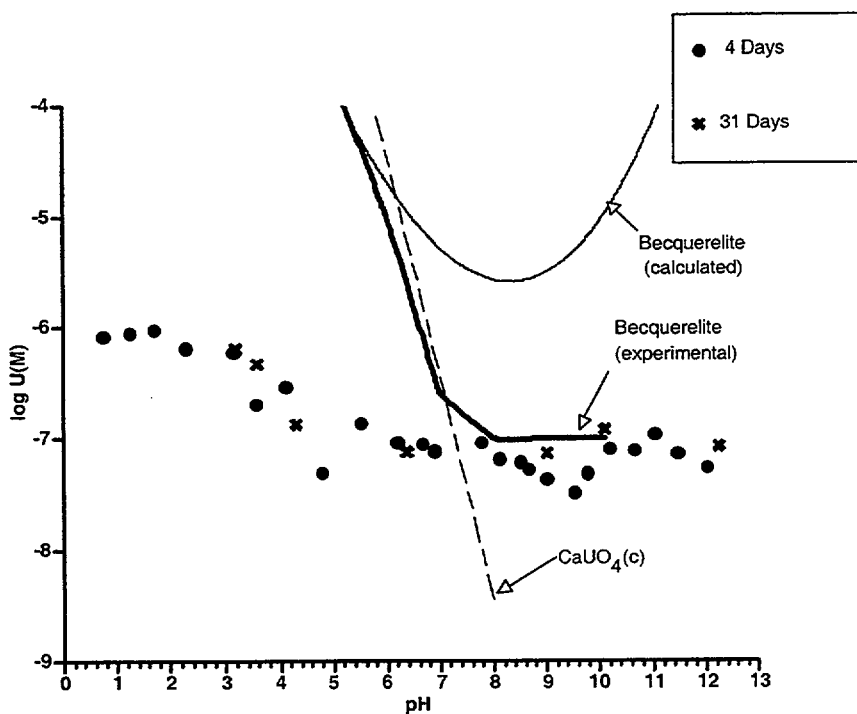
Figure 4-9. U concentrations in Site A Solubility Studies. The calculated becquerilite values use thermodynamic data taken from Grenthe et al. (1992), see Appendix C.

29
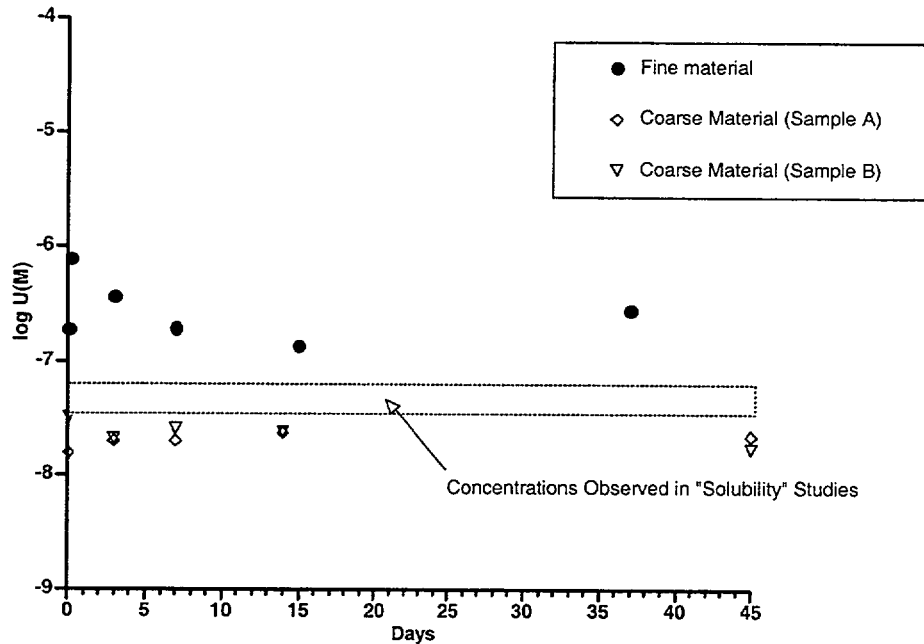
Figure 4-10. U concentrations in Site A Batch Leaching Studies. The area designated for the solubility study values represents the range of observed concentrations.

4.3.1.3 OTHER RADIONUCLIDES

Only very low concentrations of other radionuclides were detected in the solubility studies, batch studies or column studies. All Th-232 or U-238 daughters were either completely undetectable or found to be very low, typically <2pCi/ml. The only exceptions were the 14 pCi/ml of Bi-212 and 11pCi/ml of Pb-212 were found in the most acid solubility point analyzed (pH = 3.5) and Ra-226, which showed soluble concentrations in the solubility studies as high as 16pCi/ml. There was also evidence for some Pb-210, but the uncertainties of these analyses were so high as to prevent quantitiation, and Cs-137 from fallout at concentrations <2pCi/ml.

4.3.2   Site B

4.3.2.1 THORIUM

The solubility data for Th in three samples from Site B, Figure 4-11, show a very consistent trend of very low solubilities, except at the very lowest pH values. Sample C-19, the greyish green slag showed the highest solubilities consistent with the total analyzed Th concentrations in these samples. Interestingly, the observed Th solubilities for Site C samples are in general even lower than for Site A slag, with only the solubility in the C-19 sample apparently limited by thorianite, $ThO_2(c)$.

30
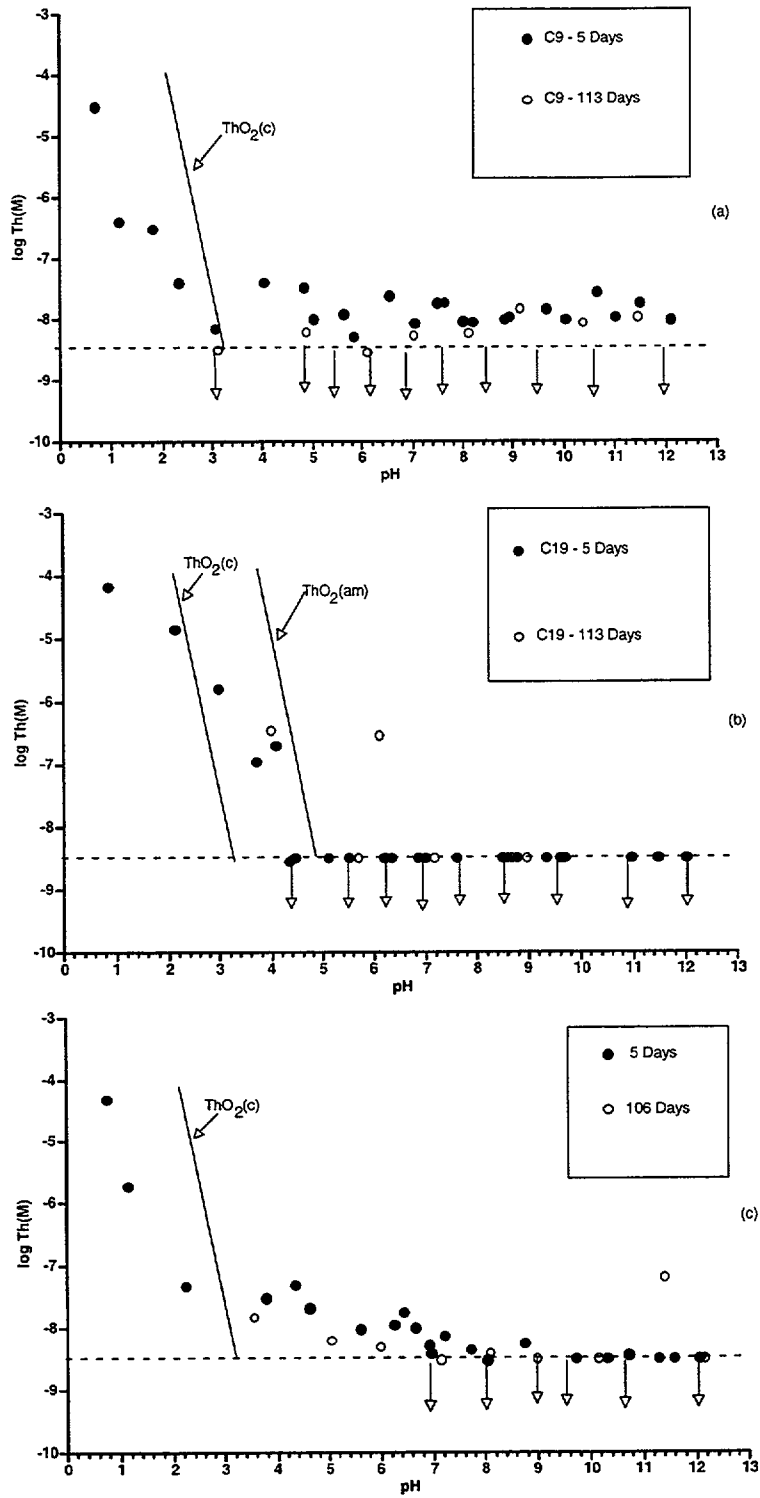
Figure 4-11. Th concentrations in Site B Solubility Studies.

In the case of the batch leaching experiments, the solution pH values were generally basic but highly variable, Table 4-14. This variability is apparently related to the changing nature of the solutions as a result of a very slow dissolution rate. The slow dissolution rate is apparent from the dissolved Ca concentrations, the dominant cation, which increase only very slowly with time. The fact that the solutions are so poorly buffered may also impact the pH meter readings. In any event, the pH values are in general between 8 and 10. The corresponding Th concentrations in the batch leaching samples in the absence of CO_2, Figure 4-12, show quite low

solubilities and bracket the range of Th concentrations expected from the solubility studies. The Th concentrations in the batch leaching studies exposed to CO_2 were also very low and close to the analytical detection limit of $10^{-8.5}M$.

The column studies, Figure 4-13, also show very low dissolved concentrations with the majority of the samples at the analytical detection limit of $10^{-8.5}M$. As was true in the previous column studies of Site A samples, the measured pH values varied only over a very narrow range (i.e. 7.9 to 8.8).

Table 4-14. Measured pH values and Ca concentrations in batch leaching studies as a function of time for Site B samples.

Leaching Time	C-9		C-19		C-20	
	pH	Ca(mg/l)	pH	Ca(mg/l)	pH	Ca(mg/l)
2 hrs.	7.86	1.5	7.83	1.5	7.57	2.9
3 days	9.97	4.7	10.5	5.1	9.90	6.3
7 days	9.12	6.9	9.30	8.7	8.93	8.6
14 days	8.37	14.4	8.70	11.8	8.03	9.9
45 days	9.12	14.6	9.70	24.3	8.54	13.1

4.3.2.2 URANIUM

Uranium solubilities in Site B samples, Figure 4-14, show very low solubilities in a similar fashion to the slag samples at Site A. At very high pH values, the solubilities could become limited by becquerelite, although the Ca concentration in these samples is about an order of magnitude lower than in Site A samples (see Figure 4-15). The observed U concentrations in the batch leaching studies in both the presence

and absence of CO_2, Figure 4-16, also show very low dissolved U concentrations, which are in good agreement with the U solubility studies. Similarly, the U concentrations in the column studies, Figure 4-13, correspond to the batch leaching studies. No particle size or surface area effect is seen. In summary, the concentration controlling mechanism for U in Site B samples is not precisely known. Becquerelite could limit the solubility at high pH values, but this is less likely than in Site A samples owing to the lower dissolved Ca concentrations. It is

possible that the U concentrations are simply controlled by slow dissolution of the solid phase material, but this also appears unlikely since the dissolved concentrations in the solubility studies, which used ground, very small particle size material yielded similar results to the batch and column studies with different particle sizes and higher solid/solution ratios (column studies). It appears more likely that the U is tightly bound in either a very insoluble or refractory phase.
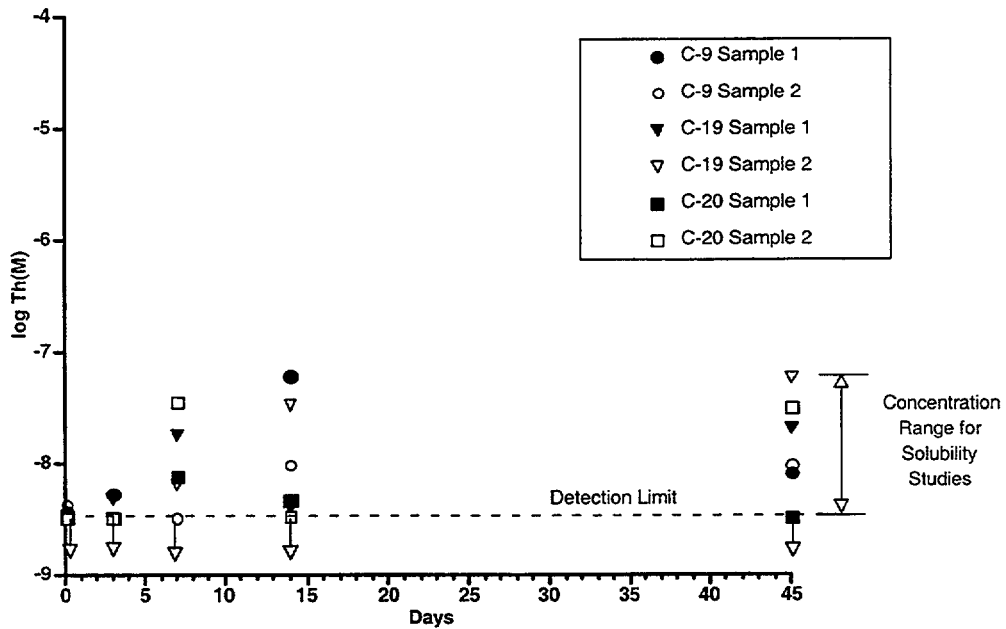
Figure 4-12. Th concentrations in Site B Batch Leaching Studies.
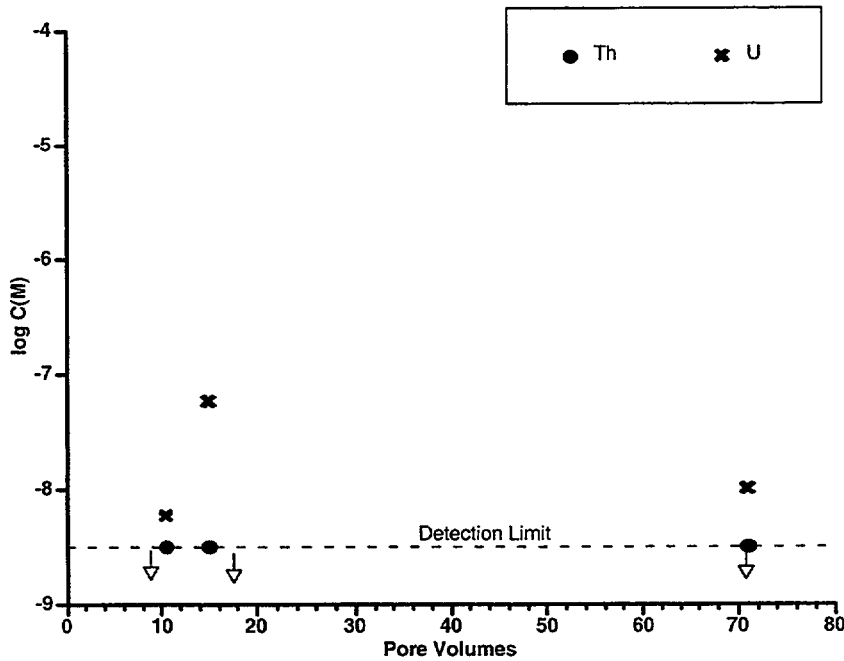
Figure 4-13. Th and U concentrations in Site B Column Studies.
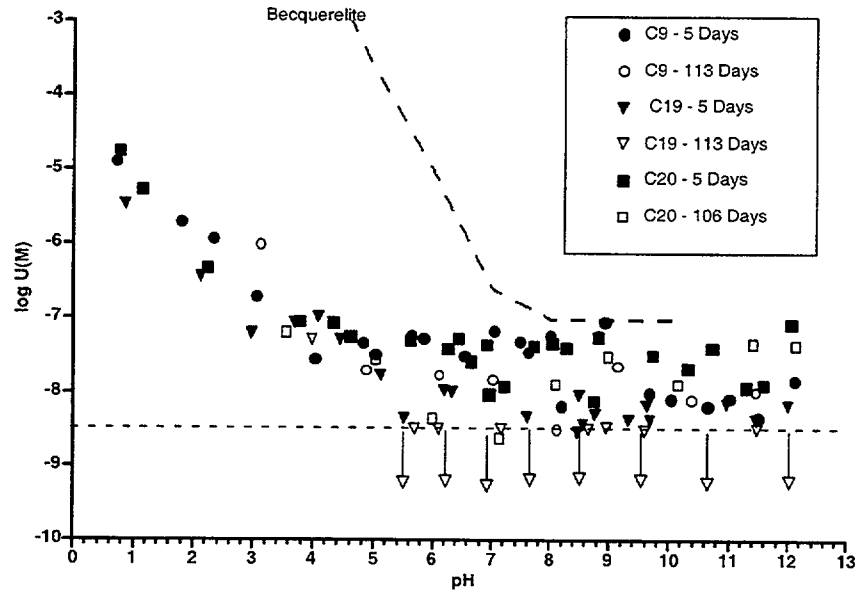
Figure 4-14. U concentrations in Site B Solubility Studies.
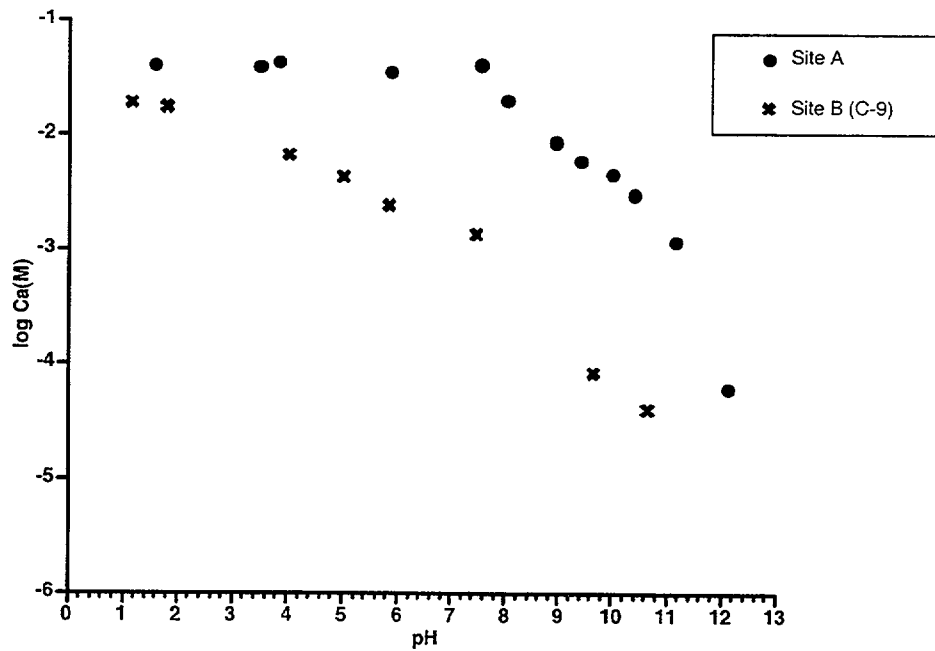
Figure 4-15. Calcium concentrations in Site A and Site B Solubility Studies.
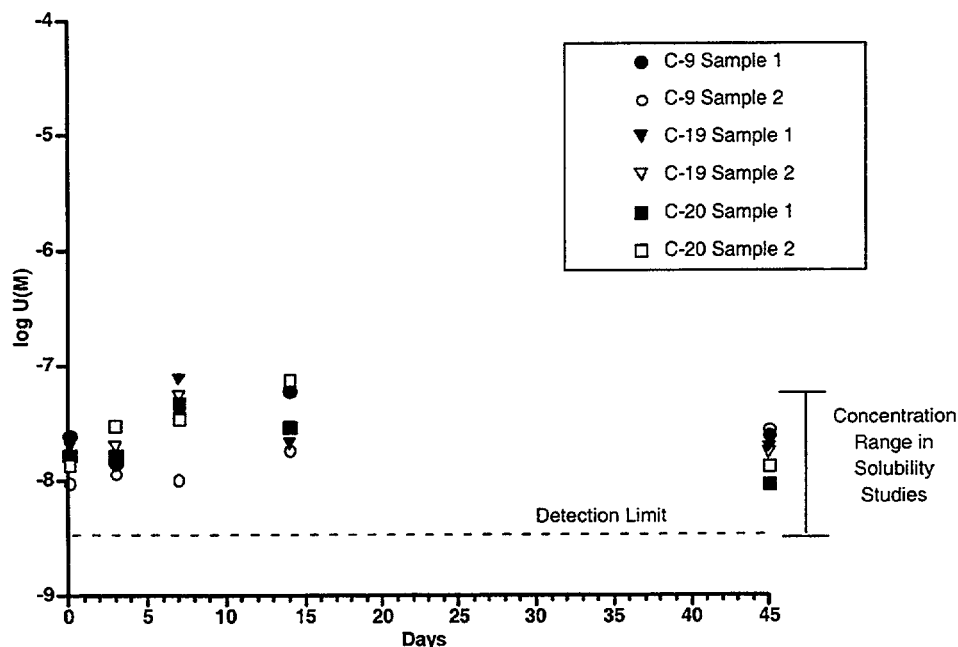
Figure 4-16. U concentrations in Site B Batch Leaching Studies.

4.3.2.3 OTHER RADIONUCLIDES

The very refractory nature of Site B samples was also reflected in the leaching of U-238 or Th-232 daughters. As was true with Site A samples, no Th-232 or U-238 daughters were detected at significant concentration in the solubility, leaching, or column studies. Bi-212 and Pb-212 were detected in a few samples, but the concentrations were so low and the uncertainty of the analysis so high that any quantification of concentration was impossible.

4.3.3 Site C

In the case of Site C only a limited number of solubility and column studies were performed to check of the results for these slag materials were consistent with the results from Sites A and B.

4.3.3.1 THORIUM

The solubility data for Th in two samples from Site C, Figure 4-17, show the same consistent trend of very low solubilities, except at the very lowest pH values, observed for samples from sites A and B. Once again this is an indication of a solubility controlling phenomena for Th in the slag samples. Upper limits on dissolved concentrations most likely being set by amorphous or crystalline thorium oxide solubility.
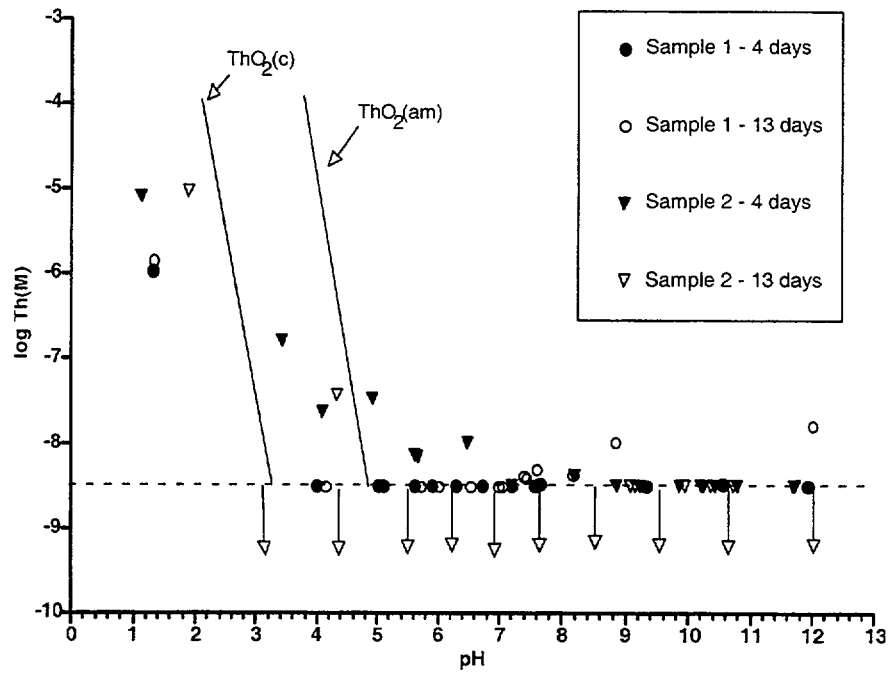
Figure 4-17. Thorium concentrations in Site C Solubility Studies.

These low solubilities are also reflected in the low dissolved concentrations seen for Site C column studies (Figure 4-18) which never exceeded the analytical detection limit of $10^{-8.5}$ M. Interestingly the pH values in the column studies showed significant variations between the two samples of slag material (Table 4-15). The higher pH values for slag sample two are consistent with the batch results for site A samples. The shorter analysis times for these samples, only approximately ten pore volumes, apparently

prevented any significant introduction of atmospheric CO_2 into the samples as happened with Site A samples in the column study. The pH values are all higher than the influent river water, Table 4-5, used in the column studies. There was no correlation between the pH values and the dissolved Ca concentrations observed in the column effluents which ranged from 27 to 74 mg/l. The Ca concentrations were all as high or higher than the influent river water (Table 4-5).

36
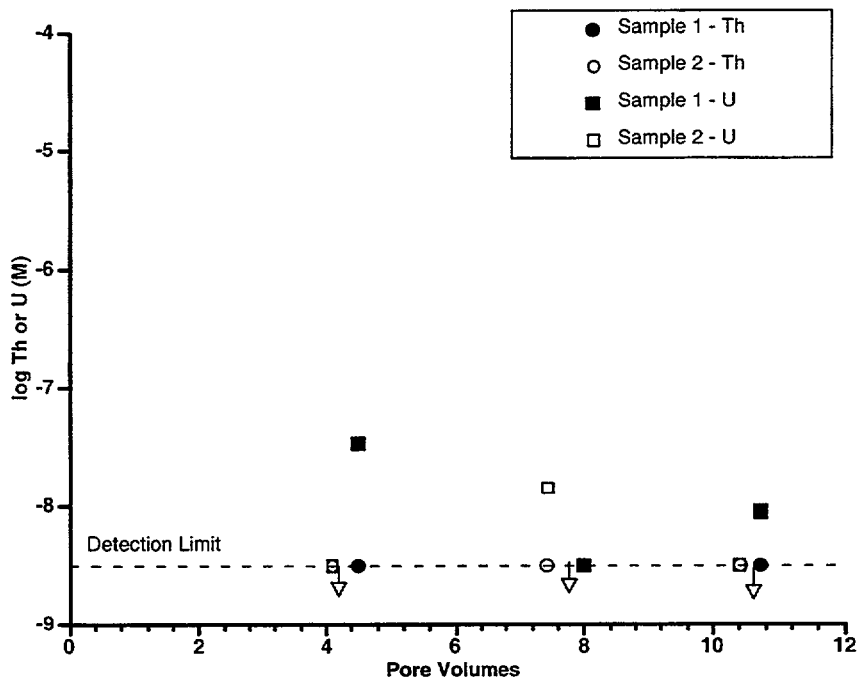
Figure 4-18. Thorium and uranium concentrations in Site C Column Studies.

Table 4-15. pH values in column studies from slags at Site C.

Pore Volumes	Sample 1	Sample 2
4.09		10.67
4.48	8.27	
7.42		9.88
7.98	8.30	
10.4		10.85
10.7	8.15	

4.3.3.2 URANIUM

Uranium solubilities in Site C samples, Figure 4-19, show very low solubilities in a similar fashion to the slag samples at Site B. In fact, the observed solubilities are even slightly lower than the values for either site A or site B (Figures 4-9 and 4-14 respectively). Similarly, the U concentrations in the column studies, Figure

4-18, correspond to the solubility studies. The uranium is most likely bound to the same type of refractory material as in Sites A or B (Table 4-4 and discussion).

In summary, the solubility and column data for Site C show that the results for these slags show the same low solubilities for both Th and U observed for both Sites A and B.

37
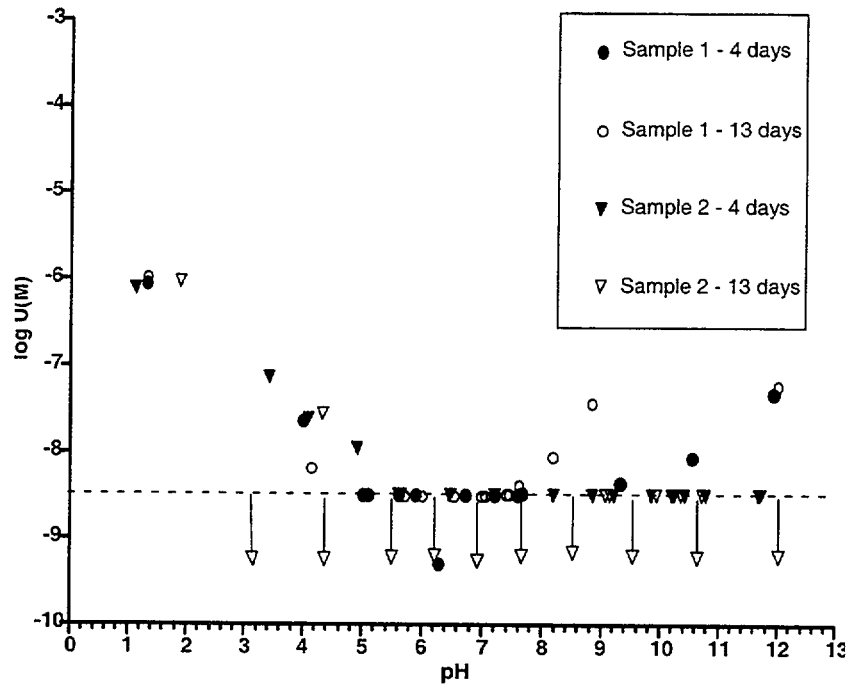
Figure 4-19. Uranium concentrations in Site C Solubility Studies.

5 CALCULATIONS OF SOLUBILITY LIMITS AND LEACHING RATES

This section presents calculations of the equilibration mass transfer (leaching) rates of Th and U from slags from Sites A, B, and C. These *leaching* rates were calculated using the highest observed dissolved concentration at the shortest equilibration time. This yielded the highest mass transfer rate for equilibration that can be calculated form the data. It is certainly possible that a higher transfer rate could have been calculated if samples were taken at earlier times (earliest times were 2hrs for batch data). Never the less, all of the samples reached equilibrium or at least steady state concentrations extremely rapidly since so little mass needed to be transfered to reach the steady state concentration. These calculations numerically demonstrate this fact.

5.1 Site A

Solubility controlled for both Th and U. Th - data from the coarse batch study were used (Figure 4-4), pH range (7-11). The highest solubility observed was $10^{-7.5}$M Th after 2hrs contact time. The solution volume was 30ml. This yields the following:

- solubility	$= 3.2 \times 10^{-8}$M
- leaching rate	$= 1.1 \times 10^{-7}$gTh/hr [1]

U - data from the coarse batch study were used (Figure 4-9), pH range (7-11). The highest solubility observed was $10^{-7.6}$M U

after 2hrs contact time. The solution volume was 30ml. This yields the following:

- solubility	$= 2.5 \times 10^{-8}$M
- leaching rate	$= 8.9 \times 10^{-8}$gU/hr [2]

5.2 Site B

Solubility controlled for both Th and U. Th - data from the batch study were used (Figure 4-11), pH range (7-9). The highest solubility observed was $10^{-7.4}$M Th after 14 days contact time. The solution volume was 30ml. This yields the following:

- solubility	$= 4 \times 10^{-8}$M
- leaching rate	$= 8.3 \times 10^{-10}$gTh/hr.

U - data from the batch study were used (Figure 4-15), pH range (7-9). The highest solubility observed was $10^{-7.2}$M U after 7 days contact time. The solution volume was 30ml. This yields the following:

- solubility	$= 6.3 \times 10^{-8}$M
- leaching rate	$= 2.7 \times 10^{-9}$gU/hr.

5.3 Site C

Solubility controlled for Th. Th - data from the solubility study were used (Figure 4-16). The highest solubility observed was $10^{-8.5}$M Th over the pH range (8-11). The shortest contact time was 4 days. The solution

---

[1]The leaching rates are calculated as follows:
(3.2×10^{-8}moles Th/l)(.03l)(232gTh/mole)/2hrs.= 1.1×10^{-7}gTh/hr.

[2]The leaching rates are calculated as follows:
(2.5×10^{-8}moles U/l)(.03l)(238gU/mole)/2hrs.= 8.9×10^{-8}gU/hr.

volume was 30ml. This yields the following:

- solubility   = 3.2×10^{-9}M
- leaching rate   = 2.3×10^{-10}gTh/hr.

U - data from the solubility study were used (Figure 4-18), pH range (8-11). The highest solubility observed was $10^{-8.05}$ M U over the pH range (8-11). The shortest contact time

was 4 days. The solution volume was 30ml. This yields the following:

- solubility   = 8.9×10^{-9}M
- leaching rate   = 6.6×10^{-10}gU/hr.

These results, converted to the units of g/cc for solubility limits and pCi/yr for release rate, are summarized in Table 5-1.

Table 5-1. Summary of Solubility and Leaching Rate Calculations at each Site.

	Th		U	
Site	Solubility Limit (g/cc)	Leaching Rate (pCi/yr)	Solubility Limit (g/cc)	Leaching Rate (pCi/yr)
Site A	7.4×10^{-9}	100	6.0×10^{-9}	260
Site B	9.3×10^{-8}	1	1.5×10^{-8}	8
Site C	7.4×10^{-10}	0.2	2.0×10^{-9}	2

6. COLLOID STUDIES

A comparison of filtered and unfiltered Th and U concentrations in the column studies at sites A and B (Table 6-1) did not show any evidence for the formation or transport of radiocolloids in any of the samples studied.

Table 6-1. Filtered and unfiltered Th and U concentrations in column studies. UF - unfiltered, F - filtered. Pore size of filters approximately 0.0018um.

Analysis	Site A	Site B (C-19)	Site B (C-21)
Th - UF	$< 10^{-8.5}$	$< 10^{-8.5}$	$< 10^{-8.5}$
Th - F	$< 10^{-8.5}$	$< 10^{-8.5}$	$< 10^{-8.5}$
U - UF	$< 10^{-8.5}$	$< 10^{-8.5}$	$10^{-8.2}$
U - F	$10^{-8.5}$	$10^{-8.3}$	$10^{-8.1}$

7 STATISTICAL ANALYSIS

Statistical analyses were performed on the batch, column, and solubility data for Th and U to better define the uncertainties involved in use of these data and for input to probabilistic site assessment models of radiological dose such as RESRAD (LePoire et al. 2000; Yu et al. 2000). Only the solubility data covering the range of expected pH values (7-10) were included in the analysis. For use of this data in probabilistic models, a known distribution and its parameters must be identified that

best match the distribution of the actual values. In order to determine the nature of these distributions we began with the data from the batch studies

7.1 Batch Studies (Sites A and B)

The data sets from site B each comprised 30 values, while the data from site A each had 16. The behavior of the data is shown in Figure 7-1.
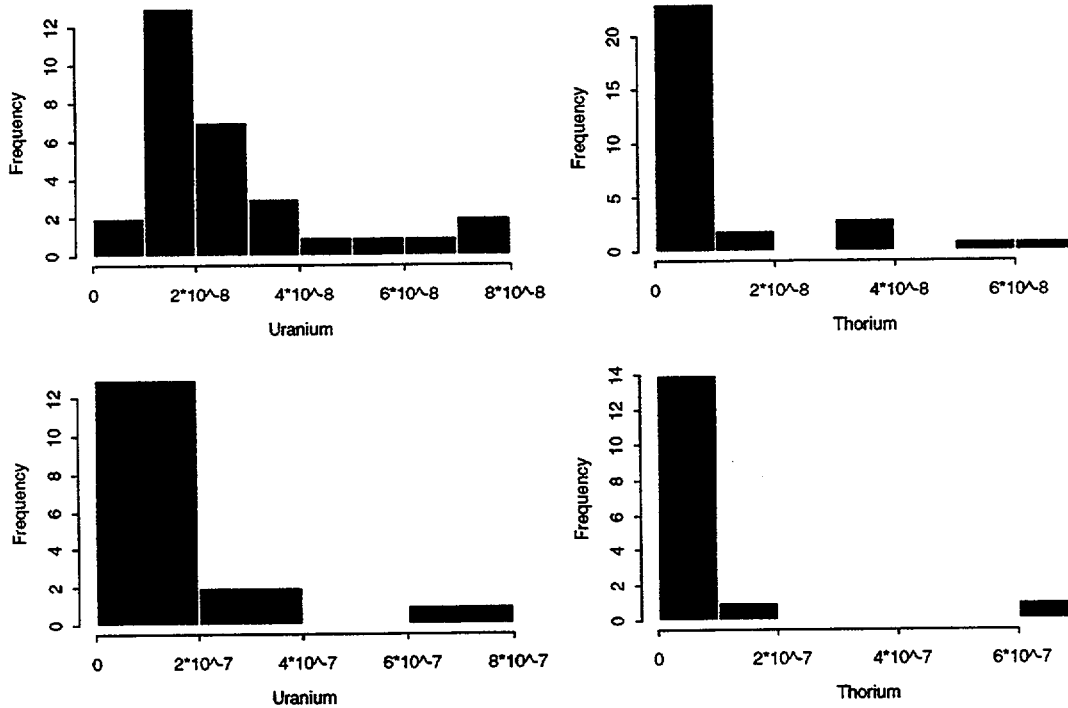
Figure 7-1. Distributions of batch data for Th and U (moles/l). (a) Site B U. (b) Site B Th. (c) Site A U. (d) Site A Th.

As can be seen, much of the data fall in the area closer to zero. This is the expected behavior since many values were close to the analytical detection limit. Also, the data is quite sparse, so the task of defining a distribution and its parameters that best match the actual data becomes a somewhat difficult problem. There are several distributions from which to choose that this data could mimic. A Kolmogorov-Smirnoff (K-S) test was used to assess the data and its parameters for goodness of fit to the specified distribution.

The K-S test assumes the hypothesis that the data in question is a certain distribution with specified parameters. The K-S statistic then collects the necessary information to

disprove the hypothesis by comparing the actual data to the hypothetical distribution. The K-S test can only show that the data is consistent with the proposed distribution. It cannot prove that the data fits this distribution.

For the Site B data, a lognormal distribution was chosen with the following parameters: meanlog=-17.7 and sdlog=.57. The K-S statistic was K-S=.1667 and p-value=.808. Since the p-value is high (> .05), there is insufficient information to refute the claim that the distribution is a lognormal with meanlog=-17.7 and sdlog=0.57. A plot of the actual data and the hypothetical data are shown in Figure 7-2.
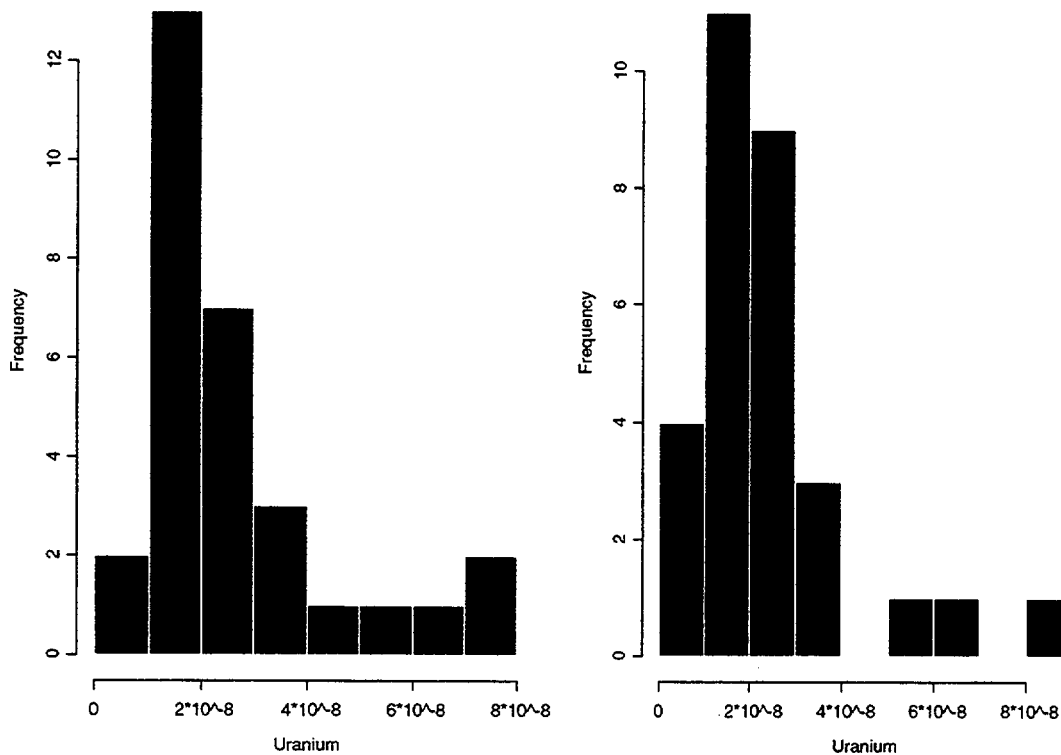
Figure 7-2. Actual (a) and hypothesized (b) distributions of U concentrations (M) in batch experiments at site B.

For the Site B thorium data, a lognormal distribution was also chosen with the following parameters: meanlog = -19.5 and sdlog=1.7. The K-S statistic was K-S = 0.2 and p-value = 0.5941. This high p-value suggests there is not enough evidence to refute the claim of a lognormal distribution with meanlog=-19.5 and sdlog=1.7. A plot of the actual data and the hypothetical data are shown in Figure 7-3.
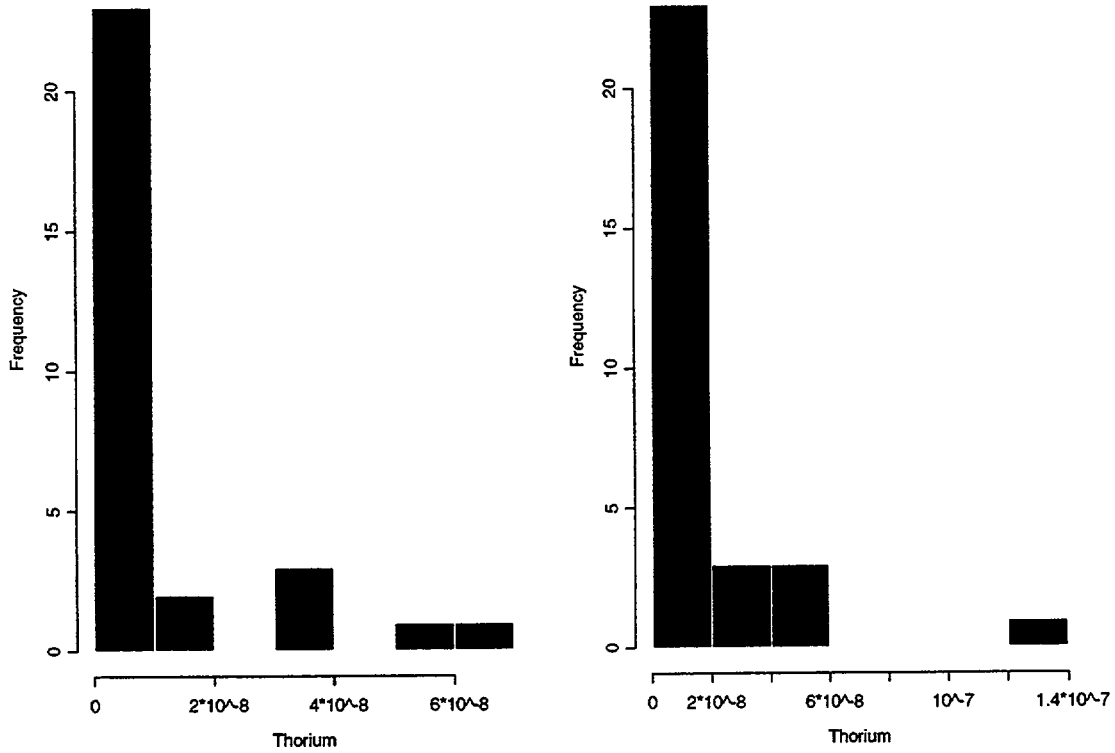
Figure 7-3. Actual (a) and hypothesized (b) distributions of Th concentrations (M) in batch experiments at site B.

For the Site A uranium data, a lognormal distribution was chosen with the same parameters as for site B (i.e. meanlog=-17.7 and sdlog=.57). The K-S statistic was 0.375 with a p-value of 0.2145. Since the p-value is high, there is insufficient information to refute the claim that the distribution is a lognormal with meanlog=-17.7 and sdlog=0.57. A plot of the actual data and the hypothetical data are shown in Figure 7-4.

45
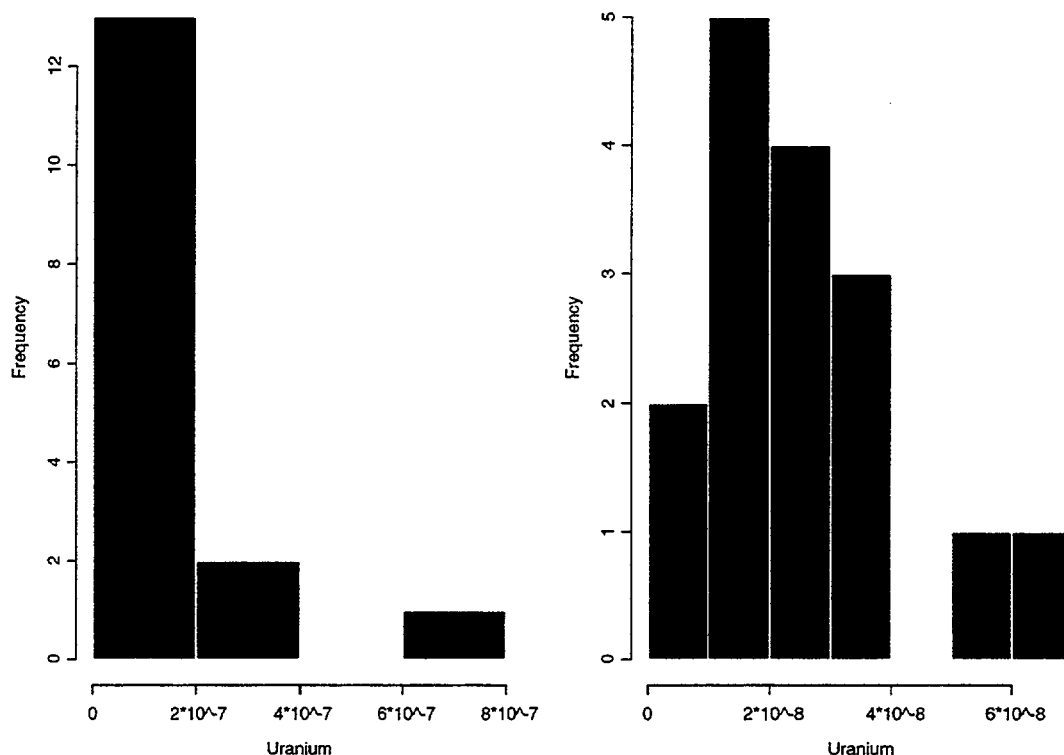
Figure 7-4. Actual (a) and hypothesized (b) distributions of U (M) concentrations in batch experiments at site A.

Similarily, for the Site A thorium data, a lognormal distribution was chosen with the same parameters as for site B (i.e. meanlog = -19.5 and sdlog=1.7. The K-S statistic was K-S = 0.25 and p-value = 0.7164. This p-value overwhelmingly suggests there is not enough evidence to refute the claim of a lognormal distribution with meanlog=-19.5 and sdlog=1.7. This fact again supports the conclusion that the Th data are solubility controlled and the hence obey similar statistical distributions. A plot of the actual data and the hypothetical data is shown in Figure 7-5.
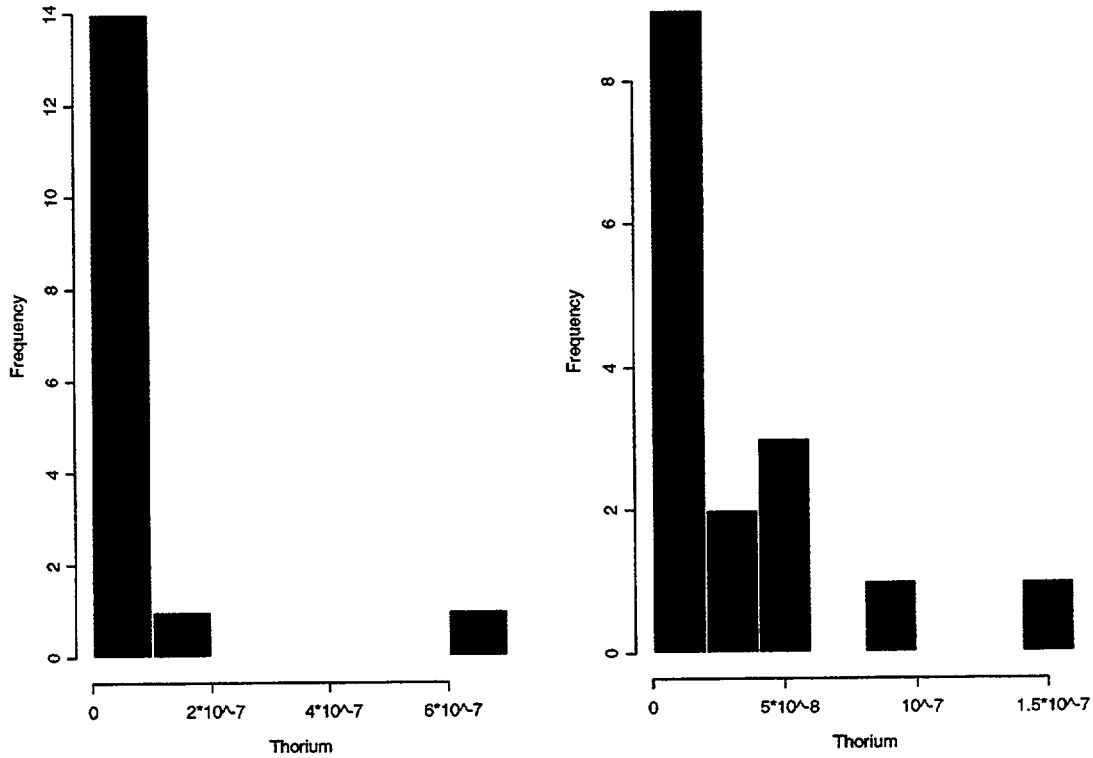
Figure 7-5. Actual (a) and hypothesized (b) distributions of Th concentrations (M) in batch experiments at site A.

7.2 Column Studies (Sites A and B)

1) Since the column study data had so few points, it is unreasonable to try to compare its distribution to a hypothetical one. Instead, a t-test was conducted to compare the means of each set of data (i.e. Site A and B,

Th and U in the batch with the corresponding data for the columns) for a significant difference.

All of these tests show a p-value above .05, which suggests there is not enough evidence to refute the claim that the data sets are equivalent. The graphs below (Figure 7-6) show each set of data on the same plot.
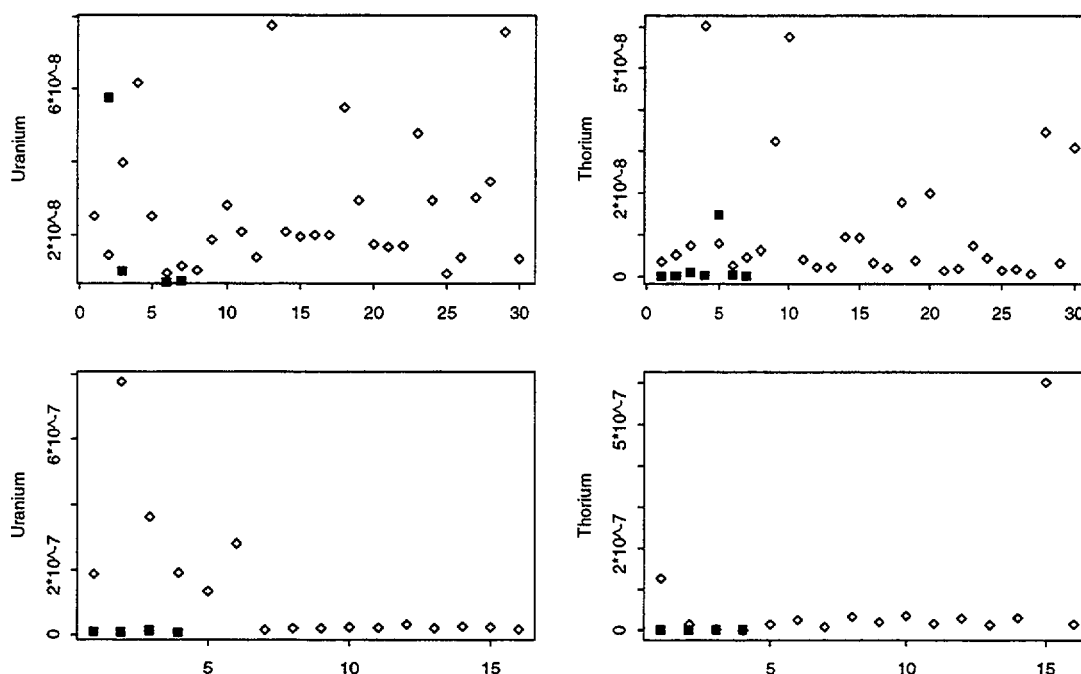
Figure 7-6. Comparisons between site A and B batch and column data for Th and U. The darkened points are the column study data, while the clear points represent the batch data. (a) Site B uranium. (b) Site B thorium. (c) Site A uranium. (d) Site A thorium.

In summary, the distributional form of the batch data is the lognormal distribution, which can be input to probabilistic models of dose assessment. Furthermore, it appears the column study data are consistent with the measurements taken during the batch studies.

7.3 Solubility Data (Sites A and B)

Since the comparison of the column and batch data showed no significant differences, the data were combined and compared to the solubility data in the same manner. All but one of these tests show a p-value above .05, which suggests there is not enough evidence to refute the claim that the data sets are equivalent. Figure 7-7 shows each set of data on the same plot.
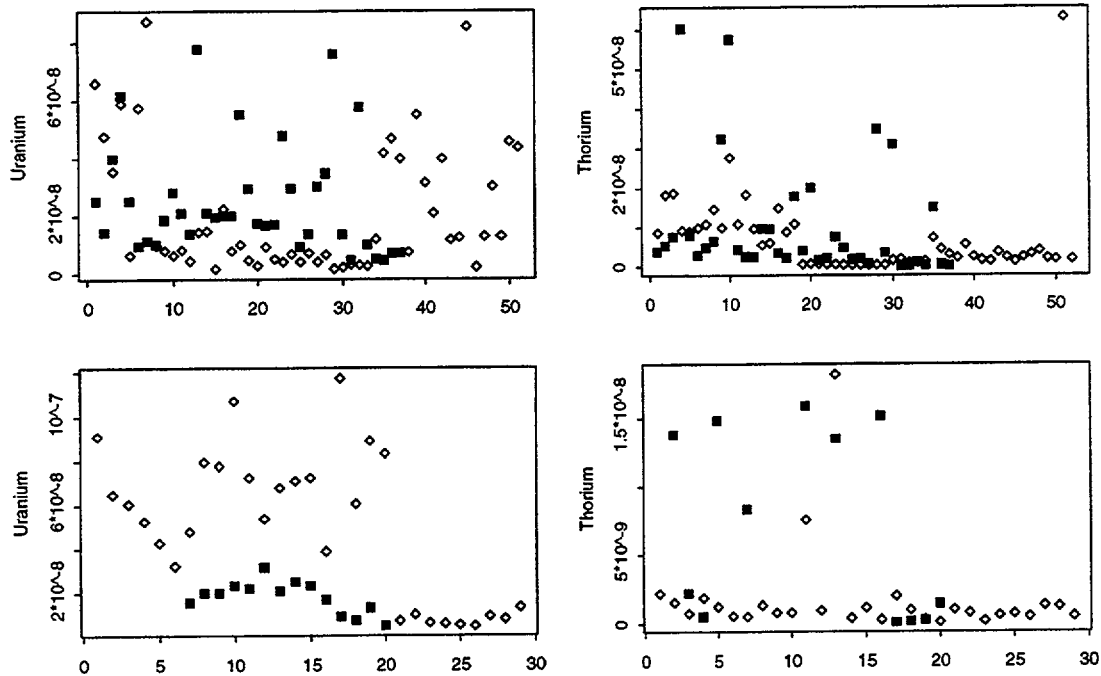
Figure 7-7. Comparisons between site A and B combined batch and column data with solubility data (pH 7-10) for Th and U. The darkened points are the batch and column study data, while the clear points represent the solubility data. (a) Site B uranium. (b) Site B thorium. (c) Site A uranium. (d) Site A thorium.

For the last test (site A thorium), the p-value=0.059, which is very close to being significant at the .05 level. From the plot, the darkened points look much more scattered than the clear points, which is probably why the t-test showed near significant differences between the data. Upon further investigation, the batch data contained the points causing the high scatter (see Figure 4-4). Never the less, these are the types of errors to be expected when measuring samples at such low concentrations even when the same chemical phenomena (solubility) is probably responsible for the observed behavior. Hence, the need for probabilistic treatments of the data.

7.4 Site C Comparison

The solubility and column data from Site C samples were more limited than for Sites A or B. The Site C solubility data comprised 29 values (pH range 7 –11 only included), while the column data comprised 6. As a result, only a t-test was done on these data. The results showed that these data could be explained by the same statistical parameters as the Th and U data at Sites A and B. A comparison between the column and solubility data is presented below.(Figures 7-8, 7-9).

49
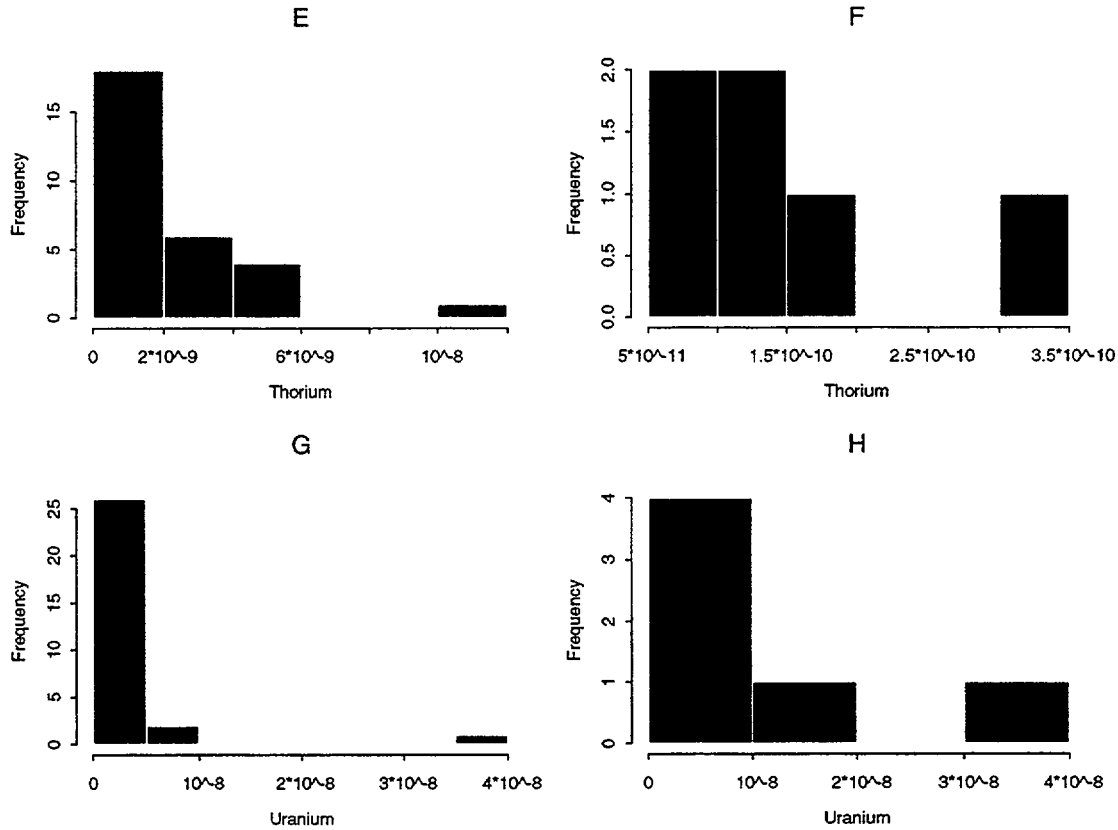
Figure 7-8. Comparisons between solubility and column data at Site C. (E) Thorium solubility data, (F) Thorium column data, (G) Uranium solubility data, (H) Uranium column data.

These tests show a p-value above .05, which suggests there is not enough evidence to refute the claim that the data sets are equivalent. Each graph below (Figure 7-9) shows both sets of data on the same plot (thorium and uranium). The darkened points are the column study data, while the clear points represent the batch data. As can be seen, the number of column points is much less that that of the solubility data, which makes a thorough comparison more difficult. A visual inspection of these graphs show that the column data could easily be combined with the solubility data.

50
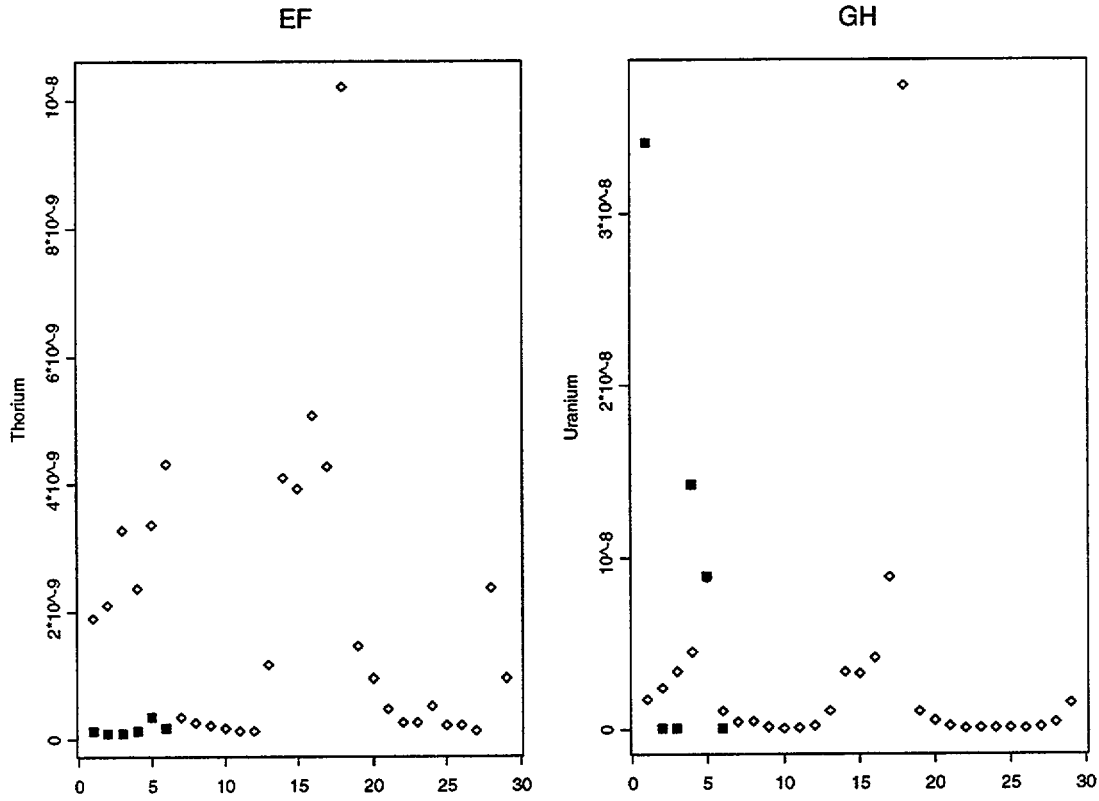
Figure 7-9. Comparisons between the column and solubility data at Site C. (EF) Thorium data, (GH) column data.

In summary, statistical analysis of the batch, column, and solubility data showed that the uncertainties in the dissolved Th and U concentrations can be described using a lognormal distribution with a meanlog of -17.7 and a sdlog of 0.57 for U and a meanlog of -19.5 and an sdlog of 1.7 for Th. These parameters are valid for all three sites.

51

8 REFERENCES

Allison, J.D., D.S. Brown, and K.J. Novo-Gradac (1991). MINTEQA2/PRODEFA2, A Geochemical Assessment Model for Environmental Systems (Version 3). UESPA, Environmental Research Laboratory, Athens GA (EPA/600/3-91/021).

Felmy, A.R., D. Rai, S.M. Sterner, M.J. Mason, N.J. Hess, and S.D. Conradson (1997). Thermodynamic Models for Highly Charged Aqueous Species: Solubility of Th(IV) Hydrous Oxide in Concentrated $NaHCO_3$ and Na_2CO_3 Solutions. J. Solution Chem., 26(3), 233-248.

Grenthe, I., J. Fuger, R.J.M. Konings, R.J. LeMire, A.B. Muller, C. Nguyen-Trung and H. Wanner (1992). *Chemical thermodynamics of uranium*, North-Holland, Elsevier Science Publishers, Amsterdam, The Netherlands.

Krupka, K.M. and R.J. Serne (1998). Effects on Radionuclide Concentrations by Cement/ground-Water Interactions in Support of Performance Assessment of Low-Level Radioactive Waste Disposal Facilities. NUREG/CR-6377.

LePoire D., J. Arnish, E. Gnanapragasam, S. Kamboj, B.M. Biwer, J.-J. Cheng, C. Yu, and S.Y. Chen (2000). Probabilistic Modules for the RESRAD and RESRAD-BUILD Computer Codes – User Guide. NUREG/CR-6692 (ANL/EAD/TM-91). U.S. Nuclear Regulatory Commission, Washington, D.C.

McKinley, J.P., J.M. Zachara, S.C. Smith, and G.D. Turner (1995). The Influence of Uranyl Hydrolysis and Multiple Site-Binding Reactions on Adsorption of U(VI) to Montmorillonite. Clays and Clay Minerals, 43(5), 586-598.

Pickett, D.A., J.D. Prikryl, D.R. Turner, and J.L. Russell (1998). Evaluation of Leach Tests for Estimating Release from Slag Sites Subject to Decommissioning: Final Report. Center for Nuclear Waste Regulatory Analysis, San Antonio, TX.

U.S. Nuclear Regulatory Commission (1995). Site Decommissioning Management Plan. NUREG-1444, Supplement 1. Washington, DC: Nuclear Regulatory Commission.

Veblen, L.A., D.J. Farthing, K.J.T. Livi, D.R. Veblen, and E. O'Donnell (2001). Long Term Performance of Radioactive Slags - Characterization and Leach Rates. DRAFT NUREG/CR 1703, March 2001, U.S. Nuclear Regulatory Commission, Washington, D.C.

Yu, C., D. LePoire, E. Gnanapragasam, J. Arnish, S. Kamboj, B.M. Biwer, J.-J. Cheng, and S.Y. Chen (2000). Probabilistic Modules for the RESRAD 6.0 and RESRAD-BUILD 3.0 Computer Codes. NUREG/CR-6697 (ANL/EAD/TM-98). U.S. Nuclear Regulatory Commission, Washington, D.C.

APPENDIX A: EARLIER STUDIES OF SITE C SAMPLES

Two sets of samples were sent to PNNL by staff at the Center for Nuclear Waste Regulatory Analyses (CNWRA), San Antonio TX. The first set containing six samples was received in December 1997 and the second set, consisting of two samples, was received in June 1998. The samples were scanned with a GM counter and the radioactive samples were analyzed by gamma spectroscopy.

A summary of the physical characteristics of the samples received in December 1997 is given in Table A1. Only two of the samples, WH-4 and WH-6, showed detectable radioactivity on the GM counter. Sample WH-6 was comprised of two types of material, an asphalt like material with embedded grayish white particles (sample A) and a pure grayish white material

(sample B). These materials were separated and analyzed by gamma spectroscopy, Table A2. The grayish white material (sample B) proved to be essentially non-radioactive. All of the radioactivity apparently being concentrated in the asphalt like sample (A). Interestingly all of the radioactivity in the asphalt like material is due to Th-232 or its daughters. This is in contrast to sample WH-4 which also shows U-238 daughters. The materials also appear to be reasonably homogeneous as different sub samples of the materials give similar radiological analyses. A alpha spectra for sample WH-4 is shown in Figure A-1.

Radiological analyses of the sample received in June 1998, Table A3, show these materials to be essentially non-radioactive.

Table A1. Physical characteristics of samples received in December 1997.

Sample	Weight (Kg)	Description	GM Activity(dpm)
WH-1	1.976	Black/green or grayish slag	none
WH-2	1.150	Blue/green to dark green slag	none
WH-3	0.743	2 pieces of blackish/gray/green slag, one piece of gray slag	none
WH-4	0.823	Dark black ash	2,500
WH-5	1.312	Numerous small pieces, grayish brown rock – light white/gray material	none
WH-6	0.909	Two types of material, asphalt like with embedded gray/white particles (A), pure grayish white material (B)	10,000

Table A2. Radiological analysis of slags at Site C (December 1997). Values in parentheses under the sample designation represent counts of different subsamples. Values in pCi/g.

	WH-4 (1)	WH-4 (2)	WH-6 (A) (1)	WH-6 (A) (2)	WH-6 (A) (3)	WH-6 (B) (1)	WH-6 (B) (2)
Th-232 Series							
Ac-228	27	30	146	151	167	nd	nd
Bi-212	31	33	152	nd	180	nd	nd
Pb-212	27	30	149	160	167	<1	<1
Ra-224	nd	nd	nd	166	170	nd	2
U-238 Series							
Ra-226	16	17	nd	nd	nd	1	<1
Bi-214	12	14	nd	nd	nd	<1	<1
Pb-214	14	15	nd	nd	nd	<1	<1

Table A3. Radiological analysis of slags at Site C (June 1998). Values in pCi/g.

	W2	W3a
Th Series		
Ac-228	1	<1
Bi-212	3	<1
Pb-212	2	<1
Ra-224	nd	1
U-238 Series		
Ra-226	3	nd
Bi-214	3	<1
Pb-214	3	<1
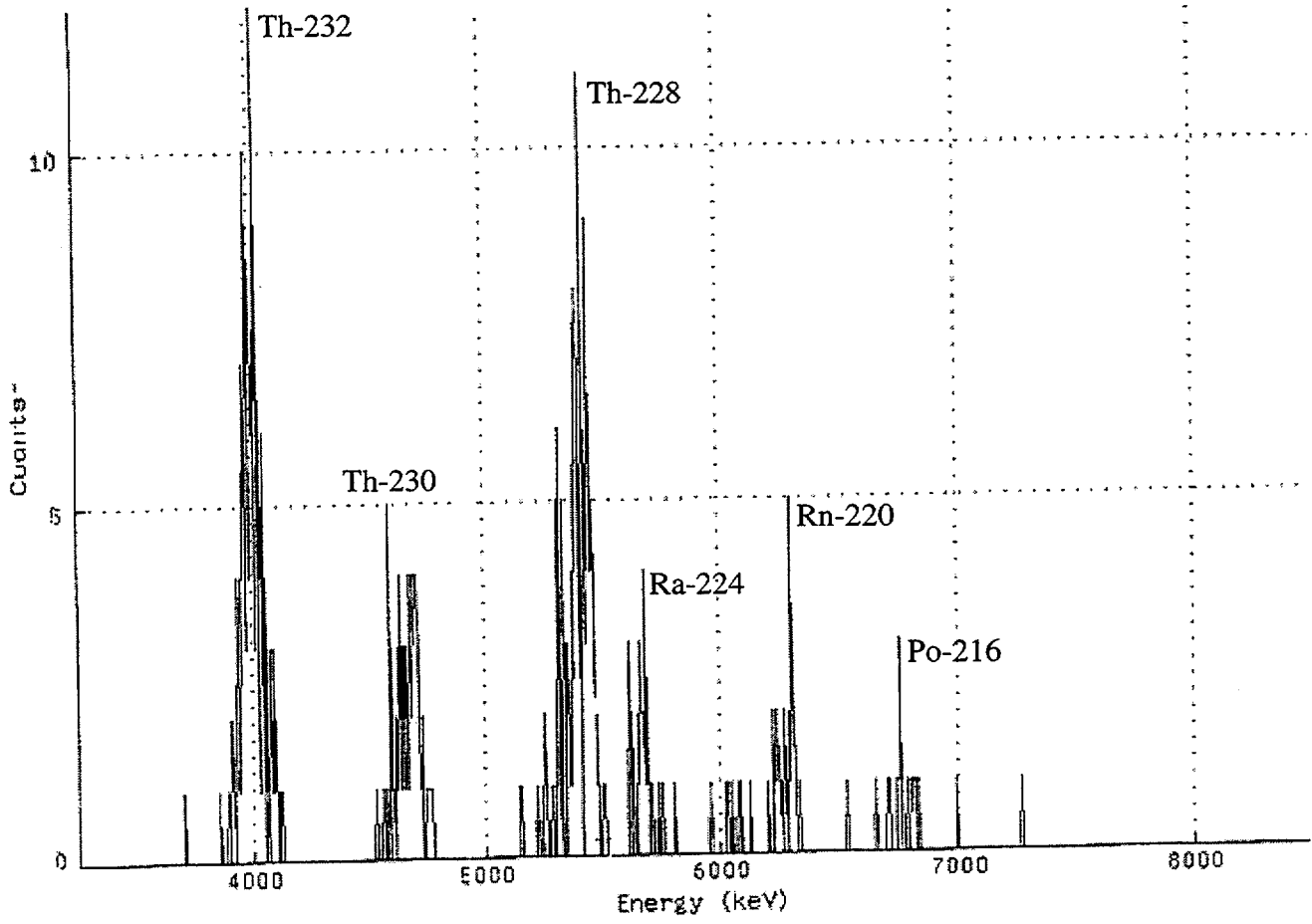
Figure A-1. Alpha spectra for sample WH-4.

APPENDIX B: TABLES OF EXPERIMENTAL DATA.

Table B1. Data Supporting Figure 4-4.

pH	log Th 4 days	log Th 31 days	log Th 275 days
0.75	-4.93		
1.24	-5		
1.7	-5.44		
2.27	-6.38		
3.14	-7.56		
3.18		-7.13	
3.31			-7.36
3.55	-7.64		
3.57		-7.88	
3.61			-7.94
4.1	-8.13		
4.31		-7.56	
4.54			-8.32
4.78	-8.5		
5.52	-8.5		
6.19	-8.5		
6.37		-8.17	
6.66	-8.5		
6.88	-8.5		
7.19			-8.5
7.77	-8.5		
8.01			-8.5
8.11	-8.5		
8.49	-8.5		
8.56			-8.5
8.66	-8.5		
9	-8.5		
9.01		-8.12	
9.24			-8.5
9.53	-8.5		
9.65			-8.5
9.76	-8.5		
10.11		-8.5	
10.16			-8.5
10.19	-8.5		
10.64	-8.5		
10.78			-8.5
11.02	-8.5		
11.45	-8.5		
11.56			-8.5
12.01	-8.5		
12.12			-8.5
12.24		-8.5	

Table B2. Data Supporting Figure 4-5.

Days	log Th 4 days Fine Material	log Th 31 days Coarse Material (Sample A)	log Th 275 days Coarse Material (Sample B)
0.08	-6.9	-8.08	-7.53
0.25	-7.86		
3	-8.5	-7.48	-7.87
7	-8.5	-7.71	-7.52
14		-7.45	
15	-7.83		
37	-7.6		
45		-7.8	-7.82

Table B3. Data Supporting Figure 4-6.

Days	Th Log(moles/L)	U Log(moles/L)
4	-8.5	-8.03
11	-8.5	-8.12
30	-8.5	-7.88

Table B4. Data Supporting Figure 4-7.

pH	log Ca(M) 4 days	log Sr(M) 31 days	log Ba(M) 275 days
1.57	-1.4	-4.16	-2.28
3.49	-1.41	-4.15	-2.29
3.84	-1.37	-4.1	-2.24
5.87	-1.45	-4.28	-2.39
7.54	-1.39	-4.19	-2.45
8.02	-1.7	-4.48	-2.78
8.93	-2.06	-4.59	-2.97
9.41	-2.23	-4.66	-3.09
10	-2.34	-4.74	-3.38
10.4	-2.52	-4.9	-3.66
11.14	-2.93	-5.24	-4.18
12.12	-4.21	-6.16	-5.01

Table B5. Data Supporting Figure 4-9.

pH	log U 4 days	log U 31 days
0.75	-6.08	
1.24	-6.05	
1.7	-6.03	
2.27	-6.19	
3.14	-6.23	
3.18		-6.2
3.55	-6.7	
3.57		-6.34
4.1	-6.54	
4.31		-6.88
4.78	-7.31	
5.52	-6.87	
6.19	-7.04	
6.37		-7.13
6.66	-7.05	
6.88	-7.12	
7.77	-7.04	
8.11	-7.19	
8.49	-7.22	
8.66	-7.28	
9	-7.37	
9.01		-7.14
9.53	-7.49	
9.76	-7.32	
10.11		-6.93
10.19	-7.1	
10.64	-7.11	
11.02	-6.97	
11.45	-7.14	
12.01	-7.27	
12.24		-7.08

Table B6. Data Supporting Figure 4-10.

Days	log U(T) Fine Material 4 days	log U(T) Coarse Material (Sample A) 31 days	log U(T) Coarse Material (Sample B) 275 days
0.08	-6.73	-7.81	-7.5
0.25	-6.11		
3	-6.44	-7.7	-7.68
7	-6.72	-7.7	-7.6
14		-7.63	-7.63
15	-6.87		
37	-6.55		
45		-7.66	-7.77

Table B7. Data Supporting Figure 4-11.

pH	log Th C9 - 5 Days	log Th C9 - 113 Days	log Th C19 - 5 Days	log Th C19 - 113 Days	log Th C1000 - 5 Days	log Th C1000 - 106 Days
0.7	-4.52					
0.75					-4.31	
0.86			-4.18			
1.15	-6.39				-5.74	
1.8	-6.51					
2.12			-4.85			
2.23					-7.33	
2.32	-7.4					
2.97			-5.79			
3.05	-8.15					
3.11		-8.5				
3.55						-7.83
3.7			-6.96			
3.78					-7.53	
3.98				-6.46		
4.03	-7.39					
4.08			-6.7			
4.33			-8.56			
4.44			-8.5			
4.61					-7.69	
4.82	-7.48					
4.86		-8.21				
5.02	-8					
5.03						-8.21
5.11			-8.5			
5.51			-8.5			
5.62					-8.03	
5.63	-7.92					
5.69				-8.5		
5.84	-8.29					
5.98						-8.31
6.1		-8.54		-6.54		
6.2			-8.5			
6.25					-7.96	
6.33			-8.5			
6.44					-7.76	
6.54	-7.62					
6.65					-8.01	
6.85			-8.5			
6.92					-8.29	
6.95					-8.42	
6.99			-8.5			
7.01		-8.27				
7.03	-8.07					
7.13						-8.52
7.16				-8.5		
7.21					-8.14	
7.47	-7.74					
7.6			-8.5			
7.62	-7.73					
7.72					-8.36	
8	-8.04					
8.04					-8.53	
8.08						-8.41
8.11		-8.23				
8.19	-8.05					
8.28					8.5	
8.48			-8.5			
8.5			-8.5			
8.57			-8.5			
8.66				-8.5		

Table B7 (Continued). Data Supporting Figure 4-11.

pH	log Th C9 - 5 Days	log Th C9 - 113 Days	log Th C19 - 5 Days	log Th C19 - 113 Days	log Th C1000 - 5 Days	log Th C1000 - 106 Days
8.75					-8.26	
8.77			-8.5			
8.83	-8.01				8.5	
8.93	-7.97					
8.96				-8.5		
8.98						-8.5
9.14		-7.83				
9.33			-8.5			
9.59				-8.5		
9.63			-8.5			
9.66	-7.84					
9.68			-8.5			
9.72					-8.5	
10.03	-8.01					
10.14						-8.5
10.31					-8.5	
10.37		-8.06				
11.48				-8.5		
10.65	-7.56					
10.72					-8.45	
10.96			-8.5			
11.01	-7.97					
11.29					-8.5	
11.39						-7.2
11.44		-7.97				
11.46			-8.5			
11.49	-7.74					
11.57					-8.5	
12			-8.5			
12.05					-8.5	
12.1	-8.02					
12.13						-8.5

Table B8. Data Supporting Figure 4-12.

Days	log Th C9 Sample 1	log Th C9 Sample 2	log Th C19 Sample 1	log Th C19 Sample 2	log Th C20 Sample 1	log Th C20 Sample 2
0.08	-8.44	-8.38	-8.48	-8.5	-8.5	-8.5
3	-8.28	-8.5	-8.5	-8.33	-8.5	-8.5
7	-8.13	-8.5	-7.75	-8.2	-8.13	-7.46
14	-7.22	-8.02	-8.41	-7.49	-8.34	-8.48
45	-8.1	-8.03	-7.7	-7.24	-8.5	-7.51

Table B9. Data Supporting Figure 4-13.

Pore Volumes	Th Log(moles/L)	U Log(moles/L)
10.29	-8.5	-8.23
14.95	-8.5	-7.24
70.92	-8.5	-8.0

Table B10. Data Supporting Figure 4-14.

pH	log U(T) C9 - 5 Days	log U(T) C9 - 113 Days	log U(T) C19 - 5 Days	log U(T) C19 - 113 Days	log U(T) C20 - 5 Days	log U(T) C20 - 106 Days
0.7	-4.89					
0.75					-4.76	
0.86			-5.47			
1.15	-5.27				-5.28	
1.8	-5.72					
2.12			-6.46			
2.23					-6.33	
2.32	-5.94					
2.97			-7.22			
3.05	-6.71					
3.11		-6.02				
3.55						-7.2
3.7			-7.08			
3.78					-7.06	
3.98				-7.3		
4.03	-7.56					
4.08			-6.99			
4.33			-7.08		-7.08	
4.44			-7.29			
4.61					-7.26	
4.82	-7.33					
4.86		-7.71				
5.02	-7.49					
5.03						-7.57
5.11			-7.78			
5.51			-8.36			
5.62					-7.29	
5.63	-7.23					
5.69				-8.5		
5.84	-7.28					
5.98						-8.36
6.1		-7.77		-8.5		
6.2			-7.97			
6.25					-7.41	
6.33			-7.99			
6.44					-7.27	
6.54	-7.52					
6.65					-7.59	
6.92					-7.36	
6.95					-8.03	
6.99			-8.04			
7.01		-7.83				
7.03	-7.18					
7.13						-8.62
7.16				-8.5		
7.21					-7.92	
7.47	-7.32					
7.6			-8.33			
7.62	-7.45					
7.72					-7.38	
8	-7.23					
8.04					-7.33	
8.08						-7.89
8.11		-8.5				
8.19	-8.19					
8.28					-7.4	
8.48			-8.54			
8.5			-8.03			
8.57			-8.44			
8.66				-8.5		
8.75					-8.12	
8.77			-8.29			

Table B10 (Continued). Data Supporting Figure 4-14.

pH	log U(T) C9 - 5 Days	log U(T) C9 - 113 Days	log U(T) C19 - 5 Days	log U(T) C19 - 113 Days	log U(T) C20 - 5 Days	log U(T) C20 - 106 Days
8.83	-7.24				-7.26	
8.93	-7.06					
8.96				-8.47		
8.98						-7.52
9.14		-7.65				
9.33			-8.38			
9.59				-8.51		
9.63			-8.17			
9.66	-8.01					
9.68			-8.37			
9.72					-7.5	
10.03	-8.09					
10.14						-7.89
10.31					-7.68	
10.37		-8.1				
11.48				-8.5		
10.65	-8.19					
10.72					-7.4	
10.96			-8.15			
11.01	-8.08					
11.29					-7.34	
11.39						-7.34
11.44		-7.99				
11.46			-8.37			
11.49	-8.35					
11.57					-7.9	
12			-8.18			
12.1	-7.84					
12.13						-7.36

Table B11. Data Supporting Figure 4-15.

pH	log Ca(T) Site A	log Ca(T) Site C(C-9)
1.15		-1.72
1.57	-1.4	
1.8		-1.76
3.49	-1.41	
3.84	-1.37	
4.03		-2.18
5.02		-2.37
5.84		-2.62
5.87	-1.45	
7.47		-2.87
7.54	-1.39	
8.02	-1.7	
8.93	-2.06	
9.41	-2.23	
9.66		-4.08
10	-2.34	
10.4	-2.52	
10.65		-4.4
11.14	-2.93	
12.12	-4.21	

Table B12. Data Supporting Figure 4-16.

Days	log U(T) C-9 Sample 1	log U(T) C-9 Sample 2	log U(T) C-19 Sample 1	log U(T) C-19 Sample 2	log U(T) C-20 Sample 1	log U(T) C-20 Sample 2	log U(T) C-9 (CO2)	log U(T) C-20 (CO2)
0.08	-7.6	-8.02	-7.68	-7.7	-7.78	-7.86	-8.5	-8.5
3	-7.84	-7.94	-7.86	-7.7	-7.77	-7.52	-7.87	-8.5
7	-7.4	-7.99	-7.11	-7.26	-7.32	-7.46	-7.6	-8.1
14	-7.21	-7.73	-7.68	-7.53	-7.53	-7.12	-7.5	-8.4
45	-7.6	-7.55	-7.71	-7.76	-8.03	-7.87	-7.5	-8.1

Table B13. Data Supporting Figure 4-17.

pH	Sample 1 - 4 days	pH	Sample 1 - 13 days	pH	Sample 2 - 4 days	pH	Sample 2 - 13 days
5.09	-8.5	6.01	-8.5	1.12	-5.09	1.89	-5.03
3.99	-8.5	4.14	-8.5	3.42	-6.8	4.32	-7.43
5.01	-8.5	5.72	-8.5	4.08	-7.64	5.62	-8.13
5.61	-8.5	6.53	-8.5	5.67	-8.16	9.15	-8.5
5.91	-8.5	7.05	-8.5	8.19	-8.37	9.94	-8.5
6.72	-8.5	6.99	-8.5	8.85	-8.5	10.24	-8.5
7.21	-8.5	7.4	-8.39	9.22	-8.5	9.85	-8.5
7.58	-8.5	7.44	-8.41	9.85	-8.5	10.21	-8.5
7.65	-8.48	7.6	-8.3	10.23	-8.5	10.73	-8.5
9.32	-8.5	8.17	-8.37	10.42	-8.5	10.36	-8.5
10.55	-8.47	8.84	-7.99	10.78	-8.5	10.78	-8.5
11.93	-8.5	12	-7.78	11.72	-8.5	11.69	-8.5
1.32	-5.98	1.32	-5.86	4.92	-7.47	7.21	-8.5
6.29	-8.5	7.2	-8.5	6.47	-7.99	9.07	-8.5

Table B14. Data Supporting Figure 4-18.

Pore Volumes	Th Log(moles/L) Sample 1	Th Log(moles/L) Sample 2	U Log(moles/L) Sample 1	U Log(moles/L) Sample 2
4.48	-8.5		-7.47	
7.98	-8.5		-8.5	
10.7	-8.5		-8.05	
4.09		-8.5		-8.5
7.42		-8.5		-7.85
10.4		-8.5		-8.5

Table B15. Data Supporting Figure 4-19.

pH	Sample 1 - 4 days	pH	Sample 1 - 13 days	pH	Sample 2 - 4 days	pH	Sample 2 - 13 days
5.09	-8.5	6.01	-8.5	1.12	-6.12	1.89	-6.04
3.99	-7.63	4.14	-8.18	3.42	-7.14	4.32	-7.56
5.01	-8.5	5.72	-8.5	4.08	-7.62	5.62	-8.5
5.61	-8.5	6.53	-8.5	5.67	-8.5	9.15	-8.5
5.91	-8.5	7.05	-8.5	8.19	-8.5	9.94	-8.5
6.72	-8.5	6.99	-8.5	8.85	-8.5	10.24	-8.5
7.21	-8.5	7.4	-8.48	9.22	-8.5	9.85	-8.5
7.58	-8.5	7.44	-8.49	9.85	-8.5	10.21	-8.5
7.65	-8.47	7.6	-8.38	10.23	-8.5	10.73	-8.5
9.32	-8.35	8.17	-8.05	10.42	-8.5	10.36	-8.5
10.55	-8.05	8.84	-7.43	10.78	-8.5	10.78	-8.5
11.93	-7.31	12	-7.22	11.72	-8.5	11.69	-8.5
1.32	-6.05	1.32	-5.99	4.92	-7.96	7.21	-8.5
6.29	-9.3	7.2	-8.5	6.47	-8.5	9.07	-8.5

APPENDIX C:

Thermodynamics of the U(VI)-Ca^{2+}-Cl^{-}-OH^{-}-H$_2$O System: Solubility Product of Becquerelite

Dhanpat Rai
Andrew R. Felmy
Nancy J. Hess
Virginia L. LeGore
David E. McCready

Pacific Northwest National Laboratory
Richland, WA 99352 USA

Thermodynamics of the U(VI)-Ca^{2+}-Cl$^-$-OH$^-$-H$_2$O System: Solubility Product of Becquerelite

Dhanpat Rai, Andrew R. Felmy, Nancy J. Hess, Virginia L. LeGore, and David E. McCready

Pacific Northwest National Laboratory, Richland, WA 99352

Summary

The solubility of synthetic becquerelite (Ca(UO$_2$)$_6$O$_4$(OH)$_6$•8H$_2$O) was determined in 0.02, 0.1, and 0.5 M CaCl$_2$ solutions and at pC_{H^+} values ranging from approximately 4 to 11. The presence of becquerelite in equilibrated samples was confirmed by a combination of techniques involving X-ray diffraction, total chemical composition, and analyses of solubility data. The solubility data were interpreted using Pitzer's aqueous thermodynamic model and the thermodynamic data for U(VI) species available in the literature. The log of the solubility product for becquerelite [Ca(UO$_2$)$_6$O$_4$(OH)$_6$•8H$_2$O + 14H$^+$ = Ca^{2+} + 6UO$_2$$^{2+}$ + 18H$_2$O] was determined to be 41.4±0.2. This value is similar to the values previously reported for other synthetic becquerelite samples, but is drastically different than a value reported for a natural sample. These data were used to interpret the observed U(VI) concentrations in solutions obtained from suspensions in water of U contaminated soils and slags collected from SDMP sites as discussed in the previous sections.

Key Words: Thermodynamics, becquerelite, solubility, solubility product, hexavalent uranium, uranium

Introduction

Uranium is one of the important constituents in the nuclear fuel cycle, in nuclear wastes, and in decommissioned nuclear facilities. In geologic environments, U exists primarily in the tetravalent and hexavalent states. Uranium in the tetravalent state readily forms hydrous oxide that has low solubility [1-3] and thus is not readily transported in subsurface groundwater. However, hexavalent U compounds (e.g., schoepites) are very soluble, and U(VI) forms strong complexes with hydroxide and carbonates [4], the most common ligands in geologic environments, making the hexavalent form the most mobile state in groundwater. However, in the presence of alkali and alkaline earth cations, common groundwater ions, U(VI) can precipitate as relatively insoluble compounds, making U(VI) far less soluble and potentially less mobile [4]. A recent review of the thermodynamic data [4] shows that reliable data for most of these compounds are not available. One of the reasons for this lack of reliable data is that a large number of compounds could possibly form with a given cation, making identification of the solubility-controlling phase difficult. For example, several of the compounds that could form in the presence of Ca, a ubiquitous cation in groundwater, are $Ca(UO_2)_6O_4(OH)_6 \cdot 8H_2O$, $Ca_2UO_5(H_2O)_{1.3-1.7}$, $CaUO_4$, Ca_3UO_6, CaU_2O_7 [5].

Members of the becquerelite structural group [becquerelite, $Ca(UO_2)_6O_4(OH)_6 \cdot 8H_2O$; and compreignacite, $K_2(UO_2)_6O_4(OH)_6 \cdot 8H_2O$] have been identified in uraninite alteration products [6] and in oxidative corrosion of synthetic $UO_2(s)$ [7,8a], and becquerelite itself is known to form from schoepite in nature. Becquerelite also appears to be an important phase in cementicious environments [5]. Uranium dioxide alteration phases including becquerelite may also form

during spent fuel alteration [8b]. Even though becquerelite appears to be a geologically

important mineral, only limited experimental data have been reported for this phase [5, 9-11],

and the reported solubility products vary over 12 orders of magnitude. To obtain reliable

thermodynamic data for becquerelite that is applicable to a wide range in environmental

conditions, experimental solubility data are required over a wide range of pH values and Ca

concentrations. However, the available data lack these attributes. Examples include Atkins *et al.*

[5], who reported solubilities of becquerelite in distilled water or in 0.5 M NaOH; they do not

report pH or Ca concentrations, and thus no thermodynamic data can be obtained from their

study. Vochten and Van Haverbeke [9] reported a solubility product of this compound based on

a limited number of samples equilibrated only in water; they do not report Ca concentrations.

Sandino and Grambow [10] studied the solubility of becquerelite $(Ca(UO_2)_6O_4(OH)_6 \cdot 8H_2O)$ at

only one Ca concentration (1.0 M $CaCl_2$) and three groups of selected pH values, and their

reported ranges in solubility product values vary by about three orders of magnitude. Casas *et al.*

[11] based their study on a naturally occurring becquerelite suspended in water and adjusted to

four different pH values at different times. They calculated log K^0 of 29 ± 1 for

$(Ca(UO_2)_6O_4(OH)_6 \cdot 8H_2O + 14H^+ = Ca^{2+} + 6UO_2^{2+} + 18H_2O)$, which differed by over 12 orders

of magnitude from the values (41.89 to 43.6) determined by Vochten and Van Haverbeke [9]

and by Sandino and Grambow [10]. Clearly, reliable thermodynamic data for becquerelite are

not available. Therefore, this study was undertaken and we determined solubilities of

becquerelite in 0.02, 0.1, or 0.5 M $CaCl_2$ solutions ranging in pC_{H^+} values from 4.4 to 11.4 using

numerous samples that were analyzed at several equilibration periods. The data obtained in this

study were then used to interpret U(VI) behavior in U contaminated soils and slags from selected

SDMP sites (see main body of this report for these details).

Methods and materials

Reagents

All solutions were prepared with deionized water that was degassed by boiling and cooling in an N_2 (99.99%) atmosphere.

For precipitating becquerelite, a 0.1 M stock solution of Ca was prepared from $Ca(NO_3) \cdot 4H_2O$ (Aldrich Products) and a solution of U(VI) from $UO_2(NO_3)_2$ (Mallinckrodt). Stock solutions (0.02, 0.1, and 0.5 M) of Ca for equilibrium solubility studies were prepared from $CaCl_2$ (Aldrich). Tetraethyl ammonium hydroxide (25%) was obtained from Kodak Chemicals and was used for adjusting pH values to avoid introduction of other alkali or alkaline earth cations into the equilibrating solutions.

Becquerelite [$Ca(UO_2)_6O_4(OH)_6 \cdot 8H_2O$, or stoichiometrically represented as $CaU_6O_{19} \cdot 11H_2O$] was prepared in a fashion similar to that described by Sandino and Grambow [10]. Briefly, uranyl and calcium nitrate stock solutions were mixed together in 50-mL plastic tubes in stoichiometric proportions (1:6 molar concentrations of Ca and U, respectively) at room temperature to obtain becquerelite solid containing approximately 107 mg of U(VI) in each tube. The pH value of the mixture was adjusted to about 4.5 with tetraethylammonium hydroxide to precipitate the solid. The precipitates were aged in mother liquor for 21 days. At the end of this period, the suspensions were centrifuged, and the supernatant was discarded. The precipitates were then washed with deionized-degassed water.

Experimental procedures

All experiments were conducted in an atmosphere-controlled chamber with a prepurified N_2

atmosphere (99.99% N_2, with <10 ppm O_2) and at 22±2°C. The solubility in all experiments

was approached from the undersaturation direction. Three sets of experiments were conducted

with the washed precipitates. These sets contained 0.02, 0.1, or 0.5 M $CaCl_2$. A 30-mL volume

of appropriate solution was added to the washed precipitates in centrifuge tubes. The pH

values of these samples were adjusted to a range between 4.4 and 11.4 using HNO_3 or

tetraethylammonium hydroxide. The tubes were capped tightly and placed on a shaker.

Periodically, the pH values of the suspensions were measured with an Orion-Ross combination

glass electrode calibrated against pH buffers. The pH meter readings were converted to

hydrogen ion concentrations using a modified Gran titration procedure [12]. In the Gran

titration method, the observed/measured pH [pH(obs)] is related to the concentration of

hydrogen ions by the equation ($pC_{H^+} = pH(obs) + A$), where pC_{H^+} is the negative logarithm of

hydrogen ion concentration in molarity units, and A is a constant. The values of A for 0.02,

0.1, and 0.5 M $CaCl_2$ solutions were determined to be 0.134, 0.161, and 0.283, respectively,

using the procedure described by Rai *et al.* [12].

At different equilibration periods, the suspensions were centrifuged at 2000 g for 10 to 15

minutes. The supernatant was filtered through Amicon Centriflo cones (Amicon Corp.) with a

25,000 molecular-weight cutoff and approximately 0.0018-μm pore size. Prior to use, the

filters were washed with deionized water followed by deionized water adjusted to the pH value

of a given sample. A 2.0-mL sample solution was passed through the filters and the filtrate

discarded before the actual sample solution was filtered. The filtrate was acidified with HNO_3,

and the concentrations of U were determined by inductively coupled plasma mass

spectroscopy. All of the solubility data are reported in the Appendix (Tables A.1 through

A.3). At the end of the study, the solid samples were separated and analyzed for crystallinity

by X-ray diffraction using Cu Kα radiation.

X-ray absorption spectroscopy experiments were conducted at Stanford Synchrotron Radiation

Laboratory (beamline 4-2). Spectra were collected at the U L_{III}-edge in fluorescence mode

using a 13-element Ge detector. All spectra were measured to a photoelectron wave vector of

13 Å^{-1}. Energy calibration was based on assigning the first inflection point of the absorption

edge of a Zr standard to 17999.35 eV. Normalization of the absorption spectrum and

extraction of the extended X-ray absorption fine structure were performed following standard

procedures described in Rai *et al.* [13].

Thermodynamic model

The ion-interaction model of Pitzer and co-workers [14, 15] was used to interpret solubility

data. This aqueous thermodynamic model emphasizes a detailed description of the specific ion

interactions in solution. The effects of specific ion interactions on the excess solution free

energy are contained in the expressions for the activity coefficients. The activity coefficients

can be expressed in a virial-type expansion as

$$\ln \gamma_i = \ln \gamma_i^{DH} + \sum_j \beta_{ij}(I)m_j + \sum_j \sum_k C_{ijk}m_jm_k + \cdots \qquad (1)$$

where m is the molality, γ_i^{DH} is a modified Debye-Hückel activity coefficient that is a universal function of ionic strength, and $\beta_{ij}(I)$ and C_{ijk} are specific for each ion interaction and are functions of ionic strength. The third virial coefficient, C, is understood to be independent of ionic strength. A detailed description of the exact form of Eq. (1) is published in Felmy and Weare [16] and Felmy *et al.* [17] and is contained in the nonlinear least-squares program (NONLIN, developed by A. R. Felmy) for estimating activity coefficients and calculating chemical equilibria involving multiple solid and aqueous species. NONLIN has been used extensively for interpreting data similar to those obtained in this study [17-20]. For interpreting the present solubility data, no attempt was made to convert molarity units to the molality units needed for modeling because even at the highest $CaCl_2$ concentrations used in these experiments (0.5 M) the error introduced by neglecting this conversion is almost negligible (1.2%), and it would be even more negligible at the lower $CaCl_2$ concentrations.

In terms of evaluating the aqueous species present in solution, we used the standard state equilibrium constants for the U(VI) species recently summarized by Grenthe *et al.* [4].

Results and Discussion

Observed Solubility

The observed aqueous U concentrations plotted as a function of pC_{H+}, $CaCl_2$ concentrations, and equilibration period (Figures 1 through 3) in general indicate that the U concentrations: 1) decrease approximately two orders of magnitude with one unit increase in pC_{H+} at all $CaCl_2$ concentrations below pC_{H+} of ~7 and appear to be nearly constant between pC_{H+} 7 and 12, 2) are similar at different equilibration periods for different $CaCl_2$ concentrations, indicating that steady-state concentrations are reached rapidly (<4 days), and 3) appear to be similar in different $CaCl_2$ concentrations (Figure 4).

Characterization of Solubility-Controlling Phase

A combination of techniques including preparation of the solid phase using a procedure recommended by Sandino and Grambow [10], X-ray diffraction (XRD), X-ray absorption spectroscopy (XAS), total chemical composition, and thermodynamic modeling of the solubility data were used to identify the solubility-controlling phase in these experiments. It was necessary to use a combination of techniques because of the difficulties involved in characterizing the phase when only one characterization technique was used. These difficulties arise from the fact that most alkali metal and alkaline earth hydrated U(VI) solids have similar chemical compositions and structures, making it difficult to unequivocally state the presence of only one phase.

X-ray Diffraction and Total Chemical Composition Analyses

Sandino and Grambow [10] have shown that, in the presence of Ca and at pC_{H^+} ~4, uranyl

hydroxide transforms quickly to becquerelite at room temperature. Therefore, we followed

their procedure to prepare the solid phase used in this study. Atkins *et al.* [5] showed that in

highly alkaline systems (pH ~12), in the presence of $Ca(OH)_2$, two Ca phases are expected,

$Ca(UO_2)_6O_4(OH)_6 \cdot 8H_2O$ and $Ca_2UO_5(H_2O)_{1.3-1.7}$, with the latter being favored. X-ray

diffraction analyses of the equilibrated phases at pC_{H^+} between 4.3 and 8.0 (Table 1, Figure 5)

show the presence of becquerelite as the major phase, along with the presence of other minor

unaccounted peaks for solids that appear to increase in concentration with the increase in pC_{H^+}.

These results are similar to the total chemical analyses of the solid phases (Table 2), showing

molar U/Ca ratios at pC_{H^+} values <8 that are similar to the theoretical values for becquerelite

(6:1), but the ratios decrease to around 2 at pC_{H^+} >8. We also noted that the color of the

precipitate changed noticeably at pC_{H^+} values around 11, indicating a significant change in the

dominant solid phase at higher pC_{H^+} values consistent with the XRD analyses, which did not

detect the presence of becquerelite. Nevertheless, these total chemical composition data

suggest that the dominant phase is becquerelite at pC_{H^+} <~8, but the presence of other minor

phases cannot be ruled out.

Sandino and Grambow [10] showed that alkali and alkaline earth compounds are readily

formed from uranyl hydroxide at room temperature. Although a number of U(VI)-Ca phases

(e.g., $Ca(UO_2)_6O_4(OH)_6 \cdot 8H_2O$, $Ca_2UO_5(H_2O)_{1.3-1.7}$, $CaUO_4$, Ca_3UO_6, and CaU_2O_7) can form in

the alkaline environment, the data of Atkins *et al.* [5] show that $Ca(UO_2)_6O_4(OH)_6 \cdot 8H_2O$ and

$Ca_2UO_5(H_2O)_{1.3-1.7}$ are the most likely phases. It can be noted that all of the other possible

U(VI)-Ca solids have lower U/Ca ratios than becquerelite. The U/Ca molar ratio for $CaUO_4$ is

1:1 and for $Ca_2UO_5(H_2O)_{1.3-1.7}$ is 1:2 as compared with 6:1 for becquerelite. The observed

lower U/Ca molar ratios (Table 2) at pH >8 are consistent with the formation of such

compounds.

X-ray Absorption Spectroscopic Analyses

Definitive identification of the solubility-limiting phase using analysis of the XAS spectra was

not possible because of the structural similarity of hydrated Ca-U(VI) phases. All samples

analyzed (pC_{H+} 5.93, 0.02 M CaCl2; pC_{H+} 6.18, 0.5 M CaCl2; and pC_{H+} 7.56, 0.1 M CaCl2)

displayed virtually identical X-ray absorption near edge structure (XANES) indicative of a

U(VI) oxidation state and similar features in the Fourier analysis of the extended x-ray

absorption fine structure (EXAFS) shown in Figure 6. Fits to the EXAFS reveal the number of

atoms and the interatomic distances to about 4.0 Å, which varied from sample to sample, but

could not be used to unequivocally identify the predominant hydrated Ca-U(VI) phase.

Solubility Data Analyses

Although becquerelite is clearly the primary phase present in our samples (XRD and total

chemical composition) at pC_{H+} values <8, this does not mean that it is the solubility-controlling

solid. To better assess this situation we turn to an initial analysis of the solubility data.

Reliable thermodynamic data for calculating the solubility of Ca uranates are available only for

CaUO$_4$. Comparison of the predicted CaUO$_4$(c) solubility in 0.1 M CaCl$_2$ using the

thermodynamic data reported in Grenthe *et al.* [4] indicates that this compound cannot be the

solubility-controlling phase (Figure 4) across the entire pC_{H+} range investigated. Although

reliable data for other phases are not available, one can compare the observed with the

expected changes in U concentrations as a function of H$^+$ and Ca^{2+} concentrations (Table 3) to

ascertain the nature of the solubility-controlling phase. First, the observed U concentrations at

pC_{H+} <~7 increase by about two orders of magnitude with an order of magnitude increase in H$^+$

concentration (one unit decrease in pC_{H+}). This is similar to the 2.33 orders of magnitude

increase expected in equilibrium with becquerelite, but drastically different than the expected

increases (3 to 8 orders of magnitude per unit decrease in pC_{H+}) in equilibrium with other Ca

uranates (e.g., Ca$_2$UO$_5$(H$_2$O)$_{1.3-1.7}$, CaUO$_4$, Ca$_3$UO$_6$, and CaU$_2$O$_7$). Second, the observed U

concentrations at pC_{H+} >~7 are essentially independent of pC_{H+}. Assuming UO$_2$(OH)$_2$(aq) is

the dominant aqueous species at pC_{H+} >~7, the observed U concentrations are close to 0.33

orders of magnitude increase in U per unit decrease in pC_{H+} as expected in equilibrium with

becquerelite, but drastically different than expected increases (2 to 6 orders of magnitude per

unit decrease in pC_{H+}) in equilibrium with other Ca uranates. Third, at all pC_{H+} values, there is

no clearly observable dependence on Ca^{2+} concentrations. This is also close to -0.17 orders of

magnitude change with one order of magnitude increase in Ca^{2+} concentrations, as expected in

equilibrium with becquerelite, but significantly different than the expected changes (-0.5 to −

3.0 orders of magnitude) in equilibrium with other Ca uranates. Finally, the expected changes

in U concentrations differ by many orders of magnitude (Table 3) as a function of H$^+$ and Ca^{2+}

in equilibrium with becquerelite and Ca$_2$UO$_5$•xH$_2$O, the only two expected solid phases [5] in

the high Ca and alkaline environments, indicating that $Ca_2UO_5 \cdot xH_2O$ could not possibly the solubility-controlling phase. Therefore, these solubility data suggest that becquerelite must be the solubility-controlling phase in most of the experimental range investigated.

In summary, although we cannot rule out the formation of minor amounts of other phases in some of our samples, the vast preponderance of the data (i.e., XRD, total chemical composition, and solubility) indicates becquerelite is the solubility-controlling solid phase at least at pC_{H+} values <8.

Thermodynamic Analysis of Data

The solubility data at the lowest ionic strength (i.e., 0.02 M $CaCl_2$) and in the low pH region, where the U(VI) hydrolysis is minimal, are best suited for determining the solubility product of becquerelite. As a first attempt to interpret these data, we used the standard state equilibrium constants for the formation of U(VI) aqueous species in the hydroxide system proposed by Grenthe *et al.* [4], along with Pitzer's [15] ion-interaction parameters for UO_2^{2+} with Cl⁻, the bulk electrolyte used in this study. In addition, the ion-interaction parameters for UO_2^{2+} with Cl⁻ were used as analogs for all of the divalent U(VI)-hydroxide species with Cl⁻, because these values are not available. With these parameters and in relatively acidic conditions, where the UO_2^{2+} species is dominant, the log of the equilibrium constant for the becquerelite solubility reaction

$$Ca(UO_2)_6O_4(OH)_6 \cdot 8H_2O + 14H^+ = Ca^{2+} + 6UO_2^{2+} + 18H_2O$$
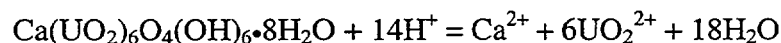
was calculated to be 41.4 ± 0.2. A close agreement, at all pC_{H^+} values, between the observed

aqueous U concentrations contacting becquerelite in 0.02 M $CaCl_2$ solutions and those

predicted using the above model (Figure 1) indicates that the model can be used to reliably

predict becquerelite behavior under these conditions.

This model was then used to predict the U(VI) concentrations in equilibrium with becquerelite

in 0.1 M $CaCl_2$ solutions. Model predictions showed close agreement with the observed

concentrations in solutions of pC_{H^+} values < 6.1 , but were up to about two orders of magnitude

higher at the higher pC_{H^+} values (Figure 2). The concentrations at the higher pC_{H^+} values are

primarily due to the dominance of $UO_2(OH)_2(aq)$ in the pC_{H^+} region 6.1 to ~9.0 and of

$UO_2(OH)_3^-$ at $pC_{H^+} > {\sim}9.0$. These results suggest that the formation constants of these species

may not be correct. In the case of $UO_2(OH)_2(aq)$ species, the formation constant is based on an

upper limit for the equilibrium constant for the formation of these species ($UO_2^{2+} + 2H_2O =$

$UO_2(OH)_2(aq) + 2H^+$; log $K^0 = {\leq}-10.3$) reported by Grenthe et al. [4] and is very likely in

error. In fact Silva [21], and Choppin and Mathur [22] report the log of the equilibrium

constants for the formation of $UO_2(OH)_2(aq)$ as -11.5 and -12.0, respectively. The formation

constant that best describes our solubility data in 0.1 M $CaCl_2$ is ~ -11.3 (because of the large

variability in solubility data for the pC_{H^+} where this species is dominant, an uncertainty of ± 1

is associated with this number) and is very near the values previously proposed/used for this

reaction [11, 21]. The limiting formation constant value of $UO_2(OH)_3^-$ ($UO_2^{2+} + 3H_2O =$

$UO_2(OH)_3^- + 3H^+$) that we calculate from our data is ≤ -21.5. This species is not important in

the pC_{H^+} region <9.0 where most of the solubility data were obtained and where becquerelite

is likely to be the equilibrium phase.

The constants and ion-interaction parameters used in the final model are reported in Tables 4 and 5. There is close agreement between the observed and predicted U concentrations in equilibrium with becquerelite in 0.02, 0.1, and 0.5 M $CaCl_2$ solutions and as a function of pC_{H+} (Figures 1 through 3), indicating that the selected modeling parameters provide reliable predictions of the solubility behavior of becquerelite over a wide range of pC_{H+} values and Ca concentrations.

It is also of interest to determine how closely this model predicts the observed solubility behavior of becquerelite in 1.0 M $CaCl_2$ in the limited range of pH values reported by Sandino and Grambow [10]. To interpret these data, values of H^+ concentrations are required. Although Sandino and Grambow [10] report pH values, they refer to the procedures used in Torrero et al. [23], which indicates that their reported pH values are really pC_{H+}. With these considerations, the U concentrations observed by Sandino and Grambow [10] are compared with the predictions using our model (Figure 7). A very close agreement between the observed and predicted concentrations indicates that our model is also consistent with the data presented by Sandino and Grambow [10]. Our value for becquerelite solubility product is identical to the value calculated from the Vochten and Van Haverbeke [9] data by Casas et al. [11] (Table 4) using the aqueous phase model reported by Grenthe et al. [4]. However, the log of the solubility product value (29±1) for natural becquerelite reported by Casas et al. [11] is drastically different than the values (41.4 to 43.7) obtained in this study or previously reported for synthetic becquerelite (Table 4). In supporting their value, Casas et al. [11] state that the differences might be due to small particle sizes or large surface areas of synthetic samples as compared with the natural bacquerelite samples. Such a large variability is noted between the

amorphous and crystalline tetravalent oxides. However, such variability is not expected for

solid phases that tend to initially precipitate as crystalline solids as is the case with

becquerelite. Casas *et al.* [11] calculate their solubility product based on only one sample that

was adjusted to four different pH values at different times. Two of their data points are for pH

values 7.4 and 8.4 where the aqueous phase model is not reliable and our study indicates

difficulty in maintaining becquerelite under highly alkaline conditions. Although, Casas *et al.*

[11] took precautions to exclude impurities from the becquerelite samples, their equilibrated

sample contained evidence of the presence of <5% soddyite and uranophane. The presence of

small percentages of impurities that are difficult to exclude and identify in natural samples can

have a significant effect on solubility. In addition, they did not investigate solubility as a

function of Ca, which is necessary to 1) obtain reliable data because Ca is one of the solid

phase components and 2) convert schoepite-type phases, which may be present as impurities

and have been shown to transform to becquerelite at room temperature in the presence of Ca,

so that reliable thermodynamic constants for becquerelite can be determined. We can only

point out the difficulties in the study, but the specific reasons for the drastically different

solubility product observed by Casas *et al.* [11] are not known. Further insights into this

problem can only be gained through extensive studies, hitherto lacking, with the natural

becquerelites.

In summary, the solubility product of synthetic becquerelite was determined through extensive

studies on solubility as a function of wide ranges in pC_{H+} and Ca concentrations. The observed

solubilities were similar to those previously reported for synthetic becquerelites (Table 4). An

unexpected reported differences of over 12 orders of magnitude [11] between the solubility

products of natural and synthetic becquerelites can only be resolved through additional

extensive studies with natural becquerelites.

Acknowledgements

References

1   Rai, D., Felmy, A. R., Ryan, J. L.: Uranium(IV) Hydrolysis Constants and Solubility
      Product of $UO_2 \bullet H_2O$(am). Inorg. Chem. **29**, 260-264 (1990).

2   Rai, D., Felmy, A. R., Sterner, S. M., Moore, D. A., Mason, M. J., Novak, C. F.: The
      Solubility of Th(IV) and U(IV) Hydrous Oxides in Concentrated NaCl and $MgCl_2$
      Solutions. Radiochim. Acta **79**, 239-247 (1997).

3   Yajima, T., Kawamura, Y., Ueta, S.: Uranium (IV) Solubility and Hydrolysis Constants
      Under Reduced Conditions. Mat. Res. Soc. Symp. Proc. **353**, 1137-1142 (1994).

4   Grenthe, I., Fuger, J., Konings, R. J. M., Lemire, R. J., Muller, A. B., Nguyen-Trung, C.,
      Wanner, H.: *Chemical Thermodynamics of Uranium,* North-Holland, Elsevier Science
      Publishers, Amsterdam, The Netherlands (1992).

5   Atkins, M., Beckley, A. N., Glasser. F. P.: Influence of Cement on the Near Field
      Environment and its Specific Interactions with Uranium and Iodine. Radiochim. Acta
      44/45, 225-261 (1988).

6   Deliens, M., Piret, P., Comblain, G.: In: *Les minéraux secondaires d'uranium du Zaire,*
      Musee Royal de l'Afrique centrale, Tervuren, Belgique, D/1981/0254/7 (1981). (quoted by
      Sandino and Grambow 1994).

7   Bates, J. K., Tani, B. S., Veleckis, E., Wronkiewicz D. J.: Identification of Secondary

    Phases Formed During Unsaturated Reaction of UO_2 with EJ-13 Water. Mat. Res. Soc.

    Symp. Proc. **176**, 499-506 (1990).

8a Wronkiewicz, D. J., Bates, J. K., Gerding, T. J., Veleckis, E., Tani, B. S.: Uranium Release

    and Secondary Phase Formation During Unsaturated Testing of UO_2 at 90°C. J. Nuc. Mat.

    190, 107-127 (1992).

8b Wronkiewicz, D.J. and Buck, E.C.: Uranium Mineralogy and the Geologic Disposal of

    Spent Nuclear Fuel. In, URANIUM: Mineralogy, Geochemistry and the Environment,

    Reviews in Mineralogy, Volume 38, 475-497 (1999), P.C. Burns and R. Finch, eds. The

    MINERALOGICAL SOCIETY OF AMERICA, Washington, DC 20036.

9   Vochten, R., Van Haverbeke, l.: Transformation of Schoepite into the Uranyl Oxide

    Hydrates: Becquerelite, Billietite and Wolsendorfite. Mineralogy and Petrology **43**, 65-72

    (1990).

10 Sandino, M. C. A., Grambow, B.: Solubility Equilibria in the U(VI)-Ca-K-Cl-H_2O System:

    Transformation of Schoepite into Becquerelite and Compreignacite. Radiochim. Acta

    66/67, 37-43 (1994).

11 Casas, I., Bruno, J., Cera, E., Finch, R. J., Ewing, R. C.: Characterization and Dissolution

    Behavior of a Becquerelite from Shinkolobwe, Zaire. Geochimica et Cosmochim. Acta

61/18, 3879-3884 (1997).

12   Rai, D., Felmy, A. R., Juracich, S. P., Rao, L.: Estimating the Hydrogen Ion Concentration in Concentrated NaCl and Na_2SO_4 Electrolytes. SAND94-1949, Sandia National Laboratories, Albuquerque, New Mexico (1995).

13   Rai, D., Hess, N. J., Felmy, A. R., Moore, D. A., Yui, M., Vitorge, P.: A Thermodynamic Model for the Solubility of PuO_2(am) in the Aqueous K^+-HCO_3^- -CO_3^{2-} -OH^- -H_2O System. Radiochim. Acta **86,** 89-99 (1999).

14   Pitzer, K. S.: Mayorga, G.: Thermodynamics of Electrolytes. II. Activity and Osmotic Coefficients for Strong Electrolytes with One or Both Ions Univalent. J. Phys. Chem. **77,** 2300-2308 (1973).

15   Pitzer, K. S.: "Ion Interaction Approach: Theory and Data Correlation." Chapter 3, pp. 75-153, *Activity Coefficients in Electrolyte Solutions.* K. S. Pitzer, ed.; CRC Press, Boca Ratan, Florida (1991).

16   Felmy, A. R., Weare, J. H.: The Prediction of Borate Mineral Equilibria in Natural Waters: Application to Searles Lake, California. Geochim. Cosmochim. Acta **50,** 2771-1783 (1986).

17   Felmy, A. R., Rai, D., Schramke, J. A., Ryan, J. L.: The Solubility of Plutonium Hydroxide in Dilute Solution and in High-Ionic-Strength Chloride Brines. Radiochim.

Acta **48**, 29-35 (1989).

18   Felmy, A. R., and D. Rai.: An Aqueous Thermodynamic Model for a High-Valence 4:2 Electrolyte Th^{4+}-SO_4^{2-} in the System Na^+-K^+-Li^+-NH_4^+-Th^{4+}-SO_4^{2-}-HSO_4^--H_2O to High Concentration. J. Solution Chem. **21,** 407-423 (1992).

19   Rai, D., Felmy, A. R., Moore, D. A.: Thermodynamic Model for Aqueous Cd^{2+}-CO_3^{2-} Ionic Interactions in High-Ionic-Strength Carbonate Solutions, and the Solubility Product of Crystalline $CdCO_3$. J. Solution Chem. **20,** 1169-1187 (1991).

20   Rai, D., Felmy, A. R., Fulton, R. W.: The Nd^{3+} and Am^{3+} Ion Interactions With Sulfate Ion and Their Influence on $NdPO_4(c)$ Solubility. J. Solution Chem. **24,** 79-895 (1995).

21   Silva, R. J.: Mechanisms for the Retardation of Uranium (VI) Migration. Mat. Res. Soc. Symp. Proc. **257,** 323-330 (1992).

22   Choppin, G. R., Mathur, J. N.: Hydrolysis of Actinyl (VI) Cations. Radiochim. Acta **52/53,** 25-28 (1992).

23   Torrero, M. E., Casas, I., De Pablo, J., Sandino, M. C. A., Grambow, B.: A Comparison Between Unirradiated $UO_2(s)$ and Schoepite Solubilities in 1 M NaCl Medium. Radiochim. Acta **66/67**: 29-35 (1994).

24 Harvie, C. E., Moller, N., Weare, J. H.: The Prediction of Mineral Solubilities in Natural

Waters: The Na-K-Mg-Ca-H-CL-SO$_4$-OH-HCO$_3$-CO$_2$-H$_2$O System to High Ionic

Strengths at 25°C. Geochim. Cosmochim. Acta **48,** 723-751 (1984).

Figure Captions

Figure 1. Aqueous uranium concentrations in solutions contacting becquerelite suspensions in

0.02 M $CaCl_2$ and a range in pC_{H^+} values that were equilibrated for different periods.

Solid line represents model predictions based on the thermodynamic data reported in

Tables 4 and 5.

Figure 2. Aqueous uranium concentrations in solutions contacting becquerelite suspensions in

0.1 M $CaCl_2$ and a range in pC_{H^+} values that were equilibrated for different periods.

The presence of becquerelite at $pC_{H^+} > 8$ is uncertain, see text for details. The lines

represent predictions based on thermodynamic data reported in Tables 4 and 5 with

the exception that the dashed line incorporates values of formation constants for

$UO_2(OH)_2^0$ and $UO_2(OH)_3^-$ from Grenthe *et al.* [4].

Figure 3. Aqueous uranium concentrations in solutions contacting becquerelite suspensions in

0.5 M $CaCl_2$ and a range in pC_{H^+} values that were equilibrated for different periods.

Solid line represents model predictions based on thermodynamic data reported in

Tables 4 and 5.

Figure 4. Aqueous uranium concentrations in solutions contacting becquerelite suspensions in 0.02, 0.1, or 0.5 M $CaCl_2$ and a range in pC_{H^+} values. Solid line represents a reference slope of -2. Dashed line represents predicted uranium concentrations in equilibrium with $CaUO_4(c)$ at 0.1 M $CaCl_2$ based on thermodynamic data reported in Grenthe *et al.* [4].

Figure 5. A representative X-ray diffraction pattern of the solid phase equilibrated in 0.1 M $CaCl_2$ at pC_{H^+} of about 8. See Table 1 for details about XRD analyses of samples at other pC_{H^+} values.

Figure 6. Comparison of the Fourier transforms of the EXAFS spectra of solids equilibrated in different molarities of $CaCl_2$ solutions (U65, 0.02 M $CaCl_2$, pC_{H^+} 5.9; U108, 0.1 M $CaCl_2$, pC_{H^+} 7.6; U209, 0.5 M $CaCl_2$, pC_{H^+} 6.2). The thin lines are the Fourier transforms of the experimental EXAFS; the thick lines are the Fourier transforms of the fit to EXAFS. Transforms were calculated over the range from 3.5 to 12.5 Å^{-1} and are offset by 0.15 units for ease of comparison.

Figure 7. Aqueous uranium concentrations in solutions contacting becquerelite suspensions in 1.0 M $CaCl_2$. The symbols representing experimental data points are from Sandino and Grambow [10] (labeled as S&G 1994). The solid line represents model predictions based on thermodynamic data reported in Tables 4 and 5.

Figure 1. Aqueous uranium concentrations in solutions contacting becquerelite suspensions in 0.02 M $CaCl_2$ and a range in pC_{H^+} values that were equilibrated for different periods. Solid line represents model predictions based on the thermodynamic data reported in Tables 4 and 5.
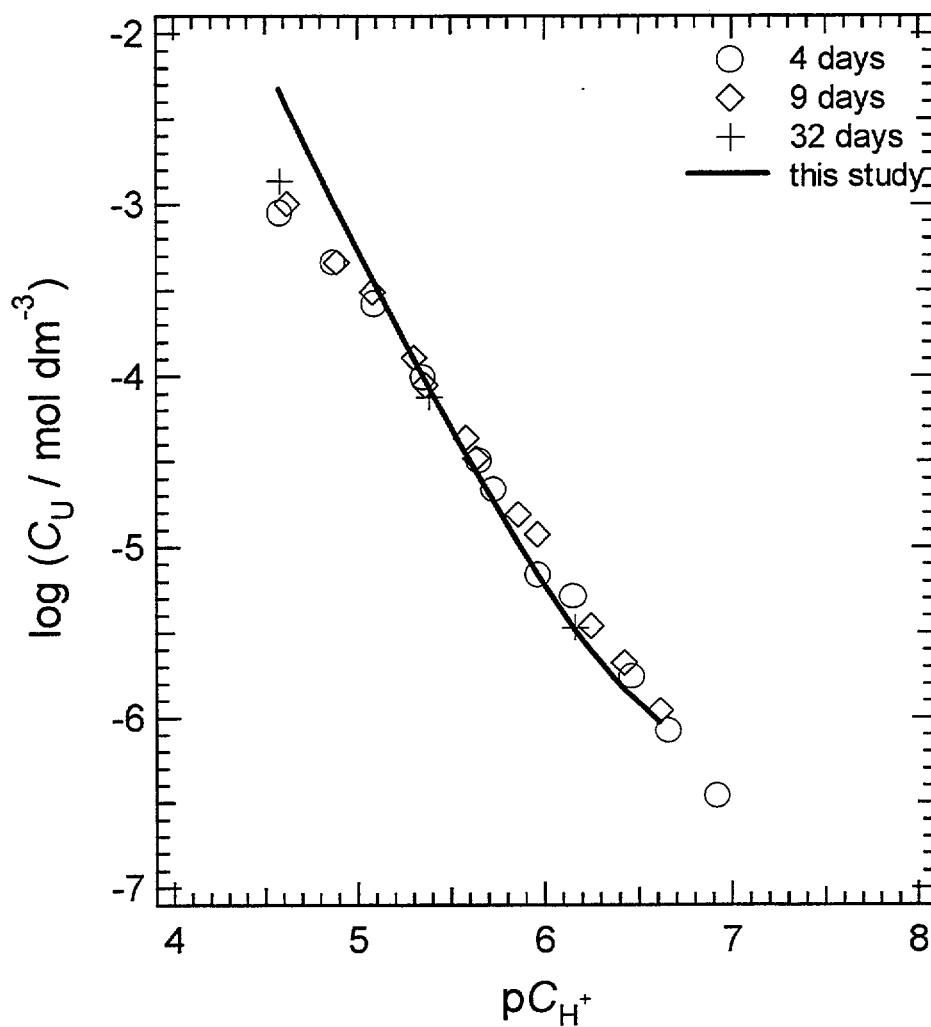
Figure 2. Aqueous uranium concentrations in solutions contacting becquerelite suspensions in 0.1 M CaCl$_2$ and a range in pC_{H^+} values that were equilibrated for different periods. The presence of becquerelite at pC_{H^+} > 8 is uncertain, see text for details. The lines represent predictions based on thermodynamic data reported in Tables 4 and 5 with the exception that the dashed line incorporates values of formation constants for UO$_2$(OH)$_2{}^0$ and UO$_2$(OH)$_3^-$ from Grenthe *et al.* [4].

Figure 3. Aqueous uranium concentrations in solutions contacting becquerelite suspensions in 0.5 M $CaCl_2$ and a range in pC_{H^+} values that were equilibrated for different periods. Solid line represents model predictions based on thermodynamic data reported in Tables 4 and 5.
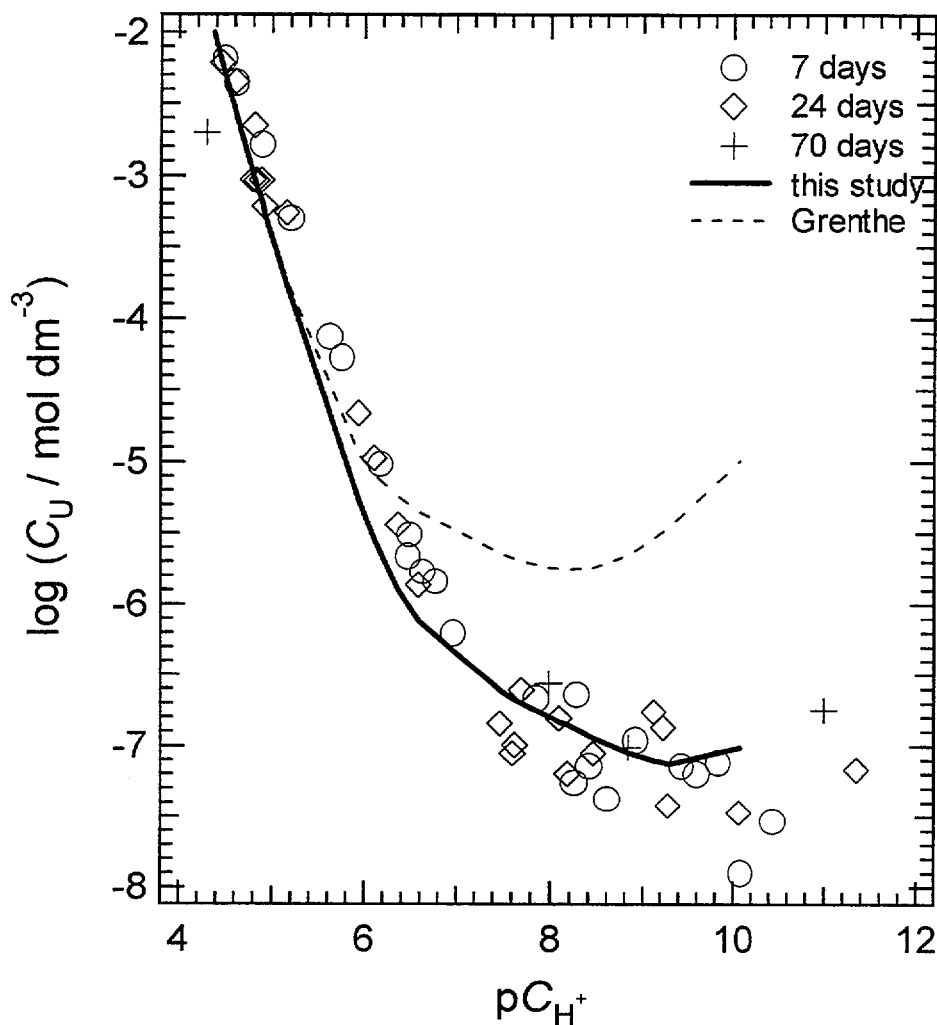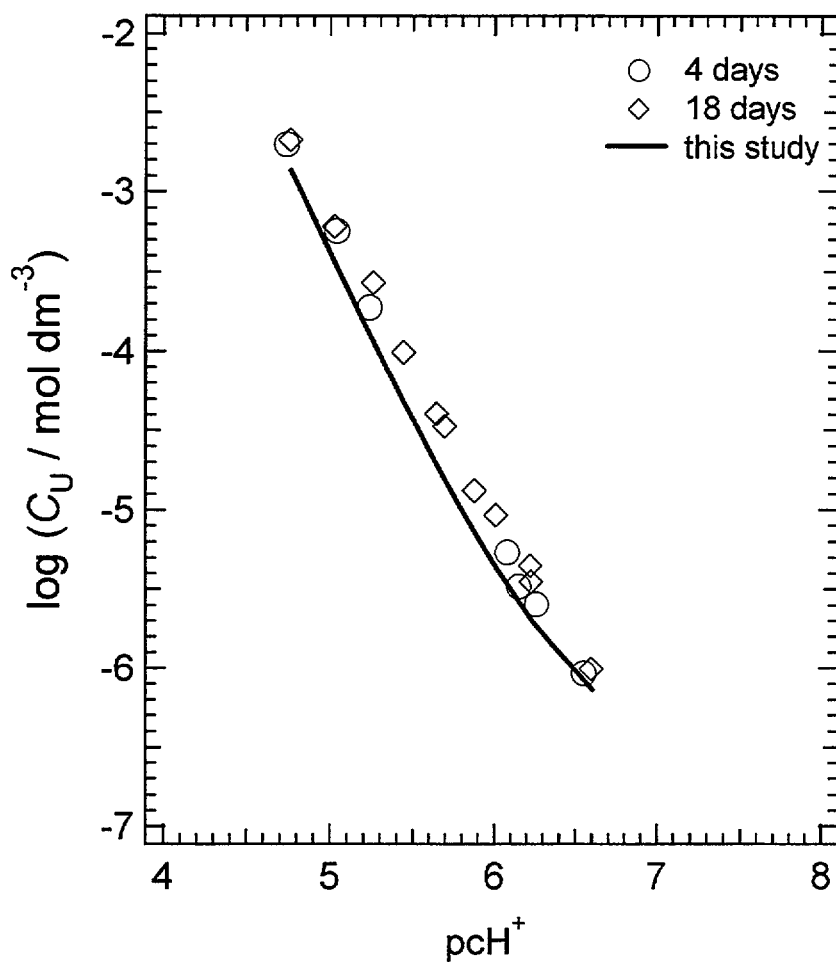
Figure 4. Aqueous uranium concentrations in solutions contacting becquerelite suspensions in 0.02, 0.1, or 0.5 M $CaCl_2$ and a range in pC_{H^+} values. Solid line represents a reference slope of –2. Dashed line represents predicted uranium concentrations in equilibrium with $CaUO_4(c)$ at 0.1 M $CaCl_2$ based on thermodynamic data reported in Grenthe et al. [4].

Figure 5. A representative X-ray diffraction pattern of the solid phase equilibrated in 0.1 M $CaCl_2$ at pC_{H^+} of about 8. See Table 1 for details about XRD analyses of samples at other pC_{H^+} values.

Figure 6. Comparison of the Fourier transforms of the EXAFS spectra of solids equilibrated in different molarities of $CaCl_2$ solutions (U65, 0.02 M $CaCl_2$, pC_{H^+} 5.9; Ul08, 0.1 M $CaCl_2$, pC_{H^+} 7.6; U209, 0.5 M $CaCl_2$, pC_{H^+} 6.2). The thin lines are the Fourier transforms of the experimental EXAFS; the thick lines are the Fourier transforms of the fit to EXAFS. Transforms were calculated over the range from 3.5 to 12.5 $Å^{-1}$ and are offset by 0.15 units for ease of comparison.

Figure 7. Aqueous uranium concentrations in solutions contacting becquerelite suspensions in 1.0 M $CaCl_2$. The symbols representing experimental data points are from Sandino and Grambow [10] (labeled as S&G 1994). The solid line represents model predictions based on thermodynamic data reported in Tables 4 and 5.

Table 1. X-ray diffraction analyses of solid samples contacting 0.1 M $CaCl_2$

pC_{H^+}	Major Phase
4.3	Becquerelite [a,b]
6.3	Becquerelite [a]
8.0	Becquerelite [a]
11.0	Inconclusive [c]

[a] Becquerelite (Ca $(UO_2)_6O_4(OH)_6 \cdot 8H_2O$) was found to be the major phase in the samples. There were some low-intensity, unaccounted peaks corresponding to unknown minor phase.

[b] The major phase in this sample was highly preferentially oriented along (00L).

[c] The experimental pattern was vaguely similar to reference powder data for bacquerelite, but the quality of the match was not conclusive.

Table 2. Molar U to calcium ratios in washed solids
that were equilibrated in different $CaCl_2$
solutions

$C_{CaCl_2}/\text{mol dm}^{-3}$	pC_{H^+}	$\dfrac{C_U/\text{mol dm}^{-3}}{C_{Ca}/\text{mol dm}^{-3}}$
0.1	4.30	5.6
0.1	7.99	5.4
0.1	8.84	3.7
0.1	11.00	1.6
0.02	11.36	2.2
0.5	11.42	2.1

Table 3. Expected changes in uranium concentrations with the changes in H^+ and Ca^{2+} concentration in equilibrium with different Ca-U(VI) solids.

Reaction	Changes in log (C_U/mol dm^{-3}) with one log unit increase in	
	C_{H^+}/mol dm^{-3}	$C_{Ca^{2+}}$/mol dm^{-3}
<u>Reactions Involving UO_2^{2+}</u>		
$Ca(UO_2)_6O_4(OH)_6x8H_2O + 14H^+ \equiv Ca^{2+} + 6UO_2^{2+} + 18H_2O$	2.33	-0.17
$Ca_2UO_5XxH_2O + 6H^+ \equiv 2Ca^{2+} + UO_2^{2+} + (x+3)\,H_2O$	6.0	-2.0
$CaUO_4(c) + 4H^+ \equiv Ca^{2+} + UO_2^{2+} + 2H_2O$	4.0	-1.0
$Ca_3UO_6 + 8H^+ \equiv 3Ca^{2+} + UO_2^{2+} + 4H_2O$	8.0	-3.0
$CaU_2O_7 + 6H^+ \equiv Ca^{2+} + 2UO_2^{2+} + 3H_2O$	3.0	-0.5
<u>Reactions Involving $UO_2(OH)_2^0$</u>		
$Ca(UO_2)_6O_4(OH)_6x8H_2O + 2H^+ \equiv Ca^{2+} + 6UO_2(OH)_2^0 + 6\,H_2O$	0.33	-0.17
$Ca_2UO_5XxH_2O + 4H^+ \equiv 2Ca^{2+} + UO_2(OH)_2^0 + (x+1)\,H_2O$	4.0	-2.0
$CaUO_4(c) + 2H^+ \equiv Ca^{2+} + UO_2(OH)_2^0$	2.0	-1.0
$Ca_3UO_6 + 6H^+ \equiv 3Ca^{2+} + UO_2(OH)_2^0 + 2H_2O$	6.0	-3.0
$CaU_2O_7 + 2H^+ \equiv Ca^{2+} + 2UO_2(OH)_2^0$	1.0	-0.5

Table 4. Thermodynamic data for reactions involving uranium species used in this study.

Reaction	log K^0	Reference
$UO_2^{2+} + H_2O \rightleftharpoons UO_2OH^+ + H^+$	-5.2	[4]
$UO_2^{2+} + 2H_2O \rightleftharpoons UO_2(OH)_2^0 + 2H^+$	~ -11.3[a]	This study
$UO_2^{2+} + 3H_2O \rightleftharpoons UO_2(OH)_3^- + 3H^+$	≤ -21.5[a]	This study
$UO_2^{2+} + 4H_2O \rightleftharpoons UO_2(OH)_4^{2-} + 4H^+$	-33.0	[4]
$2UO_2^{2+} + 2H_2O \rightleftharpoons (UO_2)_2(OH)_2^{2+} + 2H^+$	-5.62	[4]
$3UO_2^{2+} + 4H_2O \rightleftharpoons (UO_2)_3(OH)_4^{2+} + 4H^+$	-11.9	[4]
$3UO_2^{2+} + 5H_2O \rightleftharpoons (UO_2)_3(OH)_5^+ + 5H^+$	-15.55	[4]
$3UO_2^{2+} + 7H_2O \rightleftharpoons (UO_2)_3(OH)_7^- + 7H^+$	-31.0	[4]
$Ca(UO_2)_6O_4(OH)_6 \cdot 8H_2O(c) + 14H^+ \rightleftharpoons Ca^{2+} + 6UO_2^{2+} + 18H_2O$	41.4±0.2[b]	This study
	41.89±0.5[c]	[10]
	43.7±0.47[c]	[10]
	43.6±0.3[c]	[9]
	41.4 [c,d]	Calculated
	29±1[c]	[11]

[a] The value quoted by Grenthe et al. [4] for the formation of $UO_2(OH)^0_2$ and $UO_2(OH)_3^-$ are ≤−10.3 and −19.2±0.4, respectively.

[b] This value was calculated based on the data at relatively low pC_{H^+} values and is not significantly impacted by the choice of constants for the formation of $UO_2(OH)^0_2$ and $UO_2(OH)_3^-$, because these species are not dominant in the low pC_{H^+} region.

[c] The values are based on a few experiments conducted in a very narrow range of pH values and Ca concentrations. See text for details.

[d] Value calculated by Casas et al. [11] from the data reported by Vochten and Van Haverbeke [9] and using the aqueous thermodynamic model of Grenthe et al. [4].

Table 5. Pitzer ion-interaction parameters used in this study.

Binary Parameters					
Species	$\beta^{(0)}$	$\beta^{(1)}$	$\beta^{(2)}$	C^ϕ	**source**
H^+, Cl^-	0.1775	0.2945	0.0	0.00080	[24]
Ca^{2+}, Cl^-	0.3159	1.6140	0.0	-0.00034	[24]
UO_2^{2+}, Cl^-	0.4270	1.6440	0.0	-0.03690	[15]
$(UO_2)_2(OH)_2^{2+}$, Cl^-	0.4270	1.6440	0.0	-0.03690	This study [a]
$(UO_2)_3(OH)_2^{2+}$, Cl^-	0.4270	1.6440	0.0	-0.03690	This study [a]

Common-Ion Ternary Parameters (all values from Harvie *et al.* [24])	
H^+, Ca^{2+}	0.092
H^+, Ca^{2+}, Cl^-	-0.015
Cl^-, OH^-	-0.050
Ca^{2+}, Cl^-, OH^-	-0.025

[a] Assumed to be identical to UO_2^{2+}, Cl^- parameters reported by Pitzer [15].

Appendix

Complete sets of becquerelite solubility in different solutions presented in Figures 1

through 4 are reported in the following tables (Tables A.1, A.2, and A.3).

Table A.1 Solubility of becquerelite in 0.02 M $CaCl_2$ solutions at different equilibration periods.

4 days		9 days		32 days	
pC_{H^+}[a]	log C_U/mol dm^{-3}	pC_{H^+}[a]	log C_U/mol dm^{-3}	pC_{H^+}[a]	log C_U/mol dm^{-3}
4.579	-3.052	4.623	-2.996	4.582	-2.863
4.869	-3.336	4.892	-3.338	5.386	-4.120
5.087	-3.577	5.084	-3.510	6.164	-5.469
5.353	-4.008	5.306	-3.893	11.359	-6.405
5.651	-4.492	5.367	-4.054		
5.730	-4.666	5.586	-4.362		
5.965	-5.161	5.638	-4.483		
6.153	-5.283	5.861	-4.812		
6.463	-5.754	5.964	-4.928		
6.660	-6.073	6.250	-5.462		
6.922	-6.463	6.426	-5.678		
11.561	-6.642	6.617	-5.959		
		11.482	-6.857		

[a] pC_{H^+} = pH(obs) + 0.134

Table A.2 Solubility of becquerelite in 0.01 M CaCl$_2$ solutions at different equilibration periods.

7 days		24 days		70 days	
pC$_{H^+}$[a]	log C$_U$/mol dm^{-3}	pC$_{H^+}$[a]	log C$_U$/mol dm^{-3}	pC$_{H^+}$[a]	log C$_U$/mol dm^{-3}
4.497	-2.189	4.470	-2.218	4.296	-2.700
4.620	-2.355	4.619	-2.348	7.986	-6.560
4.896	-2.785	4.799	-3.030	8.838	-7.010
5.207	-3.301	4.821	-2.654	10.998	-6.750
5.629	-4.128	4.839	-3.034		
5.758	-4.277	4.889	-3.032		
6.180	-5.015	4.924	-3.217		
6.479	-5.664	5.161	-3.260		
6.499	-5.510	5.943	-4.664		
6.636	-5.772	6.113	-4.975		
6.770	-5.839	6.372	-5.442		
6.965	-6.206	6.588	-5.866		
7.860	-6.670	7.479	-6.845		
8.257	-7.263	7.613	-7.055		
8.284	-6.644	7.638	-6.996		
8.413	-7.146	7.708	-6.613		
8.603	-7.377	8.096	-6.810		
8.921	-6.963	8.186	-7.201		
9.442	-7.146	8.458	-7.055		
9.601	-7.201	9.128	-6.764		
9.839	-7.121	9.234	-6.873		
10.087	-7.900	9.287	-7.423		
10.442	-7.532	10.070	-7.474		
		11.355	-7.173		

[a] pC$_{H^+}$ = pH(obs) + 0.161

Table A.3 Solubility of becquerelite in 0.5 M $CaCl_2$ solutions at different equilibration periods.

4 days		18 days	
pC_{H^+}[a]	$\log C_U/\text{mol dm}^{-3}$	pC_{H^+}[a]	$\log C_U/\text{mol dm}^{-3}$
4.738	-2.701	4.762	-2.676
5.039	-3.243	5.026	-3.218
5.236	-3.724	5.259	-3.570
6.079	-5.265	5.445	-4.007
6.150	-5.481	5.649	-4.395
6.260	-5.593	5.698	-4.474
6.550	-6.031	5.879	-4.879
11.433	-6.449	6.011	-5.032
		6.225	-5.350
		6.229	-5.452
		6.599	-6.007
		11.422	-6.719

[a] $pC_{H^+} = pH(\text{obs}) + 0.283$

U.S. NUCLEAR REGULATORY COMMISSION

BIBLIOGRAPHIC DATA SHEET

(See instructions on the reverse)

1. REPORT NUMBER
(Assigned by NRC. Add Vol., Supp., Rev., and Addendum Numbers, if any.)

NUREG CR-6632

2. TITLE AND SUBTITLE

Solubility and Leaching of Radionuclides in Site Decommissioning Management Plan (SDMP) Slags

3. DATE REPORT PUBLISHED

MONTH	YEAR
February	2002

4. FIN OR GRANT NUMBER
W6409

5. AUTHOR(S)

Andrew R. Felmy; Dhanpat Rai; Stacey Hartley; Virginia LeGore

6. TYPE OF REPORT

7. PERIOD COVERED *(Inclusive Dates)*

8. PERFORMING ORGANIZATION – NAME AND ADDRESS *(If NRC, provide Division, Office or Region, U.S. Nuclear Regulatory Commission, and mailing address; if contractor, provide name and mailing address.)*

Pacific Northwest National Laboratory
P.O. Box 999
Richland, WA 99352

9. SPONSORING ORGANIZATION – NAME AND ADDRESS *(If NRC, type "Same as above"; if contractor, provide NRC Division, Office or Region, U.S. Nuclear Regulatory Commission, and mailing address.)*

Division of Systems Analysis and Regulatory Effectiveness
Office of Nuclear Regulatory Research
U.S. Nuclear Regulatory Commission
Washington, DC 20555-0001

10. SUPPLEMENTARY NOTES

P. Reed, NRC Project Manager

11. ABSTRACT *(200 words or less)*

Samples of disposed wastes at three U.S. Nuclear Regulatory Commission (NRC) Site Decommissioning Management Plan (SDMP) sites were studied to determine 1) the key radionuclides and their concentrations present, 2) the solubility limits and solubility limiting phases, 3) the rate of attainment of solubility equilibrium, 4) the observed leaching rate for radionuclides,, and 5) the potential for radiocolloid formation. The results for slags at all three sites show that the major radionuclides present in the wastes were Th and U with their associated daughter products. Th daughters were in secular equilibrium with the parent Th-232 in all samples. U-238 daughters were in secular equilibrium in certain highly solidified non-porous samples but escape of Rn-222 had occurred from more porous samples perturbing the U-238 secular equilibrium. Analysis of solution phase concentrations and solid phase composition indicated that aqueous Th concentrations are solubility controlled, most likely by thoranite, $ThO_2(c)$. U also appears to be solubility controlled in certain waste samples (thoriated slags) high in pH and alkaline earth cations (Ca, Sr, Ba) by the formation of alkaline earth uranates. No evidence was found for the formation of radiocolloids. Solubility limits and radionuclide leaching rates have been calculated for use in performance assessment calculations. Statistical analysis of these data showed the uncertainties in the Th and U concentrations can be represented by a lognormal distribution with a meanlog of -17.7 and an sdlog of 0.57 for U and a meanlog of -19.5 and an sdlog of 1.7 for Th.

12. KEY WORDS/DESCRIPTORS *(List words or phrases that will assist researchers in locating the report.)*

Leaching, radionuclides, SDMP, solubility, slag, thorium, uranium waste
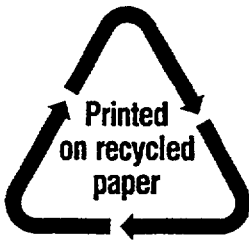
13. AVAILABILITY STATEMENT

Unlimited

14. SECURITY CLASSIFICATION

(This Page)
Unclassified

Unclassified
(This Report)

15. NUMBER OF PAGES

16. PRICE

UNITED STATES
NUCLEAR REGULATORY COMMISSION
WASHINGTON, DC 20555-0001

_____

OFFICIAL BUSINESS
PENALTY FOR PRIVATE USE, $300